*Russian Original Vol. 47, No. 2, August, 1979*

February, 1980

LS FILE

SATEAZ 47(2) 591-690 (1979)

# SOVIET ATOMIC ENERGY

АТОМНАЯ ЭНЕРГИЯ
(ATOMNAYA ÉNERGIYA)

TRANSLATED FROM RUSSIAN

c/b CONSULTANTS BUREAU, NEW YORK

# SOVIET ATOMIC ENERGY

*Soviet Atomic Energy* is a cover-to-cover translation of *Atomnaya Énergiya*, a publication of the Academy of Sciences of the USSR.

An agreement with the Copyright Agency of the USSR (VAAP) makes available both advance copies of the Russian journal and original glossy photographs and artwork. This serves to decrease the necessary time lag between publication of the original and publication of the translation and helps to improve the quality of the latter. The translation began with the first issue of the Russian journal.





Consultants Bureau journals appear about six months after the publication of the original Russian issue. For bibliographic accuracy, the English issue published by Consultants Bureau carries the same number and date as the original Russian from which it was translated. For example, a Russian issue published in December will appear in a Consultants Bureau English translation about the following June, but the translation issue will carry the December date. When ordering any volume or particular issue of a Consultants Bureau journal, please specify the date and, where applicable, the volume and issue numbers of the original Russian. The material you will receive will be a translation of that Russian volume or issue.

Subscription (2 volumes per year)

Vols. 46 & 47: $147.50 per volume (6 Issues)
Vols. 48 & 49: $167.50 per volume (6 Issues)

Single Issue: $50
Single Article: $7.50

Prices somewhat higher outside the United States.

**CONSULTANTS BUREAU, NEW YORK AND LONDON**

c/b
227 West 17th Street
New York, New York 10011

Published monthly. Second-class postage paid at Jamaica, New York 11431.

*Soviet Atomic Energy* is abstracted or indexed in *Chemical Abstracts, Chemical Titles, Pollution Abstracts, Science Research Abstracts, Parts A and B, Safety Science Abstracts Journal, Current Contents, Energy Research Abstracts,* and *Engineering Index.*

# SOVIET ATOMIC ENERGY

A translation of *Atomnaya Énergiya*

February, 1980

Volume 47, Number 2

August, 1979

## CONTENTS

# CONTENTS

(continued)



**The Russian press date (podpisano k pechati) of this issue was 7/24/1979. Publication therefore did not occur prior to this date, but must be assumed to have taken place reasonably soon thereafter.**

ARTICLES

# CHOICE OF ORGANIC DILUENTS FOR THE EXTRACTIVE REGENERATION OF THE SPENT FUEL OF NUCLEAR POWER PLANTS

G. F. Egorov, A. P. Ilozhev,
A. S. Nikiforov, V. S. Smelov, V. B. Shevchenko,
and V. S. Shmidt

UDC 621.039.59:66.061.5

At the present time the extraction of tributyl phosphate dissolved in hydrocarbon diluents is the basis for a number of engineering methods for regenerating spent fuel from nuclear power plants in the USSR [1-3], France [4], Great Britain [5], Japan [6], and the Federal Republic of Germany (FRG) [7]. The development of work in this area over a period of many years has determined the evolution of the technical requirements placed on the diluents. It is known that previous plans for using technical products with involved composition, such as Solvesso 100, "odorless" kerosene, Shell Sol, p-aminobenzine, etc., have gradually been replaced in favor of the application of individual hydrocarbons or mixtures of hydrocarbons of fairly narrow fractions (mainly synthetic products), which has limited the spectrum of possible admixtures to be controlled. The purpose of this article is to unify the physicochemical data which determine the choice of hydrocarbon diluents in extractive technology.

The main indicators which characterize the hydrocarbon diluents of the aliphate series (n-alkanes) are the length of the hydrocarbon chain and the content of admixtures of different chemical nature – olefin and aromatic hydrocarbons, alcohols, carboxylic acids, and also other admixtures which enter the diluent from the original raw material or which are formed in the synthesis. For hydrocarbon diluents in the extractive cycle, it is important to take into account the content of the products of nitrating, oxidation, and radiative-chemical interaction with the dissociation products of the extracting agent [8]. Our main attention in this article is directed to those admixtures which are found in a fresh extracting agent, having regard for their consequences as products which initiate the formation of the above technologically harmful substances as the extracting agent and diluent are used.

## Effect of the Length of the n-Alkane Chain on the Properties of the Diluent and the Extractive System as a Whole

The properties that determine the applicability of a diluent for practical use are the boiling point, freezing point, flash point, viscosity, density, surface tension, and solubility in the liquid phase. Also very important are the properties of the diluent which are responsible for its interaction with the extracting agent and extracting compound, those which affect the distribution of the extracting agent (tributyl phosphate – TBP) between the liquid and organic phases, those which affect the distribution of the system components being extracted, those which affect the compatibility of the diluent with the solvates of the compounds being extracted and the dissociation products of the extracting agent. We will consider below the effect of the length of the hydrocarbon chain of the diluent on these properties.

Boiling Point, Freezing Point, and Flash Point. The dependence of these characteristics on the length of the hydrocarbon chain of the n-alkanes (C) is shown in Fig. 1. It is seen that the freezing point of the n-alkanes becomes comparable with the lowest likely temperature of the operating area only when the number of carbon atoms in the chain is higher than 15. On the other hand, reducing C to 10 puts the diluent in the flammable category (B): the flash point becomes less than 25° higher than the maximum temperature of the surrounding medium (~35°).

The boiling point of the n-alkanes $C_{11}$-$C_{16}$ falls within the limits which are tolerable in case vacuum distillation is necessary. The addition of TBP leads only to a certain increase in the flash point and a reduction in the freezing point of the extractive mixture as compared with the individual diluent. According to the indicators shown in Fig. 1, it is thus permissible to use the n-alkane diluents $C_{11}$-$C_{15}$.

Viscosity, Density, and Surface Tension. The dependence of these characteristics is shown in Fig. 2,

Translated from Atomnaya Énergiya, Vol. 47, No. 2, pp. 75-79, August, 1979. Original article submitted January 30, 1979.

0038-531X/79/4702-0591$07.50 

where it is seen that lengthening the hydrocarbon chain causes a certain increase in the values of these characteristics. For C less than 15, however, they remain at an acceptable (as far as the rate of phase stratification in the extractive apparatus is concerned) level. The variation of the specific gravity and surface tension is quite small (in the interval $C_{11}$-$C_{15}$ it is ≈5%). The viscosity of the diluent in the same interval increases by almost a factor of two, but this does not affect the rate of stratification of the emulsions and only can have some effect on the kinetics of the mass exchange process in the organic phase. Since the kinetics of the extraction processes with TBP solutions in n-alkanes are on the whole rather satisfactory (extraction equilibrium is attained in at most 1-2 sec [9]), this variation does not play a significant role in estimating the quality of the diluents.

Solubility of the Hydrocarbons in the Liquid Phase. Hydrocarbons dissolve in the liquid phase to a very small extent, with a severalfold reduction in the solubility associated with each successive carbon atom added to the n-alkane chain. Using the available data [10] for the solubility of n-alkanes in water (n-hexane, ~120 mg/liter; n-heptane, ~50 mg/liter; and n-octane, 25 mg/liter), we derive a dependence of the form $\log S = 4.4 - 0.4n$,* from which we find by extrapolation that for n = 10 and n = 11 the solubility of alkanes in water is expected to equal, respectively, ~4 and ~1 mg/liter, and should decrease at higher values of C (n is the number of carbon atoms). Because of this characteristic, the physical distribution of n-alkanes with chain lengths greater than $C_{10}$-$C_{11}$ does not introduce any appreciable content of organic substances to the aqueous solutions in contact with the extracting agent (refinates, reextractates, and washing solutions).

Distribution of TBP between the n-Alkane Diluent and the Liquid Phase. The distribution of TBP between the n-alkane diluent and the liquid phase depends on the chain length of the alkane, since changes in the latter are associated with a change in the activity coefficient of the TBP in the organic solution. The effect of the nature of the diluent on the activity of the TBP in the extracting agent can be approximately predicted by using the theory of regular solutions [12, 13]. An increase in the chain length of the alkane and its corresponding molar volume causes an increase in solubility of the TBP in the equilibrium liquid phase as one passes to diluents with large molecular weights. Data on the concentration of TBP in the equilibrium liquid solution are shown in Fig. 3 (using the data of [14] for alkanes up to $C_{12}$, and calculated data for $C_{13}$ and higher). As one passes from $C_{12}$ to $C_{15}$, the content of TBP in the liquid phase increases by 20%, which should be taken into account in estimating the possible losses of extracting agent on contact with the large volumes of the liquid phase.

Distribution Coefficients of the Valuable Components While Extracting TBP in n-Alkanes. The length of alkyl chains of hydrocarbon diluents has practically no effect on the distribution coefficients of uranium (VI), plutonium (IV), and nitric acid during extraction by means of TBP solutions from aqueous solutions of nitric acid (Figs. 4-6). As a result, this factor has little effect on the choice of the length of the hydrocarbon chain of an n-alkane diluent. From this point of view, any n-alkane with chain length $C_{11}$-$C_{14}$ or a mixture of them can be used as a diluent.

Compatibility of the Solvates Being Extracted and the Diluents. The nitrate solvates of hexavalent actinides are quite compatible with hydrocarbon diluents. It is therefore useful to consider the compatibility of nitrate solvates with tetravalent actinides. This is determined by the maximum content of extracted element or compound (in the organic solution) for which demixing of the organic phase does not occur. Figure 7 shows the corresponding maximum concentrations of thorium extracted by a 30% solution of TBP in the form of a nitrate. As is seen, the lengthening of the n-alkane chain causes the compatibility to become worse, which agrees with theoretical conjectures [13]. When the number of carbon atoms in the n-alkane chain is around 15, however, the permissible concentrations of tetravalent actinides (~20 g/liter) far exceed those which usually occur in the reprocessing of thermal neutron reactor fuel elements [2].

Effect of the Length of an n-Alkane Hydrocarbon Chain on the Radiative-Chemical Stability. The formation of oxidation and nitrating products during the irradiation of a system consisting of a hydrocarbon with an aqueous solution of nitric acid takes place as a result of the interaction of the hydrocarbon radicals with the oxygen and the nitrating agents ($NO_2$, NO, and $HNO_2$), i.e., with the dissociation products of the nitric acid [8].

It is known [15] that the overall yield of hydrocarbon radicals is a slowly varying function of C (from 6 to 16) in the radiolysis of n-alkanes. It should therefore be expected that their yields of oxidation and nitrating products, which are used as the principal criteria of radiative-chemical stability, will be similar. However, the experimentally observed accumulations of nitrating and oxidation products on irradiation of n-octane, a $C_{10}$-$C_{12}$ hydrocarbon mixture, and also n-dodecane in contact with a 2 M solution of nitric acid indicate that the

*The solubility of aliphatic alcohols in water shows a similar dependence [11].

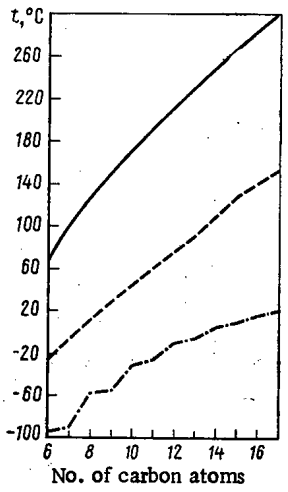


Fig. 1

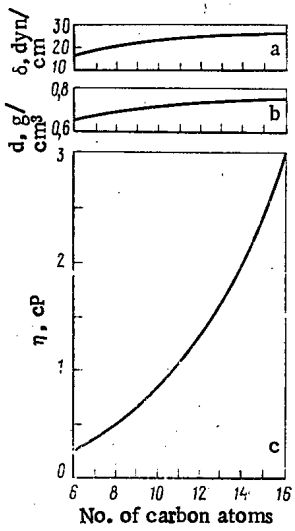


Fig. 2

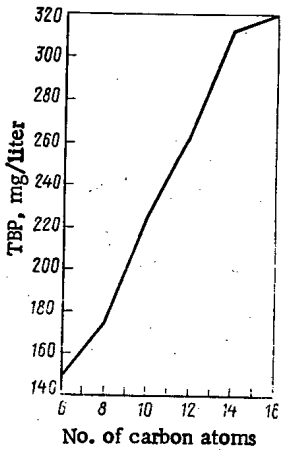


Fig. 3

Fig. 1. Dependence on the number of carbon atoms in the hydrocarbon chain of the melting point (−·−), flash point (−−−), and boiling point (——) of n-alkanes.

Fig. 2. Dependence of the density (a), surface tension (b), and viscosity (c) of n-alkanes on the number of atoms in the hydrocarbon chain.

Fig. 3. Content of TBP in the liquid phase in equilibrium at 25°C with 30 vol.% solutions of TBP in n-alkanes with a different length of hydrocarbon chain.

TABLE 1. Initial Radiative-Chemical Formation Yields of Products of Hydrocarbon Nitrating and Oxidation of Various Molecular Weights in Two-Phase Systems

| Hydrocarbon — 2 M $HNO_3$ system | G, molecule/100 eV | | | |
|---|---|---|---|---|
| | nitro compounds | organic nitrites | carbonyl compounds | dissociation of $HNO_3$ |
| n-octane | 1,2±0,2 | 0,8±0,2 | 0,6±0,1 | 2,0±0,5 |
| $C_{10}$-$C_{12}$ n-alkane mix | 0,5±0,1 | 0,3±0,1 | 0,1±0,02 | 0,8±0,2 |
| n-dodecane | 0,2±0,04 | 0,1±0,02 | 0,07±0,005 | 0,3±0,1 |
| $C_{14}$-$C_{15}$ n-alkane mix | 0,2 | 0,08 | 0,1 | — |

initial radiative-chemical yield of products that is calculated from their accumulation curves for dosages of up to $5 \cdot 10^{20}$ eV/ml becomes smaller with increasing C (Table 1). The five- to tenfold difference observed in the initial yields of the products of nitrating and oxidation on irradiation of n-octane and n-dodecane in contact with aqueous solutions of nitric acid is caused by the variation of the dissociation yield of the latter. The hydrocarbons dissolved in an aqueous solution react with OH radicals, which reduces the rate of reverse oxidation of nitrous acid to nitric acid and in this way increases the dissociation yield to an extent which depends on the hydrocarbon concentration in the aqueous phase. In addition, the hydrocarbon radicals formed in the aqueous solution by the reactions

$$RH + OH \rightarrow \dot{R} + H_2O;$$
$$RH + H \rightarrow \dot{R} + H_2$$

interact with the nitric acid by the reaction

$$\dot{R} + HONO_2 \rightarrow RNO_2 + OH$$

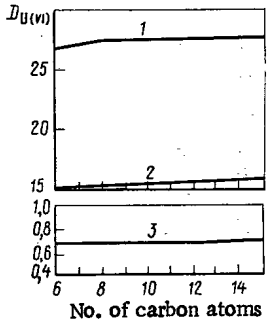


Fig. 4

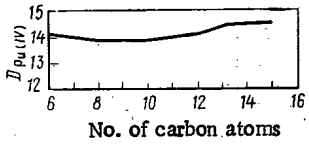


Fig. 5

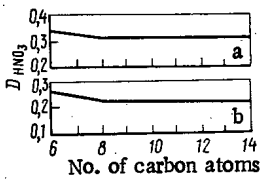


Fig. 6

Fig. 4. Coefficient of the distribution of uranium (VI) between aqueous nitrate solutions and 30 vol.% solutions of TBP in n-alkane, as a function of carbon atoms in the diluent. Initial concentration of uranium in the liquid phase ~1 g/liter, $V_{org}:V_{liq} = 1:1$, concentration of nitric acid in the liquid phase: 3 M (1); 1 M (2); 0.1 M (3).

Fig. 5. Distribution coefficient of microconcentrations of plutonium (IV) between 30% solution of TBP in n-alkane and 3 M $HNO_3$, as a function of the number of atoms in the n-alkane.

Fig. 6. Distribution coefficient of nitric acid between a 30% solution of TBP in n-alkane and the aqueous solutions, as a function of the number of carbon atoms in the hydrocarbon chain. Acid concentration in the liquid phase: 0.8 M (a) and 1.7 M (b).

and contribute to the total yield of nitrating products.

In the case of n-alkanes, it is worth noting that the transition from $C_{12}$ to $C_{14-15}$ makes no significant difference in the initial yields of the nitrating and oxidation products of these hydrocarbons (see Table 1). It should also be noted that accumulation in the irradiated system of destruction products from hydrocarbons of high molecular weight causes the rates of formation of oxidation and nitrating products in two-phase systems containing n-octane and n-dodecane to become comparable for dosages $>10^{21}$ eV/ml (>50 Wh/liter). This behavior is due to the equalization of the rate of decomposition of nitric acid between these systems.

It is seen from the data given for the radiative-chemical stablity that the quantity $C_{12-14}$ should also be considered as optimal for hydrocarbon diluents. Difficulties may arise for greater lengths of the hydrocarbon chain because of worsened removal of the high-molecular-weight products of the hydrocarbon radiolysis when they are regenerated.

Any n-alkanes with chain lengths from $C_{11}$ to $C_{15}$ or a mixture of them can be used in this way as a diluent for the extractive regeneration of spent fuel elements from nuclear power plants with thermal neutron reactors. The lengthening of the chain, while reducing the flammability of the diluent, does not affect the distribution coefficients of the valuable components. It also improves somewhat the radiative-chemical stability with practically no change in the hydrodynamic properties of the extracting agent and the solubility of the TBP in the liquid phase, but it worsens (though within allowable limits) the compatibility of the diluent with the solvates of the actinide nitrates.

## Effect of Additives on the Properties of the Diluent and the Extractive System as a Whole

The possible additives whose presence must be taken into account in order to estimate the properties of the hydrocarbon diluents are unsaturated compounds, aromatic hydrocarbons, aliphatic alcohols, and acids. The content of these additives is limited, since they worsen the properties of the extractive system. Aliphatic alcohols and acids reduce the distribution coefficients because of solvation of the functional groups of the nucleophilic extracting agents [16] (Fig. 8). Carboxylic acids have a similar effect. Branched aliphatic hydrocarbons and olefins are considerably inferior to hydrocarbons with a straight chain (n-alkanes) with respect to chemical [17] and radiative [18] resistance to the action of nitric acid, so their presence in aliphatic diluents is required to be minimal.

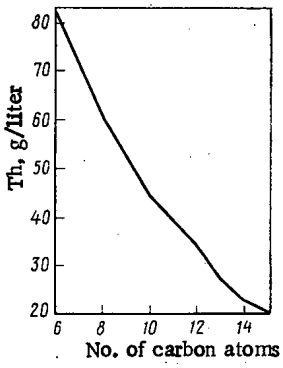


Fig. 7

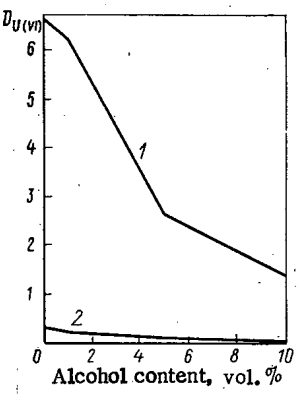


Fig. 8

Fig. 7. Maximum concentration of thorium (in nitrate form) in 30% TBP for which the organic phase is still homogeneous, as a function of the number of carbon atoms in the n-alkane chain.

Fig. 8. Coefficient of the distribution of uranium (VI) between a 10% solution of TBP in a mixture of dodecane–octanol and an aqueous solution of nitric acid, as a function of the octanol concentration in the diluent. Initial concentration of U ~ 10 g/liter; $V_{org} : V_{liq} = 1 : 1$. Concentration of $HNO_3$: 2.9 M (1); 0.23 M (2).

Certain aromatic compounds inhibit the decomposition of the extracting agent and the diluent by the transfer of energy in one or another way from molecules of the latter to molecules of the aromatic substances. The addition of 0.1 M monoisopropyldiphenyl to a solution of TBP in n-dodecane reduces by a factor of two the yield of the formation of acid products of the radiolysis of the extracting agent – DBP and MBP. However, for large contents of aromatic compounds in the extracting agents, significant unfavorable phenomena are also observed: a rapid increase in the products of nitrating and an inhibition of the fission fragment elements (zirconium) of the organic phase even for small irradiation dosages. From modeling experiments with diluents containing additions of aromatic nitro compounds, alkylphenols, and radiolysis products of TBP it can be assumed that the cause of the inhibition of zirconium may be the formation of complexes of the type $Zr_x(DBP)_y$ (PhOH). Evidently it can therefore be assumed that since the time of contact of the extracting agent with the $HNO_3$ in the apparatus amounts to 10-20 min, the presence of no more than 1% concentrations of aromatic compounds in n-alkane diluents does not cause significant impairment of the extractive characteristics and at the same time to a certain extent maintains the protective properties of the aromatic. Some simple aromatic compounds of the alkylbenzol type can be used successfully either as a diluent (e.g., for ternary amines) or as a polar additive to the aliphatic diluents. In both cases, a higher degree of purification of the plutonium from the fission fragment elements over a wide range of dosages is attained compared with systems based on aliphatic diluents [19].

The effect of the other admixtures is considered using as an illustration the radiative stability of three samples of the mixture $C_{10}$-$C_{12}$. The contents of the admixtures of unsaturated compounds and of alcohols were, respectively, 0.2 and 0.12 in sample 1, 0.02 and 0.12 in sample 2, and 0.004 and 0.012 M in sample 3. Table 2 gives the results of the investigation of the radiative-chemical stability of these samples and also of spectrally pure n-dodecane in two-phase systems containing a 2 M solution of nitric acid. The rates of formation

TABLE 2. Radiative-Chemical Stability of Samples of the Mixture $C_{10}$-$C_{12}$ at a Dose of 30 W·h/liter

| Diluent | G, molecules/100 eV | | | | $K_p$ Zr |
|---|---|---|---|---|---|
| | $RNO_2$ | RONO | $RONO_2$ | $RCOO^-$ | |
| Sample 1 | 0,98 | 1,57 | 0,13 | 0,27 | 0,5 |
| Sample 2 | 0,50 | 0,78 | 0,08 | 0,40 | 0,3 |
| Sample 3 | 0,20 | 0,15 | 0,02 | 0,05 | 0,04 |
| n-Dodecane | 0,2 | 0,1 | — | 0,07 | 0,06 |

of nitrating products of the hydrocarbon mixture used increase as the additive concentration increases. The content of olefins and alcohols in aliphatic diluents evidently should not exceed the values indicated for sample 3, which approaches that of n-dodecane with respect to its radiative-chemical stability.

## CONCLUSIONS

The length of the n-alkane chain which provides a basis for the diluent can lie within the interval $C_{11}$-$C_{15}$. Within this interval, the ratio of the separate n-alkanes in the diluent can be regulated. It is better, however, to use the hydrocarbons $C_{11}$-$C_{15}$; their rather high flash point gives them a slight edge over the higher members of the group in regard to their compatibility with the extracting solvates of the actinide nitrates and also with regard to their hydrodynamic characteristics. The content of aliphatic acids and alcohols $\leq 0.01$ M; of unsaturated compounds $\leq 0.005$ M; of aromatic hydrocarbons 1 vol.%. These requirements may change in the future as more investigations are made and a deeper study is made of the factors which affect the behavior of the diluent in the extractive cycle.

## LITERATURE CITED


1. I. D. Morokhov (editor), Nuclear Science and Technology in the USSR [in Russian], Atomizdat, Moscow (1977), p. 153.
2. V. B. Shevchenko et al., Fourth Geneva Conference (1977), Report of the USSR No. 435.
3. V. V. Fomin et al., At. Energ., 43, No. 6, 481 (1977).
4. J. Souteron et al., in: Proc. Intern. Conf. on Nuclear Power and Its Fuel Cycle. Salzburg, May 2-13, 1977, IAEA-CN-36/567.
5. R. Allardice et al., ibid., IAEA-CN-36/66.
6. K. Hasimoto et al., ibid., IAEA-CN-36/167.
7. W. Schüller et al., ibid., IAEA-CN-36/571.
8. G. F. Egorov and V. A. Medvedovskii, Khim. Vys. Energ., 5, 78 (1971).
9. V. V. Fomin, Extraction Kinetics [in Russian], Atomizdat, Moscow (1978).
10. A. M. Rozen (editor), A Handbook of Extraction [in Russian], Vol. 1; Z. I. Nikolotova and N. A. Kartasheva, Extraction by Means of Neutral Organic Compounds [in Russian], Atomizdat, Moscow (1976).
11. F. Krause and W. Lange, J. Phys. Chem., 69, 3171 (1966).
12. J. Siekiersky, J. Inorg. Nucl. Chem., 16, 205 (1962).
13. J. Hildebrand and R. Scott, Regular Solutions, New York (1950).
14. L. Burger, Nucl. Sci. Eng., 16, 428 (1963).
15. R. Hoiroyd, in: Aspects of Hydrocarbon Radiolysis. L., Academic Press, New York (1968), p. 14.
16. V. S. Shmidt, V. N. Shesterikov, and É. A. Mezhov, Usp. Khim., 36, 2167 (1967).
17. C. Black, W. Davis, and J. Schmitt, Nucl. Sci. Eng., 17, 626 (1963).
18. Reactor Fuel Proc., Vol. 4, No. 4 (1961).
19. V. A. Medvedovskii et al., in: Proceedings of the Third COMECON Symposium on Spent Fuel Reprocessing (Vol. 2), Czechoslovak Socialist Republic Atomic Energy Commission, Prague (1974), p. 302.

# POSSIBLE CORE DESIGNS FOR THE VG-400 NUCLEAR POWER PLANT

E. V. Komarov, F. V. Laptev,
A. G. Lyubivyi, F. M. Mitenkov,
O. B. Samoilov, and Yu. B. Sukhachevskii

UDC 621.039.524.2.034.3

Research in high-temperature nuclear power is designed to provide high-potential heat for various industrial purposes, including the large-scale manufacture of hydrogen, which can be used in metallurgy for the direct reduction of iron, in the chemical industry for the synthesis of hydrocarbon fuels, and also directly in engines [1, 2]. It is economically desirable to combine the production of high-potential heat with that of electrical energy [3].

Various complicated problems have to be solved in the routine production of such heat from high-temperature gas-cooled reactors (type VTGR), particularly in the production, transportation, and the use of heat at very high temperatures, which may involve helium technology, new forms of equipment, and new materials. An important step in this area is the creation of the VG-400 prototype system, as experience with this will be used in constructing commercial systems.

The VG-400 (Fig. 1) is intended to provide high-potential heat for the production of hydrogen, as well as for the production of electricity in a steam-turbine cycle. The basic characteristics are as follows:

| | |
|---|---|
| Reactor power, MW | |
| thermal | 1100 |
| electrical | 300 |
| Hydrogen output, normal $m^3/h$ | $1 \cdot 10^5$ |
| Helium pressure, $kgf/cm^2$ | 50 |
| Helium temperature, °C | |
| at outlet from reactor | 950(750) |
| at inlet to reactor | 350 |
| Number of loops | 4 |
| Steam pressure, $kgf/cm^2$ | 175 |
| Steam temperature, °C | 535 |
| Diameter and height of core, m | 6.4 and 4 |
| Number of spherical fuel elements | $8.5 \cdot 10^5$ |
| The mean time for passage of fuel elements through core, years | 3-4 |
| Standard fuel-element sizes, mm | |
| sphere (diameter) | 60 |
| six-faced prism | |
| distance between lateral bases | 400 |
| height | 840 |

In the reactor unit, the first-loop coolant circulates through four loops, which pass in turn through the core, the high-temperature heat exchanger, where some of the heat is given up to an intermediate helium loop, and the steam generator. The high-temperature heat exchanger and the steam generator work in countercurrent mode, while the steam superheater works in direct-flow.

The system with the coolant working at 950°C involves the development of new heat-resistant materials, which will delay the construction; therefore, the general scheme, the layout, and the design of the equipment have been defined for implementation in stages, with appropriate upgrading and operation.

Translated from Atomnaya Énergiya, Vol. 47, No. 2, pp. 79-83, August, 1979. Original article submitted June 20, 1978.

0038-531X/79/4702-0597$07.50 

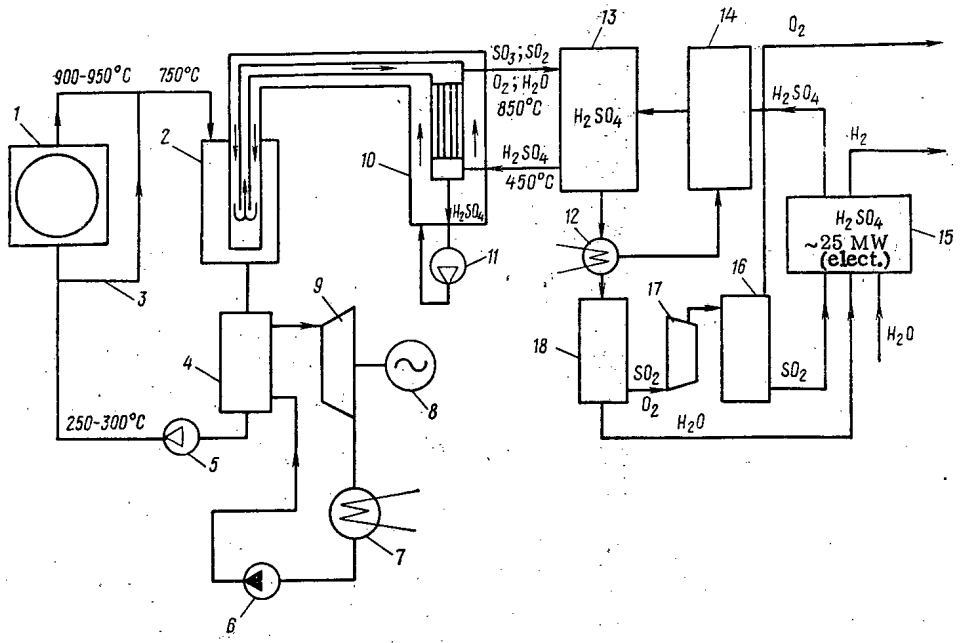


Fig. 1. General scheme of the VG-400: 1) reactor; 2) high-temperature intermediate exchanger; 3) bypass; 4) steam generator; 5) main blower; 6) feed pump; 7) condenser; 8) generator; 9) turbine; 10) thermalizer; 11) gas blower; 12) steam separator; 13) evaporator; 14) intermediate vessel; 15) electrolyzer; 16) separator; 17) compressor; 18) drum separator.

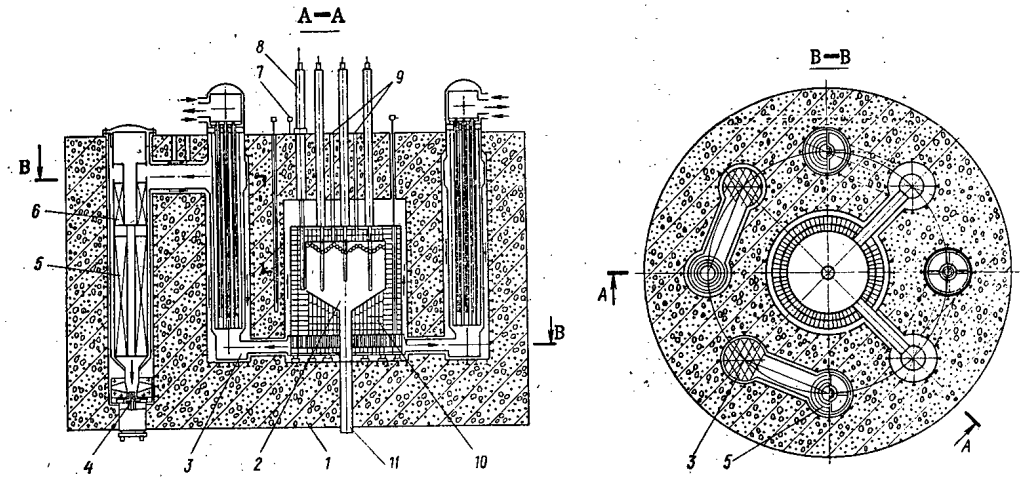


Fig. 2. The VG-400 reactor with spherical fuel elements: 1) pressure vessel; 2) core; 3) heat exchanger; 4) gas blower; 5) steam generator; 6) intermediate steam superheater; 7) ionization-chamber support; 8) control and safety rod effector mechanism; 9) charging holes; 10) graphite reflector; 11) discharge channel.

In the first stage, the system can be operated to produce only electrical power with the coolant at the exit from the reactor at 750°C, which is passed directly to the steam generator via bypass devices that replace the high-temperature heat exchangers. The design of these bypass devices allows the system to be operated without the intermediate sections for use with the core at an elevated temperature.

It is envisaged that the production of hydrogen and other substances will take place in the second stage when experience has been accumulated with the reactor equipment.

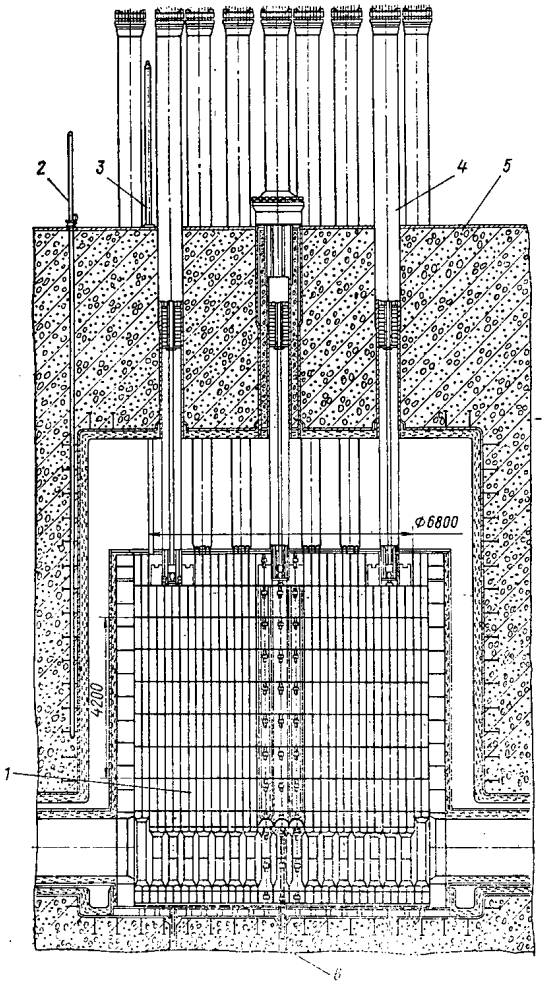


Fig. 3. The VG-400 with prismatic fuel elements: 1) core; 2 and 3) start-up and working ionization chambers; 4) control and safety rods; 5) pressure vessel; 6) thermocouple.

The reactor unit in the VG-400 has the first loop enclosed in a prestressed reinforced-concrete body. The core, the high-temperature heat exchanger, the steam generator, and the gas blowers are placed in particular parts of the body, which are linked by horizontal pipes (Fig. 2). Thermal insulation is also fitted to the inside of the pressure vessel. The use of a concrete vessel and integrated enclosure of the main equipment improves the reliability and safety, while also giving means of evaluating future assemblies for the VTGR high-power reactors. The main circulation pumps are designed to cool the system on total pressure loss and disconnection of the external electrical supplies.

A solid moderator of interchangeable type is used, which requires the movement of considerable bodies of graphite in the core. This operation has to be performed in the absence of a common removable cover in the reinforced-concrete pressure vessel, while the first loop has to remain sealed, which has imposed some specific design features on the reactor and charging unit.

The reactor is used as a source of high-potential technological heat, so the core must heat the coolant to 950°C while maintaining the fuel at the minimum temperature. The fuel cycle must be reasonably economical and the system generally must meet rigid specifications for reliability and repairability, while the fuel should be exchangeable in a minimum time or while the reactor is running. Also, the main requirements imposed on the design of the core must be formulated on the basis that the unit will be employed in devices of high unit power. These specifications define the choice of fuel-element units, the schemes for the coolant distribution, the mode of energy distribution, and the techniques for fuel recharge.

Two types of core are currently used in high-temperature gas-cooled reactors: with prismatic and spherical fuel elements [4]. Both of these have been considered for the core of the VG-400.

The core may be formed by columns of hexagonal graphite blocks containing holes for the ring fuel elements (Fig. 3). The height of a block is 840 mm, distance between faces 400 mm. Seven columns of such blocks form a modular group, which contains a central column under the control and safety rods, which is surrounded by six columns containing the fuel blocks. The end reflector and the first lateral reflector are formed by graphite blocks of analogous dimensions, while the second lateral reflector consists of stationary blocks of interlocking shape.

The physical parameters of the core are optimized along with the scope for recharging by the use of four recharge cycles during a single running cycle. In each recharge cycle one quarter of the fuel modules will be replaced. In that case, fuel blocks differing in age will be present together in the core, and these will differ in power output, so it is necessary to adjust the coolant flow rate by a regulator installed on each module.

The attainment of very high helium temperatures (950°C) subject to restrictions on the fuel temperature means that the energy distribution in the core must be appropriate. Four subzones are therefore used in the block core (two in height and two in radius), which differ in $^{235}U$ content.

A block zone is reloaded by remote control with the reactor shut down by means of an unloading–reloading machine, which involves the following operation: removal of the control and safety rod mechanisms, installation of the recharge machine, insertion of the grip into the cavity in the body, adjustment in radius, azimuth, and height on the appropriate block, extraction of the latter, transfer of the block to a container, gripping a fresh block, and setting in the appropriate position in the inverse order.

The core may be formed by free packing of spherical elements of diameter 60 mm into the cylindrical cavity bounded by the lateral and end graphite reflectors (Fig. 2). The fuel elements are loaded along tubes into the upper part of the core and moved within the core under gravity and are unloaded via an unloading hole in the lower graphite reflector. The reloading is provided by the unloading-recharge unit with the reactor working. Power control and emergency shutdown are provided by fitting rods into the spherical core; the first group of rods lies in channels in the lateral reflector, while the second is inserted directly into the spherical filling.

The reactor operates on the principle of single passage of the fuel elements through the core, where the fresh elements in the upper part of the core are in the relatively cold coolant in the area of maximum heat production, which provides favorable conditions for reducing the fuel temperature. The radial distribution of the coolant flow is difficult to manage in that case, and this means that the equalization of the radial energy production is very important. A two-zone distribution of the $^{235}U$ enrichment is employed [5]. However, it is preferable to equalize the energy distribution by controlling the speeds of movement of the fuel elements, which can be provided by the case of several unloading holes or other design measures [6].

The temperatures required by the prototype system can be provided in zones with spherical or block fuel elements; a specified helium exit temperature of 950°C can be realized for a given fuel temperature in either case. However, the precise engineering facilities required may differ substantially. In the case of a prismatic core, the system for controlling the distribution of the coolant over the modules is complicated and of inadequate reliability, while the use of four different forms of heat-producing assembly makes for additional difficulties in manufacturing the blocks and operating the equipment. Separate facilities can be used to control the energy distribution in a spherical core, although there is no doubt that considerable volume of experimental work will be required to provide a final definition of the mechanics of the fuel and the gasdynamics within the core. The thermal features of the core arising from the use of the single-pass principle indicate that there is still considerable scope for raising the temperature, which is particularly important if such reactors are to be used in metallurgy and chemistry.

The working parameters of the core will be determined to considerable extent by the details of the recharging mechanism, which must work reliably. A spherical core has certain advantages here, since this can be reloaded with the reactor working without any modification to the equipment, while the mechanisms for reloading spherical fuel elements are simpler in design and perform only standard operations, and the corresponding control system is simpler than the unloading and charging machine required for a prismatic core, where the components are of large dimensions and mass and many different operations have to be performed. There is a major disadvantage of the reloading system for a spherical core arising from the very restricted access for repair while the reactor is working, but this can be partly overcome by using backup sections for the major loading and unloading segments.

In the case of a prismatic core, control and safety rod mechanisms of traditional design can be used, similar to those in the BN-350 reactors. The control and safety absorbing rods then lie in special channels within the columns. Similar mechanisms can also be used with a spherical core if tubes are fitted to hold the control rods. However, the physical characteristics of the reactor are rather adversely affected if the tubes are placed within the spherical filling. A new design of control-rod mechanism is therefore required for a spherical core, in which the rods can be inserted directly into the filling.

In both forms of core, the reflector is formed by graphite blocks, which are subject to rigid specifications for strength and size stability. The working conditions of graphite in a high-temperature reactor are more severe than those in reactors of other types. The temperatures of the graphite blocks rise to about 1000°C and the blocks are exposed to a fluence of about $10^{22}$ neutrons/cm$^2$ during the complete period of operation. Under these conditions, the graphite blocks are subject to large internal stresses and may alter in shape considerably. It may be that graphite of existing grades cannot provide continuous operation in the reflector. In the case of the prismatic core, the inner part of the graphite reflector could be changed by means of a loading and unloading machine. No such machine is envisaged for the spherical core, while there is considerable complexity in replacing the reflector by means of special service mechanisms, and therefore the most resistant grades of graphite must be used in the reflector, which must remain in situ throughout the working life of the reactor.

An important factor in the choice of core concerns the manufacture and processing of the fuel elements; the large sizes of the elements in the prismatic case go with very severe working conditions, so careful experimental evaluation of these elements under reactor conditions is essential. However, it is impossible to perform full-scale reactor tests on such fuel elements because of the large dimensions, and therefore full viability confirmation in advance is impossible. In that respect the spherical fuel elements are undoubtedly preferable.

A spherical core has considerable possibilities, particularly with regard to further temperature rise, and it also has advantages in the creation and processing of fuel elements and the management of the graphite blocks, since simpler units and mechanisms can be used in reloading and in controlling the energy distribution, so this form is justified for the VG-400. Particular attention will then have to be given to the development of radiation-resistant grades of graphite and reliable control-rod mechanisms.

## LITERATURE CITED

1. A. P. Aleksandrov, Kommunist, No. 1, 63 (1976).
2. N. N. Ponomarev-Stepnoi et al., in: Nuclear Science and Engineering, Series Atomic-Hydrogen Power [in Russian], No. 1, Institute of Atomic Energy, Moscow (1976). p. 5.
3. F. M. Mitenkov et al., "Design features of a prototype high-temperature reactor ," in: Proceedings of the All-Union Seminar on High-Temperature Power Engineering, Moscow, April 20-22, 1977 [in Russian].
4. D. Bedenig, Gas-Cooled High-Temperature Reactors [Russian translation], Atomizdat, Moscow (1975), p. 69.
5. V. Maly, R. Schulten, and E. Teuchert, Atomwirtschaft, 4, 216 (1972).
6. G. Lohnert et al., Report IAEA-SM-200/68, Julich (1975).

# ANALYSIS OF NEUTRON YIELD PRODUCED BY HIGH-ENERGY PROTON

Y. Nakahara and H. Takahashi

Comparisons have been made between computational results obtained with the BNL code system and experimental data measured by Vasil'kov et al. for 56 × 56 × 64 cm natural and depleted uranium blocks surrounded by lead walls and primary proton energies of 400 and 660 MeV. The energetic protons from a linear accelerator are used to produce an intensive neutron source in the uranium block. The computer code system prepared at BNL to perform nuclear design analyses of linear accelerator reactors consists of six main programs: NMTC for spallation-evaporation processes above 15 MeV, HIST3D for the analysis of collision event records obtained by NMTC to get $P_3$ neutron source distribution, DLC-2 to compile 100 energy group cross sections, TAPEMAKER for format conversion, ANISN to collapse 100 group cross sections to fewer group $P_3$ cross section sets, and the principal code TWOTRAN-II which performs neutron reaction and transport calculations in the energy range below 15 MeV. Our computational method gives conservative total neutron yields, i.e., underestimates of about 16.8-29.8% in comparison with measured values depending on proton energy. Radiative capture $^{238}U(n, \gamma)$ density distributions have been compared between the calculation and experiment. The calculated distribution has the higher peak in the central part of the target system and the steeper gradient both in the r and z directions.

## 1. Introduction

Since reprocessing facilities indispensable for the conventional light water reactor to fast breeder reactor fuel cycle are now considered to increase the potential risk of nuclear weapons proliferation, evaluations have been initiated to find alternative nuclear energy systems that are not only more proliferation resistant but helpful in stretching uranium resources. A linear accelerator reactor (LAR) is one of these systems of great promise in producing fissile material in conjunction with proliferation-resistant fuel cycles.

This reactor uses a high-energy proton or deuteron beam from a linear accelerator incident on a Pb–Bi target to produce an intense neutron source. The target is surrounded by a lattice of Zr-clad rods of fertile-fissile material which is called the blanket. At the initial loading, uranium with 2% enrichment is used. The burning scheme depends on the options described below. Three options of design optimization are presented now [8]: (1) the optimization of the time-integrated production of thermal energy for conversion to power; (2) the optimization of the production rate of fissile material, without involving reprocessing; (3) the optimization of the production rate of fissile material in conjunction with reprocessing. These options correspond to the linear accelerator-driven reactor, the linear accelerator fuel regenerator, and the linear accelerator fuel producer, respectively.

The idea of using a linear accelerator to produce fissile material dates back to 1940. G. Seaborg and his group succeeded in producing tiny quantities of $^{239}Pu$ from $^{238}U$ using deuteron beams. The first practical attempts to promote the construction of accelerators to be used to generate intensive neutron sources were presented by E. O. Lawrence in the U.S.A. and N. N. Semenov in the USSR in the late 1940s. The MTA project at Livermore Radiation Laboratory, promoted by Lawrence, was abandoned in 1952, however, when high-grade ores were discovered. A Canadian team at Chalk River has always been a strong proponent of such an electronuclear facility.

Intensive theoretical works on spallation–evaporation reactions in heavy nuclei have been performed in the U.S.A. and USSR. As early as in 1948, M. L. Goldberger studied the interaction of high-energy neutrons

Brookhaven National Laboratory, Upton, New York 11973. Published in Atomnaya Énergiya, Vol. 47, No. 2, pp. 83-91, August, 1979. Original article submitted December 25, 1978.

 0038-531X/79/4702-0602$07.50 

with heavy nuclei by a Monte Carlo method under the assumption that the nucleus might be described by the statistical model [1]. From late in the 1950s to early in the 1960s, Dostrovsky et al. published a series of papers on the Monte Carlo calculations of spallation–evaporation reactions using the statistical model for degenerate Fermi gas [2-5]. The production of mesons was taken into account for the first time in the work of Metropolis et al. [6].

When a high-energy proton, neutron, or pion interacts with a nucleus, several secondary nucleons (neutrons, protons) and pions are produced. These secondary particles may have energies sufficiently high to initiate similar events with other nuclei, which develops to macroscopic cascade. Practical computer codes have been developed to follow such cascades in a heavy nucleus using the Monte Carlo method at Oak Ridge (U.S.A.), Brookhaven (U.S.A.), and Dubna (USSR). Bertini completed a medium-energy collision code using the intranuclear cascade model, which was used to calculate correlated energy-angle nucleon spectra considering the nucleus as a degenerate Fermi gas of protons and neutrons enclosed in a spherical well [7]. Chen et al. improved the method of Metropolis et al. by introducing refraction of cascade particles when going through regions of varying potential energy and considering diffuse boundaries [8]. Their Monte Carlo code is known by the name VEGAS. A similar computational method has been developed by Baraschenkov et al. [9]. The methods of Bertini and Baraschenkov et al. give good agreement with the known experimental data for the energy range above several tens of megaelectronvolts [10, 11].

Bertini's code was incorporated by Coleman to the NMTC system designed for the analysis of nucleon meson transport in a massive system [12, 13]. The NMTC code has been updated and used also at BNL and the other laboratories [14, 15].* NMTC computes the transport of nucleons and mesons up to 3.5 GeV based on the intranuclear cascade evaporation model [7] which takes into account both elastic and inelastic scattering and is also based on the 05R model [16] for the particle transport in a three-dimensional heterogeneous massive system. These processes are computed statistically by the Monte Carlo method.

In the computer code system prepared at BNL to perform nuclear design analyses of LAR's, NMTC is used to calculate all reactions down to energy 15 MeV initiated by energetic protons of energy 1 to 1.5 GeV. In the energy range below 15 MeV only the reactions induced by neutrons are calculated with the two-dimensional neutron transport theory code TWOTRAN-II [17]. The yield of neutrons produced in the spallation–evaporation process is given by the NMTC calculation; the contribution of neutron fission reactions below 15 MeV is calculated by TWOTRAN-II.

Measurements of neutron yields in uranium, lead, tin, and beryllium targets were carried out at the 3-GeV cosmotron at Brookhaven [19]. These indicate that for a uranium target the yield is about 40 neutrons/proton of energy 1 GeV and it is twice that obtained for a lead target.

Preliminary studies of the accelerator breeder concept have been performed at ANL, BNL, LASL, ORNL, and AECL (Canada). However, few experimental data have been published on neutron yields and neutron flux distributions for realistic reactor systems consisting of target, blanket, and shielding. Recently, Vasil'kov et al. published their experimental results on $56 \times 56 \times 64$ cm natural and depleted uranium blocks surrounded by lead walls for primary proton energies of 300, 400, 500, and 600 MeV [20].

The BNL computer code system for linear accelerator reactors has been applied to these Russian experimental facilities in order to estimate the accuracy and tendency of the code system. Comparisons are made in the present paper of the neutron yields, $^{238}U(n, \gamma)$ reaction density distributions, and number of fission events betweenthe measured values obtained by Vasil'kov et al. and our computational results. Discussions are also given on the differences between ours and Baraschenkov et al.'s computational models.

## II. Computational Method

The particle transport analysis part of the BNL computer code system consists of six main programs: NMTC, HIST3D [21], DLC-2 [22], TAPEMAKER [22], ANISN [23], TWOTRAN-II, and auxiliary programs: FIND [24], SURF [24], MULTSUM [25]. The overall interrelations of these programs is indicated in Fig. 1. The NMTC is used to calculate the spallation and evaporation processes above 15 MeV by the Monte Carlo method. Collision events of neutrons slowed down below 15 MeV are filed by NMTC. The collision events file is analyzed with HIST3D to get neutron distributions which are used as neutron sources for the transport calculations of neutrons in the energy range below 15 MeV. The 100 energy group DLC-2 neutron reaction cross

*Coulter improved the intranuclear code VEGAS and incorporated it into NMTC.

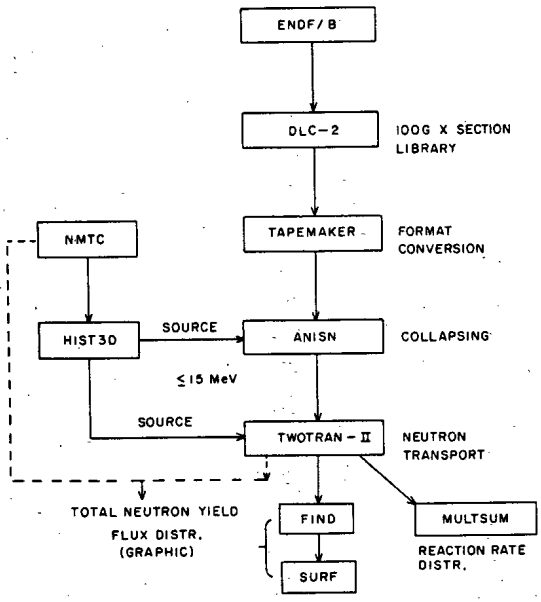


Fig. 1. Neutronics part of BNL code system for LAR'S.

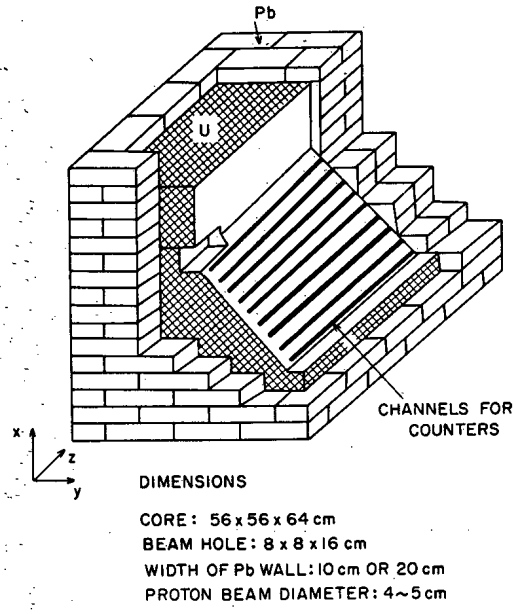


Fig. 2. Target in Russian experiments.

sections are based on ENDF/B-III [26]. The program DLC-2 is used to make a file containing cross-section data only for nuclides selected specifically. TAPEMAKER is used to convert the format of DLC-2 data to that of ANISN, i.e., FIDO format, as usually called. The DLC-2 100 group sets are collapsed to fewer energy group sets by the one-dimensional neutron transport code ANISN based on the discrete ordinate $S_n$ method. The final neutron transport calculations are performed with TWOTRAN-II, which is a two-dimensional $S_n$ method program and can take into consideration anisotropies in neutron source and scattering cross sections. MULTSUM has been programmed to calculate reaction rate distributions.

It is important to give a brief description of the nuclear models used in the NMTC and Baraschenkov et al.'s computational methods, paying attention to what are the similarities and differences between the two methods.

As for the nucleon density distribution for nucleons in a nucleus, the same three-region configuration fitted to Hofstadter's curve is used in both methods [7, 27]. The outer radius of each region is chosen by solving for r in the expression

$$\rho(r) = \alpha_i \rho(0), \quad i = 1, 2, 3, \tag{1}$$

where $\alpha = 0.9$, $\alpha_1 = 0.2$, and $\alpha_3 = 0.01$. The density in each region is set equal to the average value of the continuous distribution in that region.

Protons and neutrons are assumed to have a zero-temperature Fermi momentum distribution in each region. The momentum distribution function f(p) has the form

$$f(p) = p^2/3p_f^3(r), \tag{2}$$

where $p_f$ is the momentum of a nucleon corresponding to the Fermi energy. Depending on the particle density, the Fermi energy differs for each type of nucleon in each region. The composite momentum distribution for the entire nucleus is not a zero-temperature Fermi distribution. This assumption is employed in both methods.

The emission of particles from excited compound nucleus is treated with the statistical model due to Weisskopf. The detailed formulation was given by LeCouteur [28]. In the statistical model the level density of the residual nucleus at excitation energy E is given by the formula

$$\omega(E) = \omega_0 \exp(2\sqrt{a(E-\delta)}), \tag{3}$$

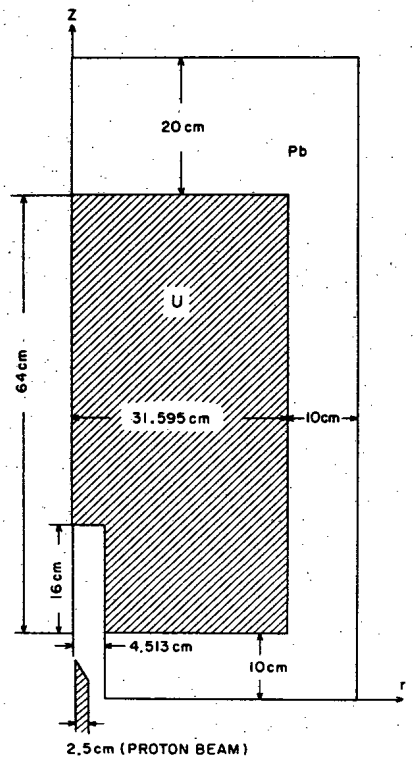


Fig. 3. Volume equivalent cylindrical target in BNL calculation.

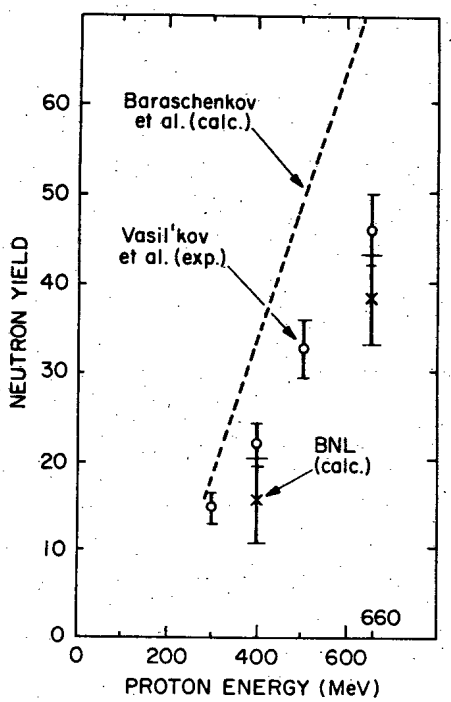


Fig. 4. Comparison of neutron yields in natural uranium target.

where $a$ and $\omega_0$ are constants for a given nucleus and $\delta$ is the pairing energy. The value of $\omega_0$ is not important, since $\omega_0$ is considered to be a slowly varying function of mass and charge number and only ratios are used in the calculation. The quantity $a$ has a significant effect on the final results. According to LeCouteur, it is given by

$$a = A/B\,[1 + Y\,(\Delta^2/A^2)], \tag{4}$$

where A = mass number, $\Delta = A - 2Z$, Z = charge number, $Y \simeq 1.5$, and $B \simeq 8$ MeV. The pairing energies $\delta$ have been tabulated by Cameron [29].

A Monte Carlo method program based on the LeCouteur formulation and a Monte Carlo scheme due to Dostrovsky et al. [3-5] was made by Dresner for calculating the evaporation of particles from excited compound nuclei [30]. The EVAP program of Dresner has been revised and updated by Guthrie [31, 32]. In the updated version nuclear mass excesses and binding energies are replaced with Mattauch et al.'s tabulation based on an atomic mass unit of 1/12 of $^{12}C$. For nuclei not tabulated by Mattauch et al. but having a mass number within ±10 of the stability valley of the periodic table, mass excesses are calculated using the semi-empirical mass formula of Cameron, which uses a set of "shell-plus-pairing" energy corrections. For these corrections for nuclides with Z or N less than 11 the values obtained by Peelle and Aebersold are used [33]. The updated version EVAP-4 has been incorporated in NMTC with the subroutine name DRES [14].

In the calculations of Baraschenkov et al. very simplified approximation is used for the level density parameter $a$. At first a constant value $a = 0.05$ MeV$^{-1}$ was recommended [34]. In their later studies of the effects of $a$ on the neutron yields for lead and uranium targets, it has been found that $a = A/10$ MeV$^{-1}$ gives the best fit to the measured values obtained with the cosmotron at BNL and the computed neutron yields are reduced by 10 to 20% from those obtained with $a = 0.05$ MeV$^{-1}$ [35].

There are some differences also in the treatments of pions $\pi^{\pm}$ and $\pi^0$ in the intranuclear cascade calculation in NMTC and Baraschenkov et al.'s method [13, 34]. The neutral pion is very unstable and for practical purposes is assumed to decay into two protons at its point of creation. As for charged pions, the $\mu$-decay of $\pi^{\pm}$ is not considered in the Baraschenkov method. Positively charged pions which come to rest as a result of ionization loss are not considered anymore. In NMTC, however, they are assumed to decay immediately into a positively charged muon and neutrino. Muon decay in flight is taken into account using the known muon life-

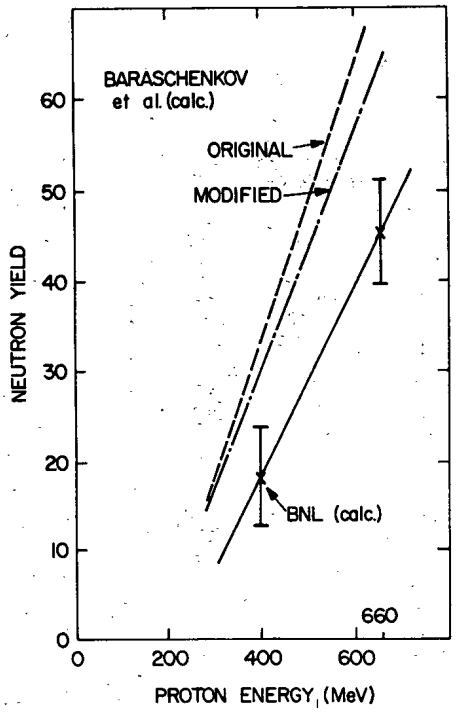


Fig. 5. Comparison of neutron yields obtained by us and Baraschenkov's calculations for effectively infinite natural uranium target.

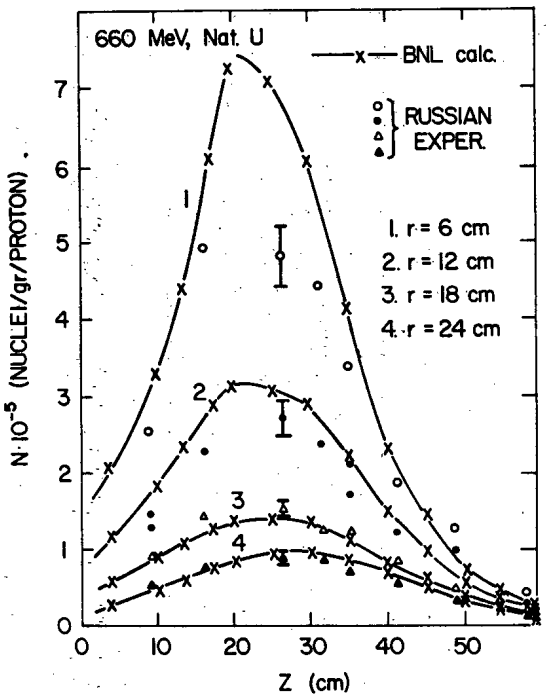


Fig. 6. $^{238}U(n, \gamma)$ reaction density distribution in natural uranium target.

time, and muons which come to rest are assumed to decay immediately. Negatively charged pions which come to rest may either decay or be captured by a nucleus, depending on the material atom density. In NMTC an option is provided as to the treatment of $\pi^-$. If decay is specified, all $\pi^-$ mesons reaching the cutoff energy are assumed to decay immediately into negatively charged muon and neutrino. If capture is specified, they are formed to undergo nuclear capture. Baraschenkov uses the capture specification only. In both methods the energy and angular distribution of the particles produced as a result of capture is obtained with the cascade-evaporation model.

The cutoff energies for proton and neutron transport in NMTC are input values. The cutoff energy for neutrons corresponds to the energy at which a transition is made from the treatment of nonelastic collisions by the internuclear-cascade evaporation model to that by the evaporation model. The most appropriate value of this cutoff is not certain, but the work of Alsmiller and Hermann gives the value ~15 MeV [36]. Incidentally, the uppermost value of the neutron energy in ENDF/B is 15 MeV. The cutoff energy is usually taken to be 15 MeV, below which the behavior of neutrons is analyzed by the neutron transport theory. Baraschenkov et al. take the cutoff energy of 10.5 MeV because they use the multigroup neutron cross section sets due to Abagian et al. [37] in the analysis of neutron transport in the energy range below the cutoff. It is not clear, however, if the cutoff energy of 10.5 MeV is not appropriate in comparison with 15 MeV and if it will result in significant effects or not.

About the computational method of neutron transport below the cutoff energy, no definite description is found in Baraschenkov et al.'s papers. In our computational method, as written in the beginning of this paper, the two-dimensional discrete ordinate $S_8$ method is used with a $P_3$ neutron source and $P_3$ scattering cross sections.

The major differences in the computational methods mentioned above are summarized in Table 1.

## III. Computational Results and Comparison with Experiments

The computer code system illustrated in Fig. 1 has been applied to Russian experimental facilities used by Vasil'kov et al. [20] in order to estimate the accuracy and tendency of the code system by making a comparison between experiments and our calculations and those of Baraschenkov et al. The reactor model em-

TABLE 1. Differences between Our Computational Methods and Baraschenkov et al.

| Methods | Ours | Baraschenkov et al. |
|---|---|---|
| Level density parameter in the statistical model | LeCouteur formulation with Cameron, and Mattauch et al. tabulation | Constant values 0.05 $MeV^{-1}$ or A/10 $MeV^{-1}$ |
| Decay of pions | $\pi^+ \rightarrow \mu^+ + \nu$ $\pi^- \rightarrow \mu^- + \nu$ or capture | Not considered $\pi^-$ capture |
| Cutoff energy for the cascade-evaporation calculation | 15 MeV | 10.5 MeV |
| Neutron cross section data below cutoff | ENDF/B-III | Abagian et al. multigroup set |
| Neutron transport below cutoff | Two-dimensional $S_n$ method with $P_3$ source and $P_3$ scattering | Monte Carlo method? |

TABLE 2. 30 Energy Group Structure

| Group | Energy range |
|---|---|
| 1 | 15.000-12.214 MeV |
| 2 | 12.214-10.000 MeV |
| 3 | 10.000-8.1873 MeV |
| 4 | 8.1873-6.7032 MeV |
| 5 | 6.7032-5.4881 MeV |
| 6 | 5.4881-2.4660 MeV |
| 7 | 2.4660-1.1080 MeV |
| 8 | 1.1080-0.49787 MeV |
| 9 | 497.87-223.71 keV |
| 10 | 223.71-111.09 keV |
| 11 | 111.09-52.475 keV |
| 12 | 52.475-24.788 keV |
| 13 | 24.788-11.709 keV |
| 14 | 11.709-7.1017 keV |
| 15 | 7.1017-4.3074 keV |
| 16 | 4.3074-2.6126 keV |
| 17 | 2.6126-1.5846 keV |
| 18 | 1.5846-0.96112 keV |
| 19 | 961.12-582.95 eV |
| 20 | 582.95-353.57 eV |
| 21 | 353.57-214.45 eV |
| 22 | 214.45-130.07 eV |
| 23 | 130.07-78.893 eV |
| 24 | 78.893-47.851 eV |
| 25 | 47.851-29.023 eV |
| 26 | 29.023-10.677 eV |
| 27 | 10.677-3.9279 eV |
| 28 | 3.9279-1.4450 eV |
| 29 | 1.4450-0.41399 eV |
| 30 | 0.41399-0.0 eV |

ployed by Baraschenkov et al. is not the same as ours, so that the comparison between the two computational methods is not exact quantitatively.

In the experiments by Vasil'kov et al. use was made of a target assembled from rectangular blocks of natural ($2 \times 4 \times 8$ cm) and depleted ($8 \times 8 \times 16$ cm) uranium. The total linear dimension of the target was $56 \times 56 \times 64$ cm covered with a lead layer having a thickness of 10 or 20 cm, as shown in Fig. 2.

The proton beam was injected into the central part of the target through the beam hole of cross section $8 \times 8$ cm and depth 16 cm from the front surface of the uranium block. The diameter of the proton beam at the entrance into the target was 4 to 5 cm.

Experiments were carried out with the extracted beam of protons having energy 660 MeV. For the experiments at proton energies 300, 400, and 500 MeV, the initial 660-MeV protons were slowed down in a polyethylene attenuator.

In the diagonal plane of the target, passing through the axis of the proton beam, a system of channels was made for the arrangement of detectors. The channels were arranged in parallel with the proton beam and located at a distance 6 to 45 cm from the axis approximately at each 3 cm. The dimension of a channel was 60 cm in length and $2 \times 0.3$ cm in cross section.

When the proton beam is absorbed in a uranium target, there is generated a source of fast neutrons with energy 1 to 100 MeV (superposition of cascade-evaporation and fission), which, being scattered by uranium nuclei, slow down to the energy range where the radiative capture of neutrons occurs.

$$^{238}\mathrm{U}\,(n,\ \gamma) \rightarrow {}^{239}\mathrm{U} \xrightarrow{\beta^-} {}^{239}\mathrm{Np} \xrightarrow{\beta^-} {}^{239}\mathrm{Pu}.$$

During the slowing down, neutrons are multiplied further in consequence of the fission of uranium nuclei.

TABLE 3. Differences between Our Computational Models and Baraschenkov et al (TWOTRAN calculation)

| | Ours | Baraschenkov et. al. |
|---|---|---|
| Geometry | Cylinder of radius = 31.595 cm, axial length = 64 cm, with lead wall of width 10 cm | Cylinder of radius = 60 cm, axial length = 90 cm, without lead wall |
| Proton source | Plane source of radius = 2.5 cm at z = 16 cm (end of beam hole) | Point source at z = 26 cm (no beam hole) |
| Cutoff energy and number of groups | 15 MeV<br>30 | 10.5 MeV<br>25 |
| Transport theory | $S_8$ with $P_3$ source<br>$P_3$ scattering | Monte Carlo method? |

TABLE 4. Analysis of Russian Experiments by the BNL Code System for LAR*

| Target | $E_p$ | F | L | N | Neutron yield |
|---|---|---|---|---|---|
| Nat. U | 660 | 0.8502 | 0.2733 | 24.28 ± 3.28 | 38.28 ± 5.17 (46 ± 4) |
| U-238 | 660 | 0.5934 | 0.2172 | 21.46 ± 3.19 | 29.53 ± 4.39 |
| Depl. U | 660 | | | | 33.55 ± 4.98 (38 ± 4) |
| Nat. U | 400 | 0.8043 | 0.2769 | 10.15 ± 3.19 | 15.51 ± 4.87 (22.1 ± 2.4) |
| Pb–Nat. U | 660 | 0.6754 | 0.2846 | 20.32 ± 2.91 | 28.26 ± 4.05 |
| Pb–U-238 | 660 | 0.4813 | 0.2350 | 19.68 ± 2.40 | 24.53 ± 3.00 |

*$E_p$ = proton beam energy (MeV). F = fission fraction normalized to one source neutron which is produced by the spallation and evaporation reaction in the energy range above 15 MeV. L = net leakage fraction from the system. N = average number of neutrons per one primary proton produced by spallation–evaporation reactions in the energy range above 15 MeV. Neutron yield = $(1 + F - L)N$. Values in parentheses are the results of Russian experiments.

TABLE 5. Number of Fission Events in Natural U Target (fissions/proton)*

| | BNL (calculated) | Russian experiment [20] |
|---|---|---|
| $n_{total}$ | 16.43 ± 2.22 | 18.5 ± 1.7 (13.7 ± 1.2) |
| $n_{235}$ | 3.38 ± 0.46 | 3.9 ± 0.4 (1.5 ± 0.1) |
| $n_{238}$ | 13.05 ± 1.76 | 14.6 ± 1.3 (12.2 ± 1.1) |

*Proton energy = 660 MeV. Values in parentheses are for depleted uranium.

The density distribution of (n, γ) capture was measured by $^{239}$Np distinguished radiochemically from the uranium sample irradiated at various points in the target. Measuring the density distribution A(z, r, θ) of the (n, γ) capture in the volume of the target and integrating this distribution, Vasil'kov et al. obtained the total number of captures ($^{239}$Pu yields) per energetic proton [20]:

$$Y = \rho \int \nu A(z, r, \theta)\, dV \tag{5}$$

(Vasil'kov et al.'s definition of neutron yield), where z is the direction of proton beam, r, θ are cylindrical coordinates, and ρ is the density of metallic uranium. Equation (5) is the definition of neutron yield per energetic proton.

The neutron yield in our calculations is defined as follows:

$$Y = [1 + (F - L)]\, N, \tag{6}$$

where N is the average number of neutrons per primary proton produced by spallation−evaporation−fission reactions in the energy range above 15 MeV, F − L is the contribution from neutron reactions in the energy range below 15 MeV per source neutron created by reactions above 15 MeV, F is the fission fraction below 15 MeV and L is net leakage from the system of neutrons below 15 MeV. On the other hand, its definition in the calculations of Baraschenkov et al. is given by,

$$Y = N_c^5 + N_c^8 + N_{esc}, \tag{7}$$

where $N_c^5$ and $N_c^8$ give the internal escape defined as the number of radiative captures of neutrons by $^{235}$U and $^{238}$U, $N_{esc}$ being the number of neutrons which escape from the block through its sides and end faces [33].

The definitions given by Eqs. (5) and (6) are consistent in that the neutron leakage fraction is not included in Y.

In our calculations the rectangular target was replaced by a volume-equivalent cylinder of metallic natural uranium with a radius of 31.595 cm and axial length of 64 cm, as shown in Fig. 3. The radius of a beam guide hole is 4.5135 cm. The proton beam radius was taken to be 2.5 cm. The atomic number densities of $^{235}$U, $^{238}$U, and Pb, in units of $10^{24}$/cm$^3$, are 0.00035148, 0.0478546, and 0.033000, respectively.

The procedure of our calculations is as follows. In the NMTC calculation, the average was taken over 10 batches of 25 protons each. Since the sampling number is small, the statistical error is somewhat large. The necessary number of samplings is not well defined.

The $P_3$ neutron source distribution was prepared for the TWOTRAN-II calculation using HIST3D. As for the anisotropy of neutron scattering, the $P_3$ approximation was employed, and 30 group cross sections sets were prepared using ANISN. The 30 energy group structure is shown in Table 2. In the TWOTRAN-II calculations the $S_8$ approximation was used. Since the $S_8-P_3-P_3-30$ group calculations by TWOTRAN are very expensive, the sufficiency of the degree of $S_n$ approximation has not been examined. These computational models are summarized in Table 3 with those of Baraschenkov et al. [34]. The target in the calculation by Baraschenkov et al. is not the same as ours. It is a cylinder with a radius of 60 cm and axial length of 90 cm without a lead wall. The proton source was assumed to be an isotropic point source at z = 26 cm from the front surface, and no beam hole is considered.

Since the entire calculation is very expensive, the calculations have been performed only for proton energies of 660 and 400 MeV. Neutron yields are summarized in Table 4 and are compared in Fig. 4 with the experimental values of Vasil'kov et al. [20] and the calculational results of Baraschenkov et al. [34]. As is clear from Fig. 4, our model gives conservative results in comparison with experiment, i.e., underestimates of about 16.8 to 29.8% in average values depending on proton energies. If we recalculate the neutron yield in the definition of Vasil'kov, we get the value $Y = 38.14 \pm 3.81$, which is smaller by 0.4% than that in our definition. This justifies the use of our definition in design calculations.

Vasil'kov et al. performed experiments also on depleted uranium targets. For the sake of comparison, calculations were performed also for the pure $^{238}U$ target, results for which are also shown in Table 4. Although the degree of depletedness is not written in Vasil'kov et al.'s paper, if we estimate it as 0.33% (number density percentage of $^{235}U$) from the data of $^{235}U$ fission events summarized in Table 5, the neutron yield for this depleted uranium can be estimated to be $33.55 \pm 4.98$, which should be compared with the experimental value $38 \pm 4$. From the values of neutron yields for natural U, depleted U, and $^{238}U$ in the case of $E_p = 660$ MeV, it is seen that the neutron yield decreases linearly in depletedness.

For a proton energy of 660 MeV, Vasil'kov et al. also measured the degree of decrease in neutron yield, replacing the uranium in the central part of the target with a lead block of the dimension $8 \times 8 \times 48$ cm [20]. The measured ratio of neutron yields for lead–uranium and uranium target was $0.48 \pm 0.2$, while our calculation gives a somewhat larger value, 0.738. The reason for this relatively large discrepancy is not yet clear. One of the reasons which can be considered is that the beam size in the experiment mightbe smaller than that in the calculation and the beam intensity may have a Gaussian distribution rather than the uniform distribution used in the calculation.

A comparison between Baraschenkov et al.'s calculations and Vasil'kov et al.'s experiments is also made in Vasil'kov et al.'s paper, but it is difficult to conclude that Baraschenkov et al.'s method gives an overestimate of neutron yield, because the target system is different.

If we neglect neutron leakage in our definition of the neutron yield, considering both our reactor system and Baraschenkov's to be effectively infinite, the comparison between the two computational methods becomes that shown in Fig. 5. The modified line for Baraschenkov's method is obtained by reducing the original value by 10%, which corresponds to the difference in the level density parameters of $a = 0.05$ MeV$^{-1}$ and $a = A/10$ MeV$^{-1}$, as was mentioned in Section II. The discrepancy in the neutron yields is still large. Although the term L in our definition is neglected, there are leaked neutrons in the energy range above 15 MeV. This high-energy neutron leakage is one of the reasons for the discrepancy.

Numbers of fission events per proton, summarized in Table 5, have been obtained by integrating the density distribution of fission events. The fission density distribution was measured with a miniature silicon surface-barrier counter covered by a uranium layer. Contributions of $^{235}U$ and $^{238}U$ were distinguished by using layers of different isotopic compositions [20]. The agreement between experiment and our calculations is quite good.

In Fig. 6 distributions of radiative capture density for $^{238}U$ are compared between our calculations and Vasil'kov et al.'s experiments [20]. The unit of distribution is the number of $^{239}Np$ nuclei per gram of uranium and per incident proton. In the central region of the target system the calculated distribution has the higher peak and steeper gradient both in the r and z directions. The agreement between calculated and measured values is quite good for curves 3 and 4. Figure 6 is, however, somewhat disconcerting. The calculated distribution is larger than the measured one, while the neutron yield obtained by integrating the distribution is smaller in the calculation. This can be interpreted as follows. The decay in the r direction is steeper in the calculated distribution than in the measured one. Since the outer region has a larger volume, the volume integral of the distribution gives the larger experimental value for the neutron yield.

What causes disagreement between theory and experiment depends on the many assumptions and approximations used in the theory and experiment. Theory is based on assumptions of nuclear structure, nuclear reactions, and their measured data. Computation brings in further approximations. When we use the code system available currently, one way of improving the calculations is to use higher-order approximations in the $S_n$ and $P_n$ treatments. In LAR, the external neutron source distribution is also important in the analysis of reactor characteristics by TWOTRAN-II. If in NMTC calculation a sufficiently large sampling number is used, the statistical fluctuations in the source distribution decreases. This would result in a better agreement of flux distribution between computation and experiment. Estimating the effects of the order of $S_n$ and $P_n$ will require tedious and costly computations.

From the comparisons presented above, it may be said that the $S_8-P_3-P_3-30$ group approximation is quite good. When much more experimental data are accumulated, more conclusive discussions will be possible.

## LITERATURE CITED


1. M. L. Goldgerger, Phys. Rev., 74, 1269 (1948).
2. I. Dostrovsky, Z. Fraenkel, and P. Rabinowitz, P/1615, Proc. Second United Nations International Conference on the Peaceful Uses of Atomic Energy, Vol. 15 (1958).
3. I. Dostrovsky, P. Rabinowitz, and R. Bivins, Phys. Rev., 111, 1659 (1958).
4. I. Dostrovsky, Z. Fraenkel, and G. Friedlander, Phys. Rev., 116, 683 (1959).
5. I. Dostrovsky, Z. Fraenkel, and L. Winsberg, Phys. Rev., 118, 781 (1960).
6. N. Metropolis, R. Bivins, M. Storm, J. H. Miller, and G. Friedlander, Phys. Rev., 110, 185 (1958).
7. H. W. Bertini, "Monte Carlo calculations on intranuclear cascades," ORNL-3383 (1963).
8. K. Chen, Z. Fraenkel, G. Friedlander, J. R. Grover, J. M. Miller, and Y. Shimamoto, Phys. Rev., 116, 949 (1968).
9. V. S. Baraschenkov, K. K. Gudima, and V. D. Toneev, "Computational scheme of intranuclear cascades," JINR R2-4065 (1968).
10. H. W. Bertini, G. D. Harp, and F. E. Betrand, Phys. Rev. C, 10, 2472 (1972).
11. V. S. Baraschenkov, A. S. Il'nov, N. M. Sobelevskii, and V. D. Toneev, Sov. Phys. Usp., 16, 31 (1973).
12. W. A. Coleman, "Thermal neutron flux generation by high energy protons," ORNL-2206 (1968).
13. W. A. Coleman, and T. W. Armstrong "The nucleon-meson transport code NMTC," ORNL-4606 (1970).
14. Radiation Shielding Information Center, ORNL, "NMTC, Monte Carlo Nucleon-Meson Transport Code System," CCC-161.
15. A. Coulter, private communication, LASL.
16. R. R. Coveyou, J. G. Sullivan, D. C. Irving, R. M. Freestone, Jr., and F. B. K. Kan, "05R, A general-purpose Monte Carlo neutron transport code," ORNL-3622 (1965).
17. K. D. Lathrop and F. W. Brinkley, "TWOTRAN-II: An interfaced, exportable version of the TWOTRAN code for two-dimensional transport," LA-4848-MS (1973).
18. Department of Nuclear Energy, Brookhaven National Laboratory.
19. J. Fraser, R. E. Green, J. W. Hilbom, L. O. D. Milton, W. A. Gibson, E. E. Gross, and A. Zucker, Phys. Can., 21, 17 (1965).
20. R. G. Vasil'kov, V. I. Gol'danskii, B. A. Pimenov, Yu. N. Potokilovskii, and L. V. Chistyakov, At. Energ., 44, 329 (1978).
21. J. F. Beerman, D. Hillman, Y. Nakahara, and H. Takahashi, in press.
22. Radiation Shielding Information Center, ORNL, "100G, 100 group neutron cross section data based on ENDF/B," DLC-2.
23. W. W. Engle, Jr., "A user's manual for ANISN. A one-dimensional discrete ordinate transport code with anisotropic scattering," K-1693 (1967), contained in CCC-82, RSIC ORNL.
24. T. Sills, private communication.
25. E. T. Balzer, Jr., and H. Takahashi, in press.
26. M. K. Drake (editor), "Data formats and procedures for the ENDF neutron cross section library," BNL-50274 (1970).
27. V. S. Baraschenkov, K. K. Gudima, F. G. Zheregi, and V. D. Toneev, "Consideration of nuclear boundary diffusivity in intranuclear cascade model," JINR-R2-6503 (1972).
28. R. J. LeCouteur, Nuclear Reactions, Vol. I, P. M. Endt and M. Demeur, eds., North Holland, Amsterdam (1958).
29. A. G. W. Cameron, Can. J. Phys., 36, 1040 (1958).
30. L. Dresner, "EVAP – A Fortran program for calculating the evaporation of various particles from excited compound nuclei," ORNL-TM-196 (1962).
31. M. P. Guthrie, "EVAP-2 and EVAP-3: Modifications of a code to calculate particle evaporation from excited compound nuclei," ORNL-4379 (1969).
32. M. P. Guthrie, "EVAP-4: Another modification of a code to calculate particle evaporation from excited compound nuclei," ORNL-TM-3119 (1970).
33. P. W. Peelle and P. M. Aebersold, "Energy parameters for light nuclides in Monte Carlo nuclear evaporation programs based on EVAP," ORNL-TM-1538 (1966).
34. V. S. Baraschenkov and V. D. Toneev, At. Energ., 35, 163 (1973).
35. V. S. Baraschenkov, V. D. Toneev, and S. E. Chigrunov, "On the calculation of electronuclear method of neutron generation," JINR-R2-7694 (1974).
36. R. G. Alsmiller, Jr., and O. W. Hermann, Nucl. Sci. Eng., 40, 254 (1970).
37. L. P. Abagian et al., Group Constants for Nuclear Reactor Calculations, Consultants Bureau, N. Y. (1974).

# CALCULATION OF THE PRESSURE CHANGE CAUSED BY SATURATED STEAM ENTERING A VESSEL

A. K. Zvonarev, V. N. Maidanik, A. P. Proshutinskii, A. G. Tolmachev, and V. K. Shanin

UDC 621.1.013.1

Our previous results [1] were concerned with the nonstationary flow of water from a pressurized vessel into a sealed vessel of volume 3.4 $m^3$ containing ceramic rings.

Calculations have been performed [2-6] on the parameters in the passage of saturated steam into a sealed vessel; however, the method used there is not applicable to the pressure variation occurring in a vessel with packing that causes additional condensation.

Here we present a method of calculating the pressure in such a drum on the basis of the uneven heating of the packing; the curves for the ring temperatures (Fig. 1) imply that the layers in the packing are heated sequentially, i.e., the air is displaced by the steam–air mixture. It is also found that the temperature distribution is almost uniform over the cross section of the packing.

The experiments indicate that the following process occurs: the steam entering the lower part of the vessel $V_0$ is instantly and uniformly mixed with the air (Fig. 2). Then the steam–air mixture passes into the ring packing, where the steam condenses.

The following assumptions were made in the mathematical description:

1) The parameters of the steam in the drum correspond to the state of saturation at the appropriate partial pressure;

2) the heating of the packing is regular (this is adequately confirmed by temperature measurements);

3) the pressure and density of the steam–air mixture are to be determined from the total of the partial pressures of the steam and air;

4) the temperature of the air in the steam–air mixture is equal to the temperature of the steam at the corresponding partial pressure.

Then the balance equations for the vapor and air take the following form:

$$\frac{dM_v}{d\tau} = G_v - \frac{dM_{1v}}{d\tau} - \frac{dM_{2v}}{d\tau}; \tag{1}$$

$$M_v = \bar{\rho}_v V_{sm}; \tag{2}$$

$$M_a = \bar{\rho}_a V_{sm}; \tag{3}$$

$$M_{1a} = \rho_a (V - V_{sm}), \tag{4}$$

where $G_v$ is the flow of the saturated vapor into the drum; $dM_{1v}/d\tau$ and $dM_{2v}/d\tau$, rates of condensation of the steam on the walls of the drum and in the packing; $M_v$, amount of vapor in the drum at time $\tau$; $V_{sm}$, volume of the steam–air mixture at time $\tau$; V, drum volume; $M_a$, mass of air in volume $V_0$; $M_{1a}$ mass of air in the rest of the drum; $\rho_a$, density of the air in that volume; and $\bar{\rho}_v$ and $\bar{\rho}_a$, partial densities of the vapor and air in the steam–air mixture.

The condensation rate $dM_{1v}/d\tau$ for the walls of the drum is given by

Translated from Atomnaya Énergiya, Vol. 47, No. 2, pp. 91-94, August, 1979. Original article submitted June 5, 1978.



0038-531X/79/4702-0614$07.50 

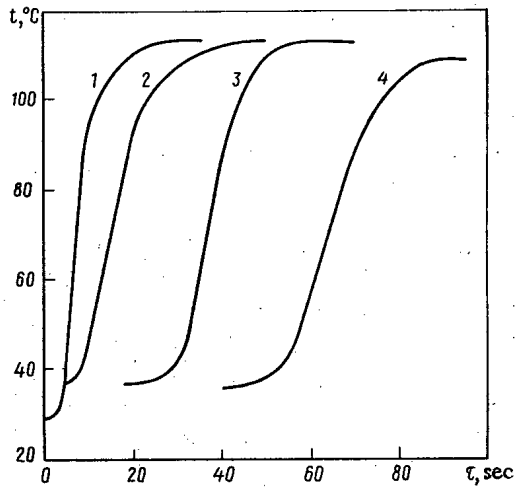


Fig. 1. Temperatures of layers of ceramic rings as functions of time: 1-4 are the numbers of the layers reckoned from the bottom.

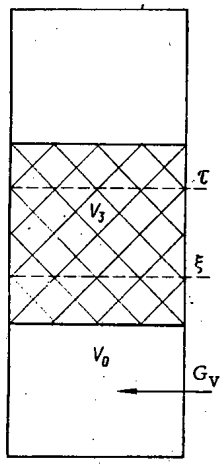


Fig. 2. Working scheme for pressure change in drum.

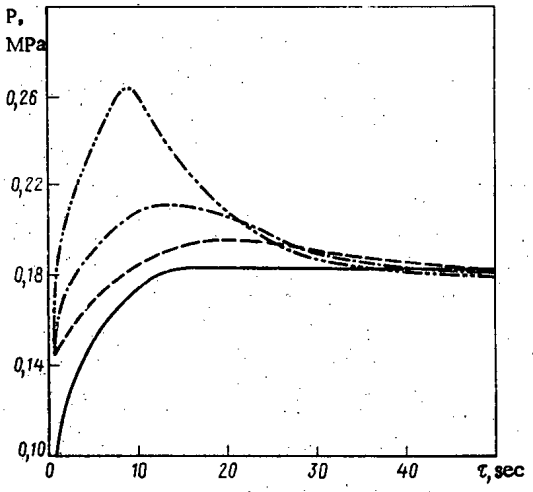


Fig. 3. Pressure variation in drum for Dy = 15 mm, $P_0$ = 12 MPa, and $T_0$ = 300°C. Upper position of pipe: solid line) from experiment, broken line) calculation for $k_2$ = 400 W/m$^2$ · deg C, dot–dash line) calculation for $k_2$ = 200 W/m$^2$ · deg C, and –•• – line) calculation for $k_2$ = 100 W/m$^2$ · deg C.

$$\frac{dM_{1V}}{d\tau} = \frac{k_1 F_1 (\bar{T}_s - T_1)}{r}, \tag{5}$$

where $k_1$ is the heat-transfer coefficient for the walls; $F_1$, area of the wall in volume $V_0$; $\bar{T}_S$, saturation temperature corresponding to the partial pressure of the vapor; r, latent heat of evaporation; and $T_1$, temperature of the inner surface of the drum wall.

This system of equations does not incorporate the change in partial pressure of the steam precisely; the heat-transfer coefficients were also taken as constant, i.e., independent of the partial pressure of steam, which is not correct. However, the experimental data are scanty, so these features were neglected.

There are also other factors such as poor contact between the insulation and the walls of the drum and swelling in the insulating material that influence $k_1$, so the value was determined by comparing the observed and calculated pressure changes. The best agreement was obtained with $k_1$ = 200 W/m$^2$ · deg C, but inexact determination of $k_1$ has only slight effects on the results.

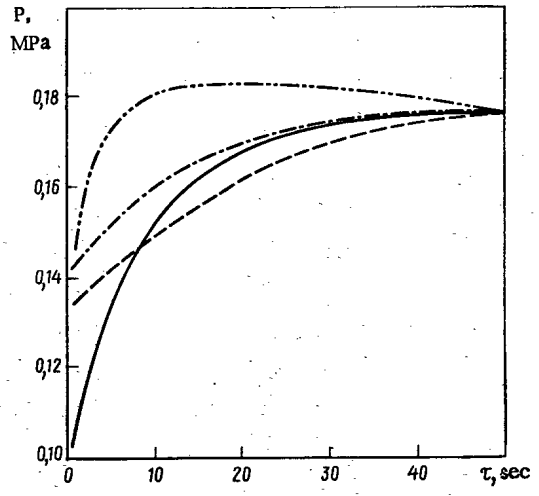


Fig. 4

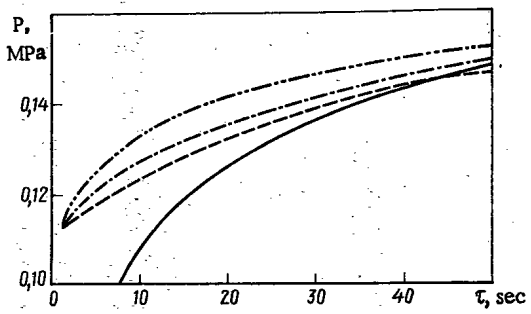


Fig. 5

Fig. 4. Pressure change in a vessel: $D_y$ = 10 mm, $P_0$ = 12 MPa, $T_0$ = 300°C. Upper position of pipe: solid line) from experiment, broken line) calculation for $k_2$ = 400 W/m$^2$ · deg C, dot–dash line) calculation for $k_2$ = 200 W/m$^2$ · deg C, and –•• – line) calculation for $k_2$ = 100 W/m$^2$ · deg C.

Fig. 5. Pressure change in vessel: $D_y$ = 6 mm, $P_0$ = 12 MPa, $T_0$ = 300°C. Upper position of pipe: solid line) from experiment, broken line) calculation for $k_2$ = 400 W/m$^2$ · deg C, dot–dash line) calculation for $k_2$ = 200 W/m$^2$ · deg C, and –•• – line) calculation for $k_2$ = 100 W/m$^2$ · deg C.

The temperature $T_1$ was determined by solving the one-dimensional nonstationary thermal conduction equation subject to the boundary conditions $\lambda_{st}(\delta T_{st}/\delta x) = k_1(\overline{T}_s - T_1)$ at the inner boundary and $\lambda_{st}(\delta T_{st}/\delta x) = 0$ at the outer one. Here we neglect the heat accumulated in the insulation, because the thickness of the latter was small by comparison with the thickness of the drum wall.

The rate of condensation on the rings $dM_{2V}/d\tau$ may be defined from the displacement of the mixture through the packing (Fig. 2). At a time $\xi$, a volume element $\Delta V(\xi)$ begins to be heated, and at the time $\tau$ the temperature rise is $T_2(\xi, \tau) - T_0$, where $T_2(\xi, \tau)$ is the temperature of the layer material at time $\tau$ for which heating started at time $\xi$, and $T_0$ is the initial temperature.

The mass of steam condensed on the packing up to time $\tau$ is

$$M_{2V} = \int_0^{V_{sm}(\tau)} \frac{c_2 m_2}{r} (T_2(\xi, \tau) - T_0)\, dV(\xi) \tag{6}$$

or on the basis that $dV(\xi) = (dV_{sm}(\xi)/d\tau)d\xi$,

$$M_{2V} = \frac{c_2 m_2}{r} \int_0^{\tau} \frac{dV_{sm}}{d\tau}(\xi)\,(T_2(\xi, \tau) - T_0)\, d\xi, \tag{7}$$

where $c_2$ is the specific heat of the packing material and $m_2$ is the mass of packing per unit free volume.

Differentiation of (7) gives

$$\frac{dM_{2V}}{d\tau} = \frac{c_2 m_2}{r} \int_0^{\tau} \frac{dV_{sm}}{d\tau}(\xi), \quad \frac{dT_2(\xi, \tau)}{d\tau}\, d\xi. \tag{8}$$

The rate of temperature change in a layer of packing in the regular state is given by

$$\frac{dT_2(\xi, \tau)}{d\tau} = \frac{k_2 F_2}{c_2 m_2}(\overline{T}_s - T_2(\xi, \tau)), \tag{9}$$

where $F_2$ is the surface area of the packing per unit volume [7] and $k_2$ is the heat-transfer coefficient for the rings.

We substitute (9) into (8) to get

$$\frac{dM_{2\mathrm{V}}}{d\tau} = \frac{c_2 m_2 k_2}{r}(A_1\bar{T}_s - A_2), \tag{10}$$

where $A_1$ and $A_2$ are intermediate integrals dependent on the upper limit $\tau$.

The differential equations for $A_1$ and $A_2$ are

$$\frac{dA_1}{d\tau} = \frac{dV_{\mathrm{sm}}}{d\tau}; \tag{11}$$

$$\frac{dA_2}{d\tau} = k_2(\bar{T}_s A_1 - A_2) + T_0\frac{dA_1}{d\tau}. \tag{12}$$

We differentiate (2)-(4) on the basis that $M_a$ and $M_{1a}$ do not vary to get

$$\frac{d\bar{P}_{\mathrm{V}}}{d\tau} = \frac{\frac{dM_{\mathrm{V}}}{d\tau}V_{\mathrm{sm}} - M_{\mathrm{V}}\frac{dV_{\mathrm{sm}}}{d\tau}}{V_{\mathrm{sm}}^2\frac{d\bar{\rho}_{\mathrm{V}}}{d\bar{P}_{\mathrm{V}}}}; \tag{13}$$

$$\frac{dV_{\mathrm{sm}}}{d\tau} = \frac{\frac{d\bar{\rho}_a}{d\bar{P}_a}\frac{d\bar{P}_a}{d\tau} + \frac{d\bar{\rho}_a}{d\bar{T}_s}\frac{dT_s}{d\bar{P}_s}\frac{d\bar{P}_{\mathrm{V}}}{d\tau}}{M_{1a}/V_{\mathrm{sm}}^2}; \tag{14}$$

$$\frac{dV_{\mathrm{sm}}}{d\tau} = \frac{M_a}{\rho_a^2}\frac{d\rho_a}{dP}\left(\frac{d\bar{P}_{\mathrm{V}}}{d\tau} + \frac{d\bar{P}_a}{d\tau}\right). \tag{15}$$

The following are expressions for the derivatives appearing in (13)-(15):

$$\frac{d\bar{\rho}_a}{d\bar{P}_a} = \frac{1}{R\bar{T}_s}, \quad \frac{d\bar{\rho}_a}{d\bar{T}_s} = -\frac{\bar{P}_a}{R\bar{T}_s^2},$$

$$\frac{d\bar{T}_s}{d\bar{P}_{\mathrm{V}}} = \frac{\bar{T}_s}{r\bar{\rho}_{\mathrm{V}}}, \quad \frac{d\rho_a}{dP} = \frac{1}{RT_0},$$

where $d\bar{\rho}_{\mathrm{V}}/d\bar{P}_{\mathrm{V}} = 0.54\cdot10^{-5}$ sec$^2$/m$^2$ is virtually constant over the pressure range involved.

System (1), (5), (10)-(15) in the unknowns $\bar{P}_{\mathrm{V}}$, $\bar{P}_a$, $V_{\mathrm{sm}}$, $A_1$, $A_2$, $M_{\mathrm{V1}}$, $M_{\mathrm{V2}}$ and $M_{\mathrm{V}}$ was solved by a fourth-order Runge–Kutta technique with automatic step size choice subject to the following initial conditions at $\tau$ = 0: $\bar{P}_{\mathrm{V}} = M_{\mathrm{V}} = M_{\mathrm{V1}} = M_{\mathrm{V2}} = A_1 = A_2 = 0$; $\bar{P}_a$ = 0.1 MPa; $V_{\mathrm{sm}} = V_0$.

Calculations were performed for an initial water temperature of 300°C in the source and pipe diameters of 6, 10, and 15 mm; Figs. 3-5 give the values for $P(\tau)$ and the measured values. To get the best agreement between theory and experiment requires some adjustment of the heat-transfer coefficients in each case, particularly when allowance is made for the delay, which is not reflected in the calculations, which were based on the assumption of regular heating and steam entering the drum and mixing instantly with the air. For example, for $D_y$ = 6 (Fig. 5) we get agreement for $k_2$ = 100 W/m$^2\cdot$deg C, while for $D_y$ = 15 the same applies for $k_2$ = 400 W/m$^2\cdot$deg C, the reason being that the steam flow rate and partial pressure increase with the diameter of the pipe, and therefore so does the heat-transfer coefficient. These values of $k_2$ agree with the observed $T_2(\tau)$ curves (Fig. 1), while special experiments are required to determine $k_2$ more precisely.

## LITERATURE CITED


1. V. N. Maidanik et al., At. Energ., 47, No. 2, 117 (1979).
2. D. Brosche, Atomkernenergie, 19, No. 1, 41 (1972).
3. D. Brosche, Ein Rechenmodell zur Berechnung von zeitlichen and örtlichen Druckverteilungen in Reaktor-Sicherheitsbehaltern. Laboratorium für Reaktorreglung und Anlagensicherung, Technische Universität München. Interner Bericht, October 1970 (to be published).
4. D. Aische, Atomkernenergie, 16, No. 2, 6 (1970).
5. M. Masarovic and B. Gaberscek, Nucl. Eng. Design, 17, No. 3, 428 (1971).
6. N. G. Rassokhin and V. S. Kuzevanov, Mosk. Eng. Inst., Issue 200, 87 (1974).
7. S. G. Gerasimov (editor), Heat Engineering Handbook, Part 2 [in Russian], Moscow–Leningrad (1957).

# METHOD OF CALCULATING THE FUNCTIONALS OF CROSS SECTIONS IN THE REGION OF FORBIDDEN RESONANCES

V. N. Koshcheev and V. V. Sinitsa

UDC 539.125.5.173.162.3

In the course of preparing constants for neutron-physical calculation of reactors and radiation shielding it is necessary to obtain various functionals of cross sections (self-shielding factors [1], transmission functions [2], etc.) under the conditions of inadequate information about the resonance structure. In these cases we usually employ the laws of statistical distributions of resonance parameters known from the theory of resonance reactions. Integration over the distributions requires a considerable expenditure of computer time; this stimulates the search for effective methods of estimating the expectation values of the functionals. In the simplest case (average cross sections) the computational difficulties are successfully overcome with generalized Gaussian quadrature formulas [3-5].

In the present paper we propose a computational scheme for estimating the expectation values of functionals of a more complex form. This scheme is based on the introduction of intermediate quantities (the moments of the cross sections) and in order to calculate them we determine the optimal parameters of the quadrature formulas of the highest algebraic degree of accuracy, i.e., optimal in relation to the considered form of the functions being integrated. The orientation of the parameters to a particular form of functional permits a substantial reduction of the number of integration points and, therefore, of the time required for estimating its mean statistical value.

Computational Scheme. The functionals of cross sections used in calculating group constants are written in the form of integrals:

$$F_x(s) = \langle \sigma_x F(\sigma, s) \rangle, \quad 0 \leqslant s < \infty. \tag{1}$$

Here $\sigma$ and $\sigma_X$ are the total and partial cross sections and $\langle \ldots \rangle$ is the averaging with respect to energy in the given energy range, which (we shall assume) contains a large number of resonances. The function $F(\sigma, s)$ determines the form of the dependence of the functional on the set of parameters. For example, $F(\sigma; \sigma_0, n) = 1/(\sigma + \sigma_c)^n$ is the dependence of the moment entering into the blocked cross section on the dilution cross section $\sigma_0$, n is the order of the moment, and $F(\sigma; t) = \exp(-\sigma t)$ is the dependence of the transmission function on the target thickness t.

We rewrite integral (1) as

$$F_x(s) = \int_{\Sigma} \int_{\Sigma_x} \sigma_x F(\sigma, s)\, p(\sigma, \sigma_x)\, d\sigma\, d\sigma_x = \int_{\Sigma} F(\sigma, s)\, \overline{\sigma_x(\sigma)}\, d\sigma, \tag{2}$$

where $p(\sigma, \sigma_X)$ is the density of the probability of occurrence of the cross sections $\sigma$ and $\sigma_X$, and $\overline{\sigma_x(\sigma)} = \int_{\Sigma_x} \sigma_x \cdot p(\sigma, \sigma_X) d\sigma_X$ is the partial cross section averaged over its distribution with a fixed value of the total cross section $\sigma$. The strong correlation of the partial cross sections, considered as a function of the energy, allows us to construct quadrature formulas for calculating the integrals (2) with points $\sigma_i$, which do not depend on the cross section type x:

$$F_x(s) = \sum_{i=1}^{N} a_i \sigma_{xi} F(\sigma_i, s). \tag{3}$$

We shall assume that cross sections due to various systems of levels of compound nuclei and characterized by particular spin and parity values have independent distributions. Then the parameters of Eq. (3) are expressed in terms of the partial parameters $a_i^{(\nu)}$, $\sigma_{xi}^{(\nu)}$, and $\sigma_i^{(\nu)}$ as follows:

Translated from Atomnaya Énergiya, Vol. 47, No. 2, pp. 94-97, August, 1979. Original article submitted April 24, 1978; revision submitted December 12, 1978.



0038-531X/79/4702-0618$07.50 

TABLE 1. Parameters of Quadrature Formulas

| No. of degrees of freedom, $\mu$ | Optimization parameters | Values of weights $a_i$ | Values of nodes $x_i$ |
|---|---|---|---|
| 1 | N = 6 | 0,0128158 | 9,178614 |
| | L = −7 | 0,2332768 | 2,783797 |
| | b = 0,0316 | 0,4187374 | 0,515245 |
| | | 0,1841195 | 0,084986 |
| | | 0,0884417 | 0,016758 |
| | | 0,0626087 | 0,001457 |
| 2 | N = 3 | 0,1971605 | 2,962740 |
| | L = −3 | 0,5973445 | 0,670028 |
| | b = 0,219 | 0,2054950 | 0,076045 |
| 3 | N = 3 | 0,1927823 | 2,595186 |
| | L = −3 | 0,6148377 | 0,770199 |
| | b = 0,316 | 0,1923800 | 0,135911 |
| 4 | N = 2 | 0,3739952 | 1,914831 |
| | L = −1 | 0,6260048 | 0,453451 |
| | b = 0,380 | | |
| 5 | N = 2 | 0,3854720 | 1,798554 |
| | L = −1 | 0,6145280 | 0,499095 |
| | b = 0,422 | | |

$$a_i = \prod_{\nu} a_i^{(\nu)}; \quad \sigma_{xi} = \sum_{\nu} \sigma_{xi}^{(\nu)}; \quad \sigma_i = \sum_{x} \sigma_{xi}. \tag{4}$$

The latter can be found from a system of equations of the form

$$\langle \sigma_x^{(\nu)} \sigma^{(\nu)n} \rangle = \sum_{i=1} a_i^{(\nu)} \sigma_{xi}^{(\nu)} \sigma_i^{(\nu)n}, \quad n = 0, \pm 1, \ldots \tag{5}$$

by the method described in [6].

In the region of forbidden resonances the left-hand sides of Eqs. (5) cannot be calculated exactly. It is natural to replace them with the expectation values obtained by averaging over the distribution p(Π) of the resonance parameters Π. Omitting the superscript $\nu$, we get

$$\overline{\langle \sigma_x \sigma^n \rangle} \equiv \int \langle \sigma_x (\Pi) \sigma^n (\Pi) \rangle p (\Pi) d\Pi. \tag{6}$$

Fluctuation Factors for Moments of Cross Sections. We define the fluctuational factor C for the moments of cross sections (6) in terms of the relation

$$\overline{\langle \sigma_x \sigma^n \rangle} = C \langle \sigma_x (\overline{\Pi}) \sigma^n (\overline{\Pi}) \rangle. \tag{7}$$

The second factor can be calculated from the exact formula obtained with any formalism, for identical equidistant resonances with account for the effects of interlevel interference and Doppler broadening [7]. Since the factor C is the ratio of the close functionals of the cross sections, it is reasonable to estimate it in the simpler approximation of the one-level Breit–Wigner formula for zero temperature. In this approximation for the moments of the cross sections entering into the fluctuation factor C, we get

$$\langle \sigma_x \sigma^n \rangle = \pi n! \frac{\sigma_m \sigma_p^n}{\overline{D}} \sum_{k=0}^{n} A_k \{\Gamma_x (\Gamma_n/\Gamma)^{k+1}\};$$

$$\langle \sigma_x / \sigma^{n+1} \rangle = \pi 2^n \frac{\sigma_m}{\overline{D} \sigma_p^{n+1}} \sum_{k=0}^{n} \sum_{i=0}^{k} B_{i,k} \left\{ \Gamma_x \frac{(\Gamma_n/\Gamma)^{2k-2i+1}}{|(\mathrm{tg}^2 \varphi + \Gamma_n/\Gamma)(1 - \Gamma_n/\Gamma)|^{n-i+1/2}} \right\}, \tag{8}$$

where $\Gamma$ and $\Gamma_x$ are the total and partial widths, respectively; $\Gamma_n$, neutron width; $\overline{D}$, mean distance between neighboring resonances; and the coefficients $A_k$ and $B_{i,k}$ depend only on the scattering phase $\varphi$:

$$A_k = \frac{1}{k!\,(n-k)!} \sum_{i=0}^{E(k/2)} \left\{ \frac{(2k-2i-1)!!}{i!\,(k-2i)!\,2^{k-i+1}} \times (1 + \mathrm{tg}^2 \varphi)^{k-2i} (\mathrm{tg}^2 \varphi^{i-k} \right\};$$

$$B_{i,k} = \frac{(2k-1)!!}{(n-k)!} 2^{n-i-1} \frac{(2n-2i-1)!!}{i!\,(2k-2i)!} (\mathrm{tg}^2 \varphi)^{n-k+1/2}; \tag{9}$$

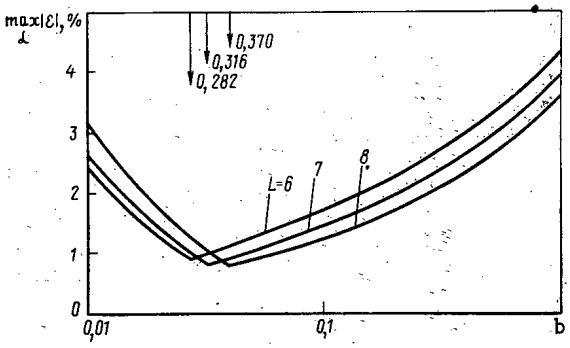


Fig. 1. Dependence of maximum error of approximation of fluctuational factor $(1+\alpha)\cdot\overline{[x/(x+\alpha)]}$ on values of optimization parameters b and L for $\mu = 1$ and N = 6.

here, $\sigma_m = 4\pi\lambda^2 g$ is the theoretical maximum cross section and $\sigma_p = \sigma_m \sin^2\varphi$ is the potential scattering cross section.

Formulas (8) and (9) are easily generalized to the case of cross-section moments of the form $\langle\sigma_x(\sigma+\sigma_0)^n\rangle$, $n = 0, \pm1, \ldots$

Parameters of the Quadrature Formulas. Let us consider the expressions in braces in Eqs. (8). These expressions contain the independent random variables $\Gamma_x$ and should be integrated over their distributions. Note that the fluctuation factor of the expressions under consideration for a separate random variable is of the form

$$C(\alpha,\ \beta) = [(1+\alpha)(1+\beta)]^{m/2} \times \int \frac{x^k p(x)}{[(x+\alpha)(x+\beta)]^{m/2}}\,dx; \quad x = \Gamma_x/\overline{\Gamma}_x. \tag{10}$$

For positive moments $\alpha = \beta$, m = 2k, k = 1, 2, ..., n+1, whereas for negative moments m = 2i+1; i = 0, 1, ..., n; k = 1, 2, ..., 2n + 1. The parameters $\alpha$ and $\beta$ depend on the random variables which do not coincide with the one separated. Since the form of Eq. (10) is invariant with respect to the choice of random variable, it is expedient to choose the parameters of the quadrature formulas for calculating the statistical integrals by the condition of a given accuracy of approximation of the fluctuation factors (10) as functions of the parameters $\alpha$ and $\beta$. The maximum error of the approximation of the fluctuation factors chosen in this way is the upper bound for the error of integration. We use the scheme of [8] to determine the parameters of the quadrature formulas of a higher algebraic degree of accuracy. Let us write the moments of distribution of the random variable x as

$$M_n(b) = \int (b+x)^n p(x)\,dx, \quad n = -L,\ -L+1,\ \ldots,\ -L+2N-1, \tag{11}$$

where N is the order of the quadrature formula and L and b are the optimization parameters [multiplicity and position of the pole introduced in the weight function p(x)]. For p(x) we take the form of the $\chi^2_\mu$ distribution ($\mu$ is the number of degrees of freedom):

$$p(x)\,dx = \frac{\mu}{2\Gamma(\mu/2)}\left(\frac{\mu x}{2}\right)^{\mu/2}\exp\left(-\frac{\mu x}{2}\right). \tag{12}$$

Then, for the moments (11) we have

$$M_n(b) = b^{n+\mu/2}\left(\frac{\mu}{2}\right)^{\mu/2}\Psi\left(\frac{\mu}{2},\ \frac{\mu}{2}+n+1;\ \frac{b\mu}{2}\right), \tag{13}$$

where $\Psi(a, b, x)$ is a degenerate hypergeometric function [9].

Table 1 gives the parameters which ensure that the error $\varepsilon$ of the calculation of the mean cross sections is not greater than 0.01. It also gives the values of the optimization parameters L and b, chosen from the con-

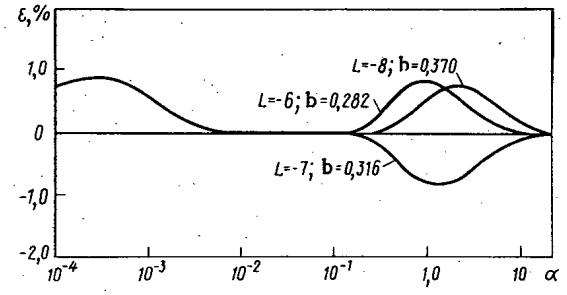


Fig. 2

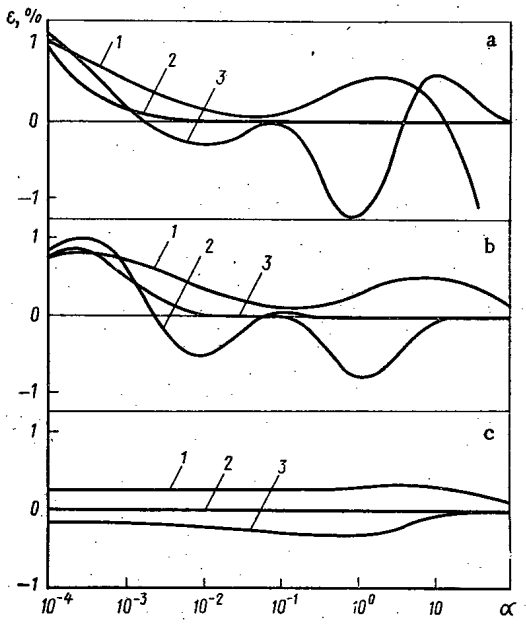


Fig. 3

Fig. 2. Error of approximation of fluctuation factor $(1+\alpha)\overline{[x/(x+\alpha)]}$ vs $\alpha$ for $\mu = 1$ and $N = 6$.

Fig. 3. Plots of approximation errors of the fluctuation factors: a) $\overline{x^2/(x+\alpha)^2}$, b) $\overline{x/(x+\alpha)}$, and c) $\overline{x/\sqrt{x+\alpha}}$ which appear in the cross-section moments $\langle\sigma_x\sigma\rangle$, $\langle\sigma_x\rangle$, $\langle\sigma_x/\sigma\rangle$ for various systems of quadrature-formula parameters: 1) equilibrium nodes [5] (N = 20); 2) Gauss–Legendre parameters [4] (N = 10); 3) present paper (N = 6).

dition of the best approximation of functions (10), for $\alpha = \beta$, m = k = 1. By changing the parameter b, we can somewhat reduce the maximum error $\max_{\alpha} |1 - f_n(\alpha)/f(\alpha)|$, distributing it uniformly along the entire curve (Fig. 1). The parameter L has a smaller effect on the maximum error $\varepsilon(\alpha)$, but it does allow the deviation to be made of alternating sign (Fig. 2) and this, generally speaking, improves the accuracy of calculation of multiple integrals.

The possibility of using the nodes obtained in order to calculate cross-section moments of higher order was examined for integrals with respect to the distribution of the neutron width in the moments of cross sections for reactions differing from the inelastic scattering reaction. The appropriate fluctuation factor $C(\alpha)$ for the random parameter $x = \Gamma_n/\overline{\Gamma_n}$ is obtained from Eq. (10) as the limit as $\beta \to \infty$. Exact values of it are calculated from the formula

$$C(\alpha) = (1+\alpha)^{m/2}\,\alpha^{k-m/2}\left(\frac{\alpha\mu}{2}\right)^{\mu/2}\frac{\Gamma(k+\mu/2)}{\Gamma(\mu/2)}\;\Psi\left(k+\frac{\mu}{2};\; k+\frac{\mu-m}{2}+1;\; \frac{\alpha\mu}{2}\right). \qquad (14)$$

Figure 3 gives the plot of approximation error $\varepsilon$ vs the parameter $\alpha$ for fluctuation factors appearing in the cross-section moment $\langle\sigma_x\,\sigma^n\rangle$, $-1 \leqslant n \leqslant 1$. It also gives the results of calculations with Gauss–Legendre parameters [4] and with parameters with equal weights [5]. With almost equal maximum errors of approximation the parameters obtained require substantially fewer nodes in the physically important range of the parameter $\alpha$.

Conclusions. The proposed scheme makes it possible to estimate the expectation values of a broad class of cross-section functionals and to find the limits of error for these estimates. The parameters obtained for the quadrature formulas are much more economical than those ordinarily used for these purposes, which is especially noticeable in the calculation of integrals of high multiplicity. The approximations used in the estimation of the fluctuation factor are valid only for determining the optimal parameters which can then be used directly in calculating cross-section moments from more stringent formulas of the theory of resonance reactions.

The authors are deeply indebted to M. V. Nikolaev and L. P. Abagyan for their useful discussion and attention to the work.

LITERATURE CITED

1. L. P. Abagyan et al., Group Constants for Nuclear Reactor Design [in Russian], Atomizdat, Moscow (1974).
2. V. F. Khoknlov et al., in: Nuclear Constants [in Russian], No. 8, Part 4, Izd. Tsentr. Nauchn. Issled. Inst. Atominform (1972), p. 154.
3. M. Beer, Nucl. Sci. Eng., 50, 171 (1973).
4. R. Hwang and H. Henyson, Trans. Am. Nucl. Soc., 22, 712 (1975).
5. L. P. Abagyan, "Methods of calculation of resonance effects in group constants for fast reactor design," Candidate's Dissertation, NIIAR, Dimitrovgrad (1971).
6. V. V. Sinitsa and M. N. Nikolaev, At. Energ., 35, No. 6, 429 (1973).
7. A. A. Luk'yanov, Moderation and Absorption of Resonance Neutrons [in Russian], Atomizdat, Moscow (1974).
8. V. I. Krylov and L. T. Shul'gina, Handbook of Numerical Integration [in Russian], Nauka, Moscow (1966).
9. G. Bateman and A. Erdelyi, Higher Transcendental Functions [Russian translation], Nauka, Moscow, Vol. 1 (1973); Vol. 2 (1974).

# PRINCIPLES OF CONSTRUCTION OF CRYSTAL COORDINATE DETECTORS FOR NUCLEAR RADIATION

B. M. Lebed' and I. I. Marchik

UDC 539.1.074.5:538.221

One of the major problems of experimental nuclear physics is that of obtaining high coordinate resolution when recording fission fragments, protons, neutrons, etc. In the present paper we expound some of the physical ideas about the possibility of realizing crystal coordinate detectors (CCD) and give experimental results.

Physical Basis. How to construct CCD is considered with the example of ferromagnets, but the procedure is equally applicable to other ferroelectrics as well.

It is well known that ferromagnets in the ground state are divided up into regions of spontaneous magnetization, i.e., domains. When a constant magnetic field exceeding a certain value is applied, a ferromagnet goes over into a state without domains, i.e., into the saturation state. This transition is a phase transition of the first kind [1].

Suppose that the ferromagnet is in a constant field H which diminishes quasistatically from values determining the saturation state to values which only slightly exceed the field $H_0$ corresponding to the onset of the formation of the domain structure. If the difference $H-H_0$ is small so that in respect of order of magnitude the energy $M|H-H_0|$ is equal to the thermal fluctuations of the spin density (magnetization), then the nuclei of the new magnetic phase (domains) will be localized in space near precisely such fluctuations. The process of nucleation can be controlled if the thermodynamic fluctuations M are suppressed by slightly increasing the difference $H-H_0$ and can be controlled by external perturbations of the spin density. The latter can be achieved in several ways, the most feasible of which seem to be processes of the interaction of nuclear radiation with a solid. A simpler method, resulting in sufficient fluctuations of the spin density, is that of local thermodynamic heating of the substance along the particle track. Such a process is characteristic of heavy, multiply charged particles of the fission-fragment type. It is known [2] that a channel in which multiply charged particles travel heats up to a temperature considerably above the temperature of magnetic phase transitions. The transverse dimension of the heating region is several thousand interatomic distances and is quite sufficient for nucleation of a new magnetic phase whose characteristic dimensions are comparable with those of the domain wall ($\leq 10^{-7}$ m).

Translated from Atomnaya Énergiya, Vol. 47, No. 2, pp. 97-100, August, 1979. Original article submitted September 1, 1978; revision submitted January 11, 1979.



0038-531X/79/4702-0622$07.50 

During motion in a solid, fast neutrons also form large-scale defects, "displacement peaks" [2], whose size is of the order of $10^2$ interatomic distances. At the moment of formation the substance in the displacement peak heats up to $10^4$ °K.*

For relativistic particles the current of a moving charged particle may be the characteristic form of perturbations of the spin system. The magnetic field produced by the current is sufficient to cause rapid spatiotemporal changes in magnetization at distances of the order of $10^{-7}$ m, and intensive excitation of spin waves should be observed in the process. The excited spin waves can be induced directly during their relaxation (spin scintillation) and are also a cause of nucleation.

The inhomogeneities observed in a magnetically ordered medium are arranged spatially along the particle trajectory, thus ensuring the possibility of its being instrumentally observed and measured.† The maximum spatial resolution in this case will be determined by the minimum size of thermodynamically stable nuclei ($10^{-7}$ m) and the means of detecting them.

The considered mechanisms of the interaction of nuclear particles with a solid do not, naturally, encompass the entire multitude of such processes, but the processes indicated are characteristic perturbations of ordered subsystems of a solid (spin and charge density, polarization) and hold out the greatest promise for the construction of nuclear radiation detectors with high coordinate resolution. The possibilities of amplifying the effect of the interaction are considered below. There are two possible ways of determining the coordinates of a particle: strictly speaking, nuclei and domains forming right along the trajectory of the particle are recorded or disturbances to the regular structure previously formed in the solid are recorded.

Experimental Investigations and Ways of Constructing CCD. Experimental results obtained when square-loop ferrites were irradiated with fast electrons were the decisive element in studies on the construction of CCD. It was found that there was a decrease in the amplitude of the signal from an undamaged unit during irradiation in an information-storage mode. In ferrites in the state of residual magnetization there are nuclei of inverse magnetization and these nuclei are pinned on lattice inhomogeneities. The spin waves excited by electrons are conducive to nucleation since the process of the formation growth of nuclei in systems in the state of residual magnetization is accompanied by a decrease in the free energy. At some integrated electron flux the nucleus grows enough for the demagnetization of the specimen to become noticeable (this is observed experimentally).

In order to assess the possibility of realizing nuclear-particle detectors on the basis of these interactions, additional model experiments were carried out on the influence of glow microdischarges in various stages, right up to breakdown. The experiments showed convincingly that chains of cylindrical magnetic domains (CMD) form along discharge channels in thin layers of single crystals of orthoferrites which are CMD carriers [13]. In addition to experiments with single-crystal media, studies were also made of the effect of discharges on artificial magnetic structures in polycrystalline materials. To this end, spatially regular transparencies were recorded by a video recorder on chromium dioxide tape. Remagnetization of the tapes was established from the variation of the recorded information. It was established that microdischarges cause the recorded image to change markedly, especially under the conditions of microbreakdowns. Subsequent rerecording of the image and examination of the tape under a microscope showed that erasure of information is not a result of mechanical damage to the film.

Experiments with $^{235}U$ fission fragments confirmed the possibility of a localized annular domain being formed as a result of a single interaction. The experimental verification was carried out on thin plates (up to 50 $\mu$m) of ferrites and thin films. A thin film of $^{235}U$, deposited on a metallic substrate, was placed on the specimens under study and the entire composition was irradiated in the channel of a VVRM reactor. After irradiation the specimens were separated from the uranium films and studied under a microscope in polarized light which allowed the domain structure before and after irradiation to be observed.

*At this temperature in optically transparent media radiation should be observed from the region of the displacement peaks. Optical radiation of the displacement peaks was observed by the authors when quartz, polystyrene, etc. were irradiated with fast neutrons. At the same time, low-energy x rays were detected. It must be pointed out that both forms of radiation can be used for the indication of neutron fluxes.

†The idea of constructing a magnetic analog of the Wilson cloud chamber was recently stated by V. I. Ozhogin in the foreword to [3]. However, the effect on which this idea is based, i.e., the effect of the particle spin on the magnetic structure, is too small for realizing a chamber.

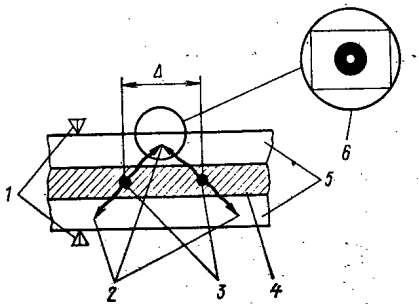


Fig. 1. Schematic diagram of neutron (proton) detector: 1) magnetic head; 2) fission-fragment tracks; 3) coordinates of neutron capture; 4) fissionable material; 5) ferrite; 6) photograph of annular domain on site of fission-fragment track.

The experiments showed that after irradiation the domain structure in separate local and extended segments (the latter being the result of several fission fragments striking close to each other) experiences considerable distortions. By visual observation under a microscope it is possible to determine regular band structures which take on a serpentine character after irradiation.

The tracks of fission fragments were most distinctly revealed in plates of orthoferrites and ferrites with rare-earth additives. With the application of a magnetic bias field (not quite sufficient for saturating the ferrite) annular domains (hollow CMD [3]) were formed after irradiation (Fig. 1). The size of the inner circle (and, therefore, the counter resolution) $\lesssim 15 \cdot 10^{-6}$ m. It may be that the empty space inside the annular CMD is due to the channel of radiation damage.

This example does not mean that orthoferrite is the most applicable material. Materials with the smallest possible size of domains and domain boundaries should be chosen. As is known, the size of a domain is proportional to the thickness of the tape and the thickness of the boundaries is inversely proportional to the area of the anisotropy. Tapes with metallic ferromagnets (e.g., cobalt) with a thickness of $0.5 \cdot 10^{-6}$ m are also promising, are easily produced, and can have considerable dimensions. Also of some interest is the possibility of using ferrites with exact compensation in which use is made of hysteretic effects in the interaction of compensated magnetic sublattices as well as domain structures in antiferromagnets.

In addition to polarized light, promise is held out by the recording of damage with magnetic video heads (MH) scanning over the image. As shown by tests, domain structures with a size of about $10^{-4}$ cm can be easily recorded by using commercially manufactured MH with a gap of $0.7 \cdot 10^{-6}$ m. If necessary, this resolution can be improved considerably.

The schematic diagram of a slow-neutron counter is shown in Fig. 1. The difference between it and the experiment described above is that two ferrite films on either side of a $^{235}U$ film are used. This is because of the need to eliminate the error which arises in determining the neutron-capture coordinate because fission fragments fly apart with spatial isotropy. The coordinates of annular domains are determined with an MH. Once the coordinates have been measured the system is put into the initial state by remagnetizing the ferrites over a whole cycle.

In order to increase the probability of nucleation of a new phase (counting efficiency) as a result of each flight of a weakly ionizing particle through a magnetic film it is necessary to amplify the effect of the interaction; this can be accomplished by additional current heating of the radiation channel or by employing a streamer mode. For this purpose the surfaces of the ferrite are metallized and a constant voltage is applied to them. The ferrite acts as a dielectric in a spark chamber [4] with the advantage that the size of the domain formed, i.e., the counter resolution, does not depend on the channel diameter but is determined only by the ferrite parameters [5]. Magnetoresistive transducers (see [3]), shunting the high-voltage circuit, can serve as clipping discharge gaps. Crystal coordinate detectors based on metallic ferromagnetic films with a semiconductor or dielectric sandwiched between them are very attractive.

Undoubtedly, in view of the intensive development of new computing techniques [3] crystalline coordinate detectors based on CMD are most promising for the future since the CMD generated by particles can be re-

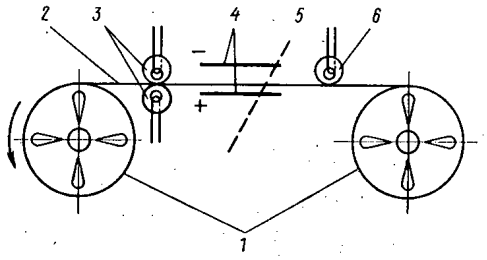


Fig. 2. Schematic diagram of charged-particle detector based on magnetic carrier: 1) reel; 2) magnetic tape; 3) magnetic reading heads; 4) electrodes; 5) particle track; 6) magnetic recording head.

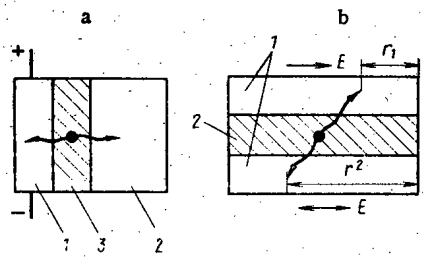


Fig. 3. a) One-coordinate neutron counter and b) diagram of detector for studying the anisotropy of fission fragments (a one-coordinate detector is realized when $E_1 = -E_2$): 1) Gunn diode; 2) fissionable material; 3) fission-fragment counter.

corded by a computer. At the present time, it would seem that more realistic for CCD is a combination of magnetic tape as the recording medium and a spark chamber which makes it possible to create a detector combining all the advantages of the spark chamber with the high coordinate resolution and in-line processing of results of the irradiation of magnetic tapes.

The schematic diagram of such a detector for charged particles is shown in Fig. 2. The transit of a particle is recorded here by coincidence circuits in the spark chamber and the coordinates of the particle at the time of its transit through the spark chamber are determined with the aid of a magnetic carrier on which, in addition to the coordinates, additional data could also be recorded at the same time. The information is read out from the carrier by magnetic video heads. In this case either a television image of the recorded scanned transparency is formed (the coordinate measurements are made from the visually detectable distortions in the transparency) or a pulsed signal is produced. In the latter case, the reading is done by two magnetic video heads, one of which is used as a reference head in a comparison circuit for eliminating the background produced by the magnetic structure recorded on the carrier.

Phase transitions in materials other than ferromagnets can also be used to create CCD. It was pointed out earlier that ferroelectrics, e.g., Gunn-effect semiconductors, are suitable for this purpose. In these materials, charge-density instabilities ("electric domains") moving through the specimen are formed at a certain value of the electric field E.

Upon reaching the edge of the crystal a domain produces an abrupt current drop which can be reproduced as a signal. The coordinates of the formation of a domain in an ideal specimen are random, although in practice inhomogeneities in E are introduced artificially in order to ensure monochromatic generation. Such an inhomogeneity can be produced by charged particles. Figure 3a gives the diagram of a one-coordinate neutron detector. With the incidence of fission fragments formed as the result of neutron capture by nuclei of the fissionable material in the Gunn diode and in any ordinary counter a pulse is formed in the diode with a delay of $\tau = r/v$, where r is the coordinate of the fission fragment and v is the velocity of the domain. The real velocity

at the present time is $10^5$ m/sec. The resolution of such a detector will be determined by the electrical circuitry (see Fig. 3b). The fields E in the Gunn diodes are connected in the same way and the spatial anisotropy, as is clear from Fig. 3, is measured from the difference of $\tau_1$ and $\tau_2$. A one-coordinate detector is realized when two diodes are counter connected. It may also prove useful to employ Gunn diodes in time-of-flight spectrometry. The generation frequencies attained at the present time are $10^{12}$ Hz, i.e., it is possible to record the formation of a domain in $10^{-12}$ sec. This means that two diodes separated by $10^{-2}$ m enable the highest possible particle velocities to be measured.

Conclusions. The physical principles for the construction of CCD considered in the present paper with the example of ferrites and semiconductors are primarily qualitative in character, although the coordinate resolution of $15 \cdot 10^{-6}$ m obtained for fission fragments in the initial stage of the experiments indicates the feasibility of constructing such detectors. The prospects for the use of such counters lies in the simplification of many experimental arrangements for nuclear-physical research as well as in new possibilities being discovered in the formulation of experiments, e.g., in neutron-diffraction analysis. By using the dependence of the cross section and scattering on the mutual orientation of the scattering vector and M it is possible with the aid of an external magnetic field in the specimen to set the direction of M so that magnetic and nuclear scattering take place with respect to one coordinate and only nuclear scattering with respect to the other. The difference in the intensity of the diffraction rings as a function of the modulus of the coordinates directly yields the magnetic neutron-diffraction pattern.

## LITERATURE CITED


1. S. V. Vonsovskii, Magnetism [in Russian], Nauka, Moscow (1971).
2. S. T. Konobeevskii, The Effect of Radiation on Materials [in Russian], Atomizdat, Moscow (1967).
3. T. H. O'Dell, Magnetic Bubbles, Halsted Press (1974).
4. A. A. Vorob'ev, N. S. Rudenko, and V. I. Smetanin, Spark Chamber Technique [in Russian], Atomizdat, Moscow (1978).
5. D. Ballock and D. Epstein, "A new technique for generating magnetic bubbles," Proc. IEEE, 59, No. 12 (1971).


# PRODUCTION OF $^{109}$Cd by IRRADIATING $^{107}$Ag WITH REACTOR NEUTRONS

A. G. Beda, A. V. Davydov, A. V. Lyakhov, and K. I. Shchekin

UDC 539.122.03

One of the radionuclides most widely used in x-ray radiometric analysis is $^{109}$Cd. Its virtues are a long half-life (452 days) [1] and a simple radiation spectrum containing strongly converted 88-keV $\gamma$ radiation of the daughter nucleus $^{109}$Ag and x rays accompanying the internal conversion process (the K lines which result from this process have energies of ~22 keV). The $^{109}$Cd isotope is employed in quantitative and qualitative analysis of: a) materials containing elements with atomic numbers from 22 to 44 (for the excitation by x rays of the K series of the elements being investigated) and b) materials containing elements with atomic numbers from 74 to 92 (for the excitation of the L series). The K series of heavy atoms can also be excited by the 88-keV $\gamma$ radiation from sufficiently intense $^{109}$Cd sources.

At the present time $^{109}$Cd is produced in the USSR exclusively by the cyclotron irradiation of silver, using the $^{109}$Ag(p, n)$^{109}$Cd or $^{109}$Ag(d, 2n)$^{109}$Cd reactions. However, the cyclotron production of $^{109}$Cd requires prolonged irradiation of silver, and this greatly limits the possibilities of the wide introduction of this nuclide into x-ray radiometric analysis. In addition, $^{109}$Cd sources made by cyclotron irradiation are very expensive and since the physical properties of these sources make them particularly suitable for x-ray radiometric analysis, any new inexpensive method for producing $^{109}$Cd sources on a broader scale is very important.

Recently it has appeared possible to produce radionuclides in a reactor having a high neutron flux (up to $2 \cdot 10^{15}$ neutrons/cm$^2$ · sec). In such a reactor $^{109}$Cd can be very efficiently produced by irradiating $^{107}$Ag, using the double neutron capture reaction $^{107}$Ag(n, $\gamma$)$^{108}$Ag → $^{108}$Cd(n, $\gamma$)$^{109}$Cd.

Translated from Atomnaya Énergiya, Vol. 47, No. 2, pp. 101-103, August, 1979. Original article submitted August 7, 1978.



0038-531X/79/4702-0626$07.50 

Estimate of the Possibilities of the Method. Natural silver is a mixture of $^{107}$Ag (51.3%) and $^{109}$Ag (48.7%). A $^{109}$Cd source of adequate activity can be produced by irradiating natural silver and subsequently separating the cadmium formed, but there are two reasons why it is undesirable to work with natural silver. The irradiation of natural silver leads to the reaction $^{109}$Ag(n, $\gamma$)$^{110}$Ag in addition to the reactions indicated above. This results in the formation of $^{110}$Ag both in the ground state with a half-life of 24 sec [2] from which it is transformed into $^{110}$Cd, and in the metastable state with a half-life of 253 days [3]. The final result of both $^{110}$Ag decay processes is the formation of an excessive amount of cadmium, which lowers the specific activity of the next product $^{109}$Cd. Here the decay from the short-lived ground state of $^{110}$Ag plays a fundamental role. For example, for neutron flux of $2 \cdot 10^{15}$ neutrons/cm$^2$ · sec and an irradiation time of ~100 days, 75% of the $^{109}$Ag is transformed into $^{110}$Cd. The decay of $^{110}$Ag from the long-lived metastable state is characterized by a high $\gamma$ constant ($K_\gamma$ = 14.25 R · cm$^2$/h [4]). In view of this it may be very difficult to ensure safe conditions in the radiochemical processing of irradiated samples. Thus the silver irradiated should be enriched in $^{107}$Ag with a minimum $^{109}$Ag content.

The accumulation of $^{109}$Cd nuclei in the irradiation of $^{107}$Ag by thermal neutrons in a reactor is determined by the following expression which neglects the capture of neutrons by $^{108}$Ag because of its short lifetime:

$$n_{109}(t) = n_{107}\frac{J\sigma_{107}\sigma_{108}}{\sigma_{107}-\sigma_{108}}\left[\frac{1}{J\sigma_{109}+\lambda_{109}-J\sigma_{108}}\left(e^{-J\sigma_{108}t}-e^{-(J\sigma_{109}+\lambda_{109})t}\right)-\frac{1}{J\sigma_{109}+\lambda_{109}-J\sigma_{107}}\right.$$
$$\left.\times\left(e^{-J\sigma_{107}t}-e^{-(J\sigma_{109}+\lambda_{109})t}\right)\right]=n_{107}\frac{10^{24}\sigma_{107}\sigma_{108}}{\sigma_{107}-\sigma_{108}}F(t)=1.28\cdot10^{-4}n_{107}F(t), \quad (1)$$

where $n_{109}(t)$ is the number of $^{109}$Cd nuclei accumulated during the irradiation time t; $n_{107}$, initial number of $^{107}$Ag nuclei; J, thermal neutron flux; $\sigma_{107}$, $\sigma_{108}$, and $\sigma_{109}$, respectively, the $^{107}$Ag, $^{108}$Cd, and $^{109}$Cd thermal neutron absorption cross sections; $\lambda_{109}$, $^{109}$Cd decay constant.

To determine the specific activity of the $^{109}$Cd formed it is necessary to consider the accumulation of other cadmium isotopes in the sample. If silver enriched more than 99% in $^{107}$Ag is irradiated, the amount of cadmium formed after the absorption of neutrons in $^{109}$Ag can be neglected, since it comprises no more than 2 to 3% of the total amount of cadmium formed in silver. Each neutron capture by $^{107}$Ag nuclei in the final analysis leads to the formation of cadmium isotopes in accord with the chain of transformations:

$$^{107}\mathrm{Ag}\,(n,\ \gamma)^{108}\mathrm{Ag}\xrightarrow{\beta^-}{}^{108}\mathrm{Cd}\,(n,\ \gamma)^{109}\mathrm{Cd}\,(n,\ \gamma)\,{}^{110}\mathrm{Cd}.$$

The total number of cadmium nuclei $n_{Cd}$ accumulated during an irradiation time t is given by the expression

$$n_{\mathrm{Cd}} = n_{107}\left[1-\exp\left(-J\sigma_{107}t\right)\right]. \quad (2)$$

From Eqs. (1) and (2) we obtain the following expression for the specific activity C of $^{109}$Cd in the cadmium fraction separated from the irradiated sample:

$$C=\frac{\lambda_{109}N_A J\sigma_{107}\sigma_{108}\left[\frac{1}{J\sigma_{109}+\lambda_{109}-J\sigma_{108}}\left(e^{-J\sigma_{108}t}-e^{-(J\sigma_{109}+\lambda_{109})t}\right)-\frac{1}{J\sigma_{109}+\lambda_{109}+J\sigma_{107}}\left(e^{-J\sigma_{107}t}-e^{-(J\sigma_{109}+\lambda_{109})t}\right)\right]}{A\left(\sigma_{107}-\sigma_{108}\right)\left(1-e^{-J\sigma_{107}t}\right)}= \quad (3)$$
$$=3.32\,f(t)\ \mathrm{Ci/g},$$

where $N_A$ is Avogadro's number and A is the average atomic mass of the cadmium isotopes formed.

If a standard ampoule with a 5-mm inside diameter completely filled with $^{107}$Ag is irradiated in the SM-2 reactor, the average effective neutron flux is ~59% of the unperturbed flux as a result of self-shielding. Figure 1 shows the functions F(t) and f(t) calculated for the following values of the constants appearing in Eqs. (1) and (2); $J_0 = 2 \cdot 10^{15}$ neutrons/cm$^2$ · sec, $J = J_{eff} = 0.59J_0$, $\sigma_{107}$ = 35 b [5], $\sigma_{108}$ = 1.24 b (average from [6, 7]), $\sigma_{109}$ = 700 b [6], $\lambda_{109} = 1.76 \cdot 10^{-8}$ [sec$^{-1}$ [1], A = 109. The coefficients $1.28 \cdot 10^{-4}$ and 3.32 in Eqs. (1) and (3) were obtained from the values listed above for quantities appearing in these equations.

Analysis of Eq. (3) shows that the maximum specific activity of 4.23 Ci/g is reached for an irradiation of ~400 days, but Fig. 1 shows that the specific activity reaches 92% of its maximum value in 100 days.

Experimental Results. To test the efficiency of the reactor method of producing $^{109}$Cd, a 26.4-mg sample of metallic silver enriched to 99.46% $^{107}$Ag and containing 0.54% $^{109}$Ag was irradiated in the SM-2 reactor in a thermal neutron flux of $2 \cdot 10^{15}$ neutrons/cm$^2$ · sec. The effective irradiation time was 25.7 days, which corresponds to the length of one reactor run. Six months after irradiation ceased, the cadmium formed in the ir-

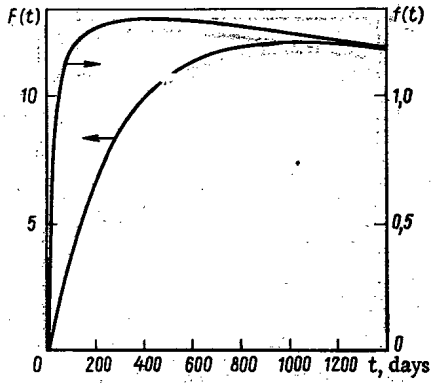


Fig. 1. F(t) and f(t) as functions of irradiation time.

radiation of the sample was separated radiochemically. The measured activities of the $^{109}$Cd separated from the irradiated sample and the $^{110}$Ag in the irradiated sample were as follows (the numbers in parentheses refer to the instant irradiation was terminated): the activity of $^{109}$Cd was 6.6 ± 0.6 mCi (8.6 mCi); the activity of $^{110}$Ag was 6.5 ±0.6 mCi (10.6 mCi); the specific activity of $^{109}$Cd was 3.0 ±0.6 Ci/g (3.9 Ci/g).

Within the limits of error these values agree with the calculations if it is kept in mind that as a result of the small amount of irradiated material the neutron flux was practically unperturbed.

The only radioactive cadmium isotope formed in the irradiated silver sample was $^{109}$Cd, and since cadmium is easily separated from silver chemically, the $^{109}$Cd source obtained in this way has a very low level of background radiation. The measurements of the background activity of the $^{109}$Cd sample separated from the irradiated silver showed that the possible admixture of $^{110}$Ag radioactivity did not exceed $10^{-6}$ of the $^{109}$Cd activity.

Conclusions. The data obtained permit a rather confident assessment of the prospects of this method of producing $^{109}$Cd for making sources for x-ray radiometric analysis. It is possible to irradiate 7.1 g of metallic silver simultaneously in a standard ampoule in the SM-2 reactor. Table 1 lists data on the number of sources which can be made from this silver as a function of the irradiation time and the source diameter. The amount of cadmium required for a source depends on the source dimensions, since the low specific activity requires an increase in the source thickness as the diameter is decreased, and this increases the absorption of 22-keV x rays in the source itself.

In the fabrication of a source there are unavoidable losses of time in delivering the irradiated material to the source manufacturer, in the technological process itself, and in delivering the sources to the user. The average time between the cessation of irradiation of the silver and the delivery of a finished source to the user is 6 months. The data in Table 1 apply to a preparation cycle of this length.

Estimates show that expenditures for fabricating one source (cost of enriched silver plus cost of irradiation) are decreased slightly for an irradiation time of more than three reactor runs, and reach a minimum for an irradiation time equal to five reactor runs. If only the above expenditures are taken into account, the cost of one $^{109}$Cd source (equivalent to a thin 10-mCi source) obtained by the reactor method is tens of times less than the current cost of a source of the same activity produced by the cyclotron method. In addition, the reactor method makes it possible to obtain $^{109}$ Cd in amounts sufficient to satisfy fully the acute demand for these sources.

It should be noted that while the radioisotopic purity of $^{109}$Cd sources obtained by the reactor method are not inferior to $^{109}$Cd sources produced by the cyclotron method, they are significantly inferior to them in specific activity. Cyclotron sources may reach a specific activity of more than 100 Ci/g, which permits the fabrication of a 1-mm-diameter source with an activity of 10 mCi.

By irradiating enriched silver in a reactor for three runs it is possible to make a source 3.4 mm in diameter which is equivalent in the yield of 22-keV radiation to a thin 10-mCi source, and for a 10-mm-diameter source the effective activity can be increased to 87 mCi, which is high enough for the excitation of the K x-ray lines of heavy elements by the 88-keV $\gamma$ radiation. In using 88-keV $\gamma$ radiation the dimensions of the sources can be decreased substantially by increasing their thickness, since the self-absorption of this radiation in the source material is small. Reactor $^{109}$Cd can be used to fabricate a wide range of sources for x-ray

TABLE 1. $^{109}$Cd Yield as a Function of Irradiation Time

| Irradiation time (No. of reactor runs) | Total yield of $^{109}$Cd radioactivity, B* (mCi) | No. of sources with a surface activity corresponding to the activity of a thin 10-mCi source | |
|---|---|---|---|
| | | diameter 6 mm | diameter 10 mm |
| 1 | 861 | 63 | 77 |
| 2 | 2220 | 179 | 206 |
| 3 | 3350 | 292 | 330 |
| 4 | 4686 | 393 | 433 |
| 5 | 5841 | 497 | 548 |
| 6 | 6770 | 573 | 637 |
| 7 | 7775 | 661 | 732 |

*$B = B_0(M/m)\,(F(t)/F_0(t))$, where $B_0 = 6.6$ mCi and m = 26.4 mg are the activity and mass of the experimental silver sample, M = 7.1 g, F(t) from Fig. 1, $F_0(t) = 1.4$ is the value of F(t) for unperturbed flux at t = 25.7 days.

radiometric analysis, including a source of annular shape. In this case the fact that the specific activity of reactor $^{109}$Cd is lower than that of cyclotron $^{109}$Cd is not a disadvantage, since such sources have a rather large area. Estimates show that the reactor method retains a number of advantages (both with respect to the total $^{109}$Cd yield and with respect to the cost of the sources made from it) when somewhat lower neutron fluxes of the order of several times $10^{14}$ neutrons/cm$^2$ · sec are used.

Thus, the investigations performed show the practical expediency and economic advantage of making reactor sources of $^{109}$Cd for x-ray radiometric analysis. It should be noted that the production of $^{109}$Cd by irradiating silver in a reactor was studied in [6], but because silver of natural isotopic composition was irradiated by a relatively low thermal neutron flux of $\sim 2.5 \cdot 10^{14}$ neutrons/cm$^2$ · sec, the results obtained did not permit conclusions about the prospects of this method of producing $^{109}$Cd.

The authors thank Yu. G. Sevast'yanov for performing the radiochemical separation of $^{109}$Cd.

## LITERATURE CITED

1. H. Leutz, K. Schneckenberger, and H. Wenninger, Nucl. Phys., 63, 263 (1965).
2. F. Boley, Phys. Rev., 94, 1078 (1958).
3. K. Geiger, Phys. Rev., 105, 1539 (1957).
4. N. G. Gusev, V. P. Mashkovich, and B. V. Verbitskii, Radioactive Isotopes as γ Radiators [in Russian], Atomizdat, Moscow (1964).
5. Nuclear Data, Part 2 [in Russian], Atomizdat, Moscow (1970), p. 6.
6. R. Lewis and F. Beitter, Isotop. Radiat. Tech., 6, No. 1, 43 (1968).
7. A. G. Beda, P. N. Kondrat'ev, and E. F. Tret'yakov, At. Energ., 16, No. 2, 145 (1964); S. Mangal and P. Gill, Nucl. Phys., 36, 542 (1962).

# CALCULATION OF RADIATION BURDEN FROM SECONDARY NEUTRONS DURING PROTON IRRADIATION OF TUMORS

V. I. Kostyuchenko, B. I. Reznik, and A. P. Shchitov

UDC 534.106:539.107.37

When sessions of radiation therapy are given with proton accelerators the dose of a single irradiation of large volumes of tumors not infrequently runs to several tens of kilorads. Dosimetry preceding such irradiations should provide information not only about the dose at the focus but also about the secondary radiation which places a radiation burden on the patient's healthy tissue outside the irradiated target. Such elements of the beam-shaping system as the preliminary and final collimators as well as the irradiated targets themselves are also secondary radiation sources.

Most critical in this respect is a single massive irradiation of patients with osteogenic sarcomas and other tumors of extremities with a beam of 155-MeV protons. Depending on the size of the tumors, such irradiation was carried out by superposing one to three areas of 7 × 9 cm each. The maximum dose was ~20 krd per area [1]. Problems of shielding against secondary radiation also arise when internal objects are irradiated by a wide beam (diameter up to 50 mm).

The purpose of the present paper is to calculate the influence of secondary particles from a total-absorption target, imitating a real irradiated object, to obtain experimental data and to compare them with calculations, as well as to compare the efficiency of various materials for local radiation protection. The choice of an optimal computational method will make it possible further on to avoid extremely laborious measurements of radiation burdens due to secondary particles, replacing this procedure with comparatively simple computations for a given irradiation geometry.

Calculation of Fluence of Secondary Fast and Ultrafast Neutrons. Secondary radiation arising in a total-absorption target comprises ultrafast, fast, intermediate, and thermal neutrons as well as $\gamma$ rays. As follows from [2], the absorbed dose behind the radiation shielding is determined by the contribution of fast and ultrafast neutrons.

In order to calculate the fluence of ultrafast neutrons, we use the scheme presented in [2]. With a view to increasing the accuracy of the calculations, we split the total-absorption target (lead block with a thickness of 5 cm) into a number of layers. We use the mean energy of protons in a layer to calculate the sought parameters.

Then, the neutron yield from the i-th layer is

$$q_i = 10^3 (L/A)\, I_i \nu_i x_i (\delta_{in})_i, \tag{1}$$

where L is Avogadro's number; A, atomic mass of the target; $I_i$, number of primary protons before the i-th layer; $\nu_i(E)$, number of neutrons per inelastic collision; $x_i$, target thickness (kg/m$^2$); and $(\delta_{in})_i (E_p)$, inelastic interaction cross section (m$^2$).

The primary proton flux is an exponential function of the target thickness:

$$I_i = I_0 \exp\{-10^3 (L/A) (\delta_{in})_i x_i\}, \tag{2}$$

where $I_0$ is the initial number of protons and $I_i$ is the number of protons before the i-th layer.

The values of $\delta_{in}$ for each layer are found from an equation given in [3]:

$$\delta_{in}(E_p) = \frac{1}{400} \exp\left\{\sum_{j=0}^{N} a_j \left(\frac{E_p}{400}\right)^j\right\}, \tag{3}$$

Translated from Atomnaya Énergiya, Vol. 47, No. 2, pp. 104-107, August, 1979. Original article submitted July 17, 1978.



0038-531X/79/4702-0630$07.50 

where N = 3-4, $a_j$ is a coefficient which depends on the target material and $E_p$ is the proton energy (MeV).

The values of $\nu_i$ in the energy range from 50 to 200 MeV were obtained by extrapolation of the data of [2] to the point with energy 20 MeV, which is the threshold energy for ultrafast neutrons, where by definition $\nu_i = 0$.

In accordance with [2], the fluence of ultrafast neutrons emitted inside a solid angle $d\Omega'$ is

$$\Phi_i = \frac{q_i}{r_i^2} \frac{\int_0^{\Omega'} f(\theta, E_p)\, d\Omega}{\int_0^{4\pi} f(\theta, F_p)\, d\Omega}. \tag{4}$$

Hence, going over from $\Omega$ to $\theta$, we get

$$\Phi_i = \frac{q_i}{r_i^2} \frac{2\pi \int_0^{\theta'} f(\theta, E_p) \sin\theta\, d\theta}{2\pi \int_0^{\pi/2} f(\theta, E_p) \sin\theta\, d\theta}, \tag{5}$$

where $r_i$ is the distance from the i-th layer to the point of detection; $\theta$, angle between the directions of the secondary and primary particles; $\theta'$, angle of detection; and $f(\theta, E_p)$, angular distribution of the secondary ultrafast neutrons, described in the range from 100 to 700 MeV by the following expression [4]:

$$f(\theta, E_p) = \begin{cases} \cos[1.05(\theta/\theta_{1/2})]; & 0 \leqslant \theta \leqslant \theta_{1/2}; \\ 1/2 \exp[-4.2(E_p/660)^{2/3}(\theta - \theta_{1/2})]; & \theta_{1/2} \leqslant \theta \leqslant \pi/2, \end{cases} \tag{6}$$

where $\theta_{1/2}$ is the half-width of the angular distribution,

$$\theta_{1/2} = \eta (660/E_p)^{2/3}, \tag{7}$$

and $\eta$ is an empirical coefficient which is equal to 0.3 for materials with $A \geq 27$ [4].

Since $f(\theta, E_p)$ is defined only for $E_p \geq 100$ MeV, the value of $\int_0^{\pi/2} f(\theta, E_p) \sin\theta\, d\theta$ for a layer with $E_{eff}$ = 50 MeV can be found by extrapolation.

We make use of the fact that for the threshold energy of 20 MeV the angular distribution of the neutrons is isotropic, i.e., $2\pi \int_0^{\pi/2} f(\theta, E_p) \sin\theta\, d\theta = 4\pi$, and we construct the curve of $F(\theta, E_p) = \int_0^{\pi/2} f(\theta) \sin\theta\, d\theta$ as a function of the energy $E_p$ (Fig. 1). From this we find that the value of this integral at the point where $E_p$ = 50 MeV is 1.23. It can further be easily shown that in the range $0 \leq \theta \leq 5°$ this integral is practically independent of the energy. The latter remark is pertinent to the comparison of the calculation presented here with the experiment which will be described below. Upon summing the values of $\Phi_i$ over all layers of the target with the appropriate $r_i$, we get the density of the current of ultrafast neutrons at the point of detection.

For fast neutrons the distribution is isotropic, i.e., inside the detection angle $\theta_i$ we have

$$\Phi_{f.n.} = (q_i/r^2)(\theta_i/\pi). \tag{8}$$

The values of $\nu_i$ for fast neutrons were obtained by extrapolation by analogy with the procedure for ultrafast neutrons. The following assumptions were made in the calculations: the neutron source was assumed to be a point source, the shielding was assumed to be unbounded, and the albedo was not taken into account. In order to assess the extent to which these assumptions affect the accuracy of the calculations, we set up two experiments.

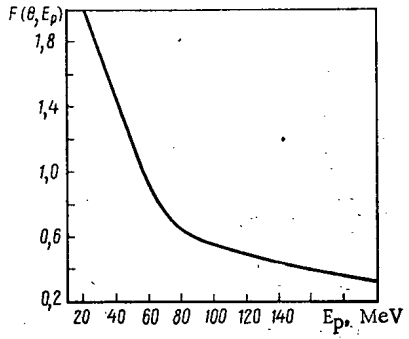


Fig. 1. Plot of $F(\theta, E_p)$ vs proton energy $E_p$.

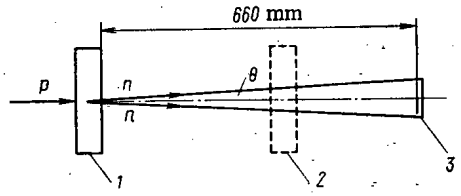


Fig. 2. Geometry of experiment with scintillation detector: 1) total-absorption target of lead; 2) block of variable-thickness radiation shielding; 3) scintillation detector.

Geometry of "Point" Source. In this experiment we verified the technique for calculating the yield of ultrafast neutrons from a total-absorption target in the geometry of a "point" source and also studied their attenuation as a function of the thickness of the radiation shielding.

The geometry of the experiment is shown in Fig. 2. The primary-proton beam of diameter 10 mm ($E_p$ = 200 MeV) impinged on a total-absorption target. A $^{12}C$ scintillation detector of diameter 70 mm and thickness 10 mm was set up on the axis of the beam at a distance of 660 mm from the target. The activity induced in the detector by secondary neutrons was established by the technique described in [5]. Radioactive $^{11}C$ formed in the $^{12}C(n, 2n)^{11}C$ reaction with a threshold energy $E_{thr}$ = 20.6 MeV has a half-life of 20.4 min. Since the cross section for this reaction for $E_n \geq 40$ MeV is assumed to be constant and equal to 21 mb [6], such a detector records the number of neutrons. The cross section of the attendant $^{12}C(\gamma, n)^{11}C$ reaction is negligible.

The number of primary protons incident on the target was recorded by an induction transducer with an error of ± 5%. The density of the flux of ultrafast neutrons, obtained as the result of the experiment (without shielding blocks), was 19.8 neutrons/cm$^2$ · sec. The error of measurement was roughly ± 15%. The value calculated for the same quantity by the technique described above with the parameters used in the experiment (r = 66 cm, $t_0$ = 68 sec, $\theta_1 = 3°$, $I_0 = 10^{10}$ protons) turned out to be equal to 18.1 neutrons/cm$^2$ · sec. The difference between the experiment and calculations < 10%.

In the same experiment we studied the shielding properties of aluminum, lead, and tungsten blocks which were successively placed on the beam axis between the target and the detector (Fig. 3). In each separate experiment the thickness and material of the radiation shielding was varied. The values of the coefficients of attenuation of ultrafast neutrons, obtained experimentally, are given in Fig. 3 (normalization to particle-flux density in absence of shielding).

It should be noted that, according to [2], the ratio of the flux density of the ultrafast and fast neutrons inside the shielding remains constant. The attenuation coefficients obtained characterize the shielding properties of the material within the limits of the entire neutron spectrum. By using the proposed computational procedure, we can get the following values of the total yield of neutrons with an energy exceeding 25 MeV for a beam of protons with an energy of 200 MeV: for $^9Be$, $^{27}Al$, $^{64}C$, and $^{207}Pb$, respectively, yields of $1.96 \cdot 10^{-1}$, $2.01 \cdot 10^{-1}$, $1.93 \cdot 10^{-1}$, and $1.62 \cdot 10^{-1}$ neutrons/proton. Thus, within the limits of 10% the total neutron yield is independent of the target material.

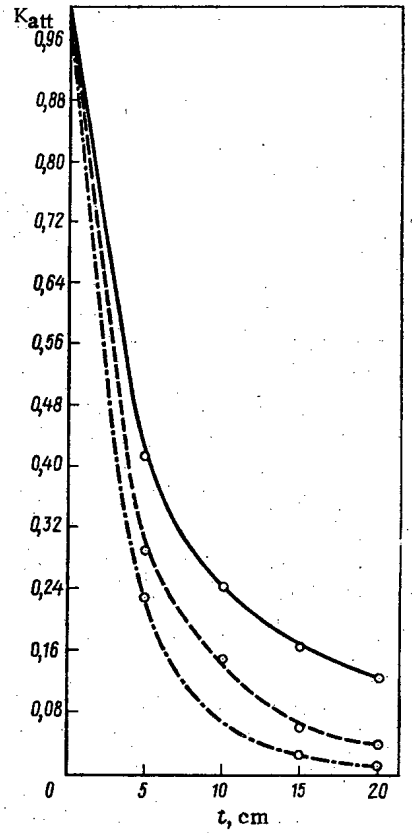


Fig. 3. Dependence of coefficient of attenuation of ultrafast neutrons on thickness of shielding of: ——) Al; – – –) Pb; and –·–·–) W [○) experiment].

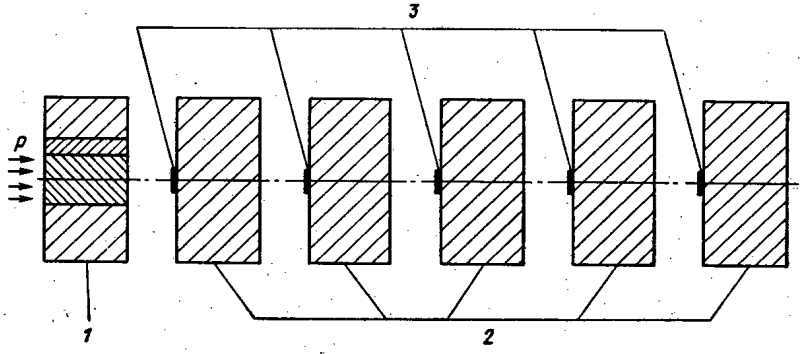


Fig. 4. Geometry of experiment with track detector: 1) total-absorption target; 2) radiation shielding blocks; 3) track detectors.

Geometry of "Extended" Source. In the second experiment we studied the yield of both ultrafast and fast neutrons from a total-absorption target in the case when the beam diameter is greater than the detector size and the distance between the detectors is comparable with the beam diameter.

The geometry of the experiment is shown in Fig. 4. A beam of 200-MeV protons with a diameter of 30 mm struck a total-absorption lead target at a distance of 30 mm from the target and then at intervals of 30 mm we set up tungsten shielding blocks with track detectors mounted on them. Each detector constituted a "sandwich" of $^{238}U$ plates of 5 × 10 mm and a glass substrate. The number of fission-fragment tracks for each plate were measured with an MBI-3 microscope (×630). It was shown in [7] that such a detector is a rem-

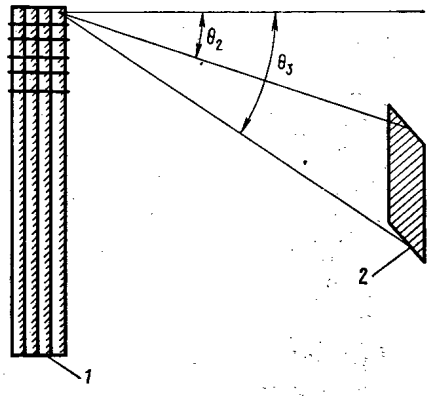


Fig. 5. Diagram for calculation of density of the secondary-neutron flux in experiment with track detector: 1) total-absorption target subdivided into layers and levels; 2) track detector.

TABLE 1. Calculation of Radiation Burdens on Critical Organs

| Critical organs | r, cm | Ultrafast neutrons, neutrons/cm$^2$ | Fast neutrons, neutrons/cm$^2$ |
|---|---|---|---|
| Eye | 50 | $3{,}1 \cdot 10^7$ | $4{,}0 \cdot 10^8$ |
| Gonads | 32 | $7{,}6 \cdot 10^7$ | $1{,}0 \cdot 10^9$ |
| Healthy extremity | 19 | $2{,}1 \cdot 10^8$ | $1{,}8 \cdot 10^9$ |

meter and records the equivalent dose of ultrafast and fast neutrons. Prior calibration of the track detectors showed that in the energy range considered 1 track/mm$^2$ corresponds to a value of $0.96 \pm 0.29$ rem.* With a shielding thickness of 0, 5, 10, 15, and 20 cm the dose is 497.0, 79.1, 24.5, 7.9, and 3.0 rem. The fluence of protons incident on a total-absorption target is $2 \cdot 10^{13}$ cm$^{-2}$. The error of dose measurement with track detectors was ~30%.

In calculating the particle fluence in such a geometry, as in the first case we divided the total-absorption target into four layers and, moreover, within the limits of each layer we further divided it into a series of circular levels ($K_i$ over the beam cross section). Each circular level, in turn, was subdivided into 100 segments so that any of them could be taken to be a point source. Having calculated the angles at which the detector is seen from a given point ($\theta_2$ and $\theta_3$ in Fig. 5), we find the particle fluence incident on the surface of the detector from a given point as the difference of the values of $\Phi_i$ from Eq. (4) for the angles $\theta_2$ and $\theta_3$. Thus, having integrated the values over the entire area occupied by the beam on the target, we calculate the fluence of particles incident on the given layer of the total-absorption target. Further, by summing the values over all layers, we find the sought value $\Phi_i$ for the entire target as a whole.

Calculation by this method for the case when there was no shielding gave values of $4.2 \cdot 10^8$ (for ultrafast neutrons) and $7.3 \cdot 10^9$ neutrons/cm$^2$ (for fast neutrons), which correspond to 23.7 and 386.9 rem, respectively [8], i.e., a total dose of 410.6 rem. Thus, the difference between the experimental and calculated values does not exceed 22%.

In considering the geometry of massive irradiation, we specify the set of parameters necessary for calculating the fluence of ultrafast and fast neutrons incident on critical organs ($E_p$ = 155 MeV, $I_0 = 3 \cdot 10^{13}$ protons,

*The unit rem is used here as a unit of measurement of radiation burdens on an organism during irradiation, although according to [8] it is applicable only for estimating the risk of chronic professional irradiation with low doses. However, in our opinion the absence of regulation values for radiation therapy practice and the limited number of persons subjected to such irradiation allows an analog to be drawn between our cases and those considered in [8].

$\theta$ = 90). Using the data given in Table 1, we find, in accordance with [8], values of 23 rem on an eye, 57.3 rem on the gonads, and 106.7 rem on a healthy extremity. Such radiation burdens on critical organs are unacceptably high. In view of this, obviously, the problem arises of creating local radiation shielding for the patient in order to reduce the radiation burdens on the entire organism (or separate parts of the patient's body) during irradiation of tumors. In our opinion, such local protection should ensure a reduction of the radiation burdens to the level of a "dose of justified risk" to the patients subjected to radiation therapy. As an example, we point out that for cosmonauts the dose of justified risk has been taken equal to 50 rem [9].

## LITERATURE CITED

1. M. F. Lomanov et al., Med. Radiol., No. 7, 40 (1975).
2. D. L. Broder et al., Concrete in Shielding for Nuclear Facilities [in Russian], Atomizdat, Moscow (1973).
3. R. Alsmiller et al., Rep. ORNL-4046 (1967).
4. M. M. Komochkov, JINR Preprint R-1349, Dubna (1963).
5. N. G. Guseva et al. (editors), Dosimetric and Radiometric Techniques [in Russian], Atomizdat, Moscow (1966), p. 282.
6. S. L. Kuchinin et al., IFVÉ ORI Preprint 77-94.
7. M. F. Lomanov et al., At. Energ., 34, No. 3, 185 (1973).
8. Radiation Safety Standards NRB-76 [in Russian], Atomizdat, Moscow (1978), p. 3.
9. E. E. Kovalev, Radiation Risk on Earth and in Space [in Russian], Atomizdat, Moscow (1976).

LETTERS

# VACUUM FISSION CHAMBERS FOR NEUTRON MONITORING

A. B. Dmitriev, E. K. Malyshev, and O. I. Shchetinin

UDC 539.1.074;539.1.074.8

In the practice of monitoring high fluxes a characteristic recent development has been the extensive introduction of various emission detectors in which current is produced by the motion of charged particles in the interelectrode space, particles which are formed directly when neutrons are captured by nuclei of an active substance [(n,$\beta$), (n,$\alpha$), (n, p), and other reactions]. Those which have come into most widespread use have been the $\beta$-emission self-powered detectors (SPD) with rhodium or silver as the radiator of charged particles. Disadvantages which $\beta$-emission SPD suffer include comparatively low sensitivity as well as inertia due to the half-life of the radionuclides formed. Moreover, in a number of cases it is desirable to have a detector with a spectral sensitivity corresponding to the energy dependence of the fission cross section of the nuclear fuel. In this respect, of interest are vacuum fission chambers which utilize electronic emission under the action of fission fragments [1, 2]. These chambers are practically inertialess (electron collection time $< 1 \cdot 10^{-9}$ sec) instruments and the relatively low energy of the electrons emitted permit continuous control of the detector current (sensitivity) [3, 4]. The fission-fragment radiator (it is also the electron emitter) is usually deposited directly on the electrodes of the chamber. If the electrodes have a different electron emissivity, then even in the absence of an external voltage at the instant of irradiation of the chamber a difference current is established in the closed circuit of the electrodes. Because of the small space charge, the detector current remains proportional to the neutron flux density [3]. The current of the vacuum fission chamber is determined by the emitted electrons since their total charge is much greater than the charge of the fission fragments. The present authors carried out measurements of the electron emission coefficient with a plane-parallel three-electrode vacuum cell consisting of disk-shaped emitter and collector of emission electrons with a control grid between then. The surface of the emitter was coated electrolytically with a layer of $U_3O_8$ (90% $^{235}U$). The current of the electrons emitted by the surface of the emitter during the escape of a fission fragment or by the surface of the collector under bombardment by fission fragments was measured as a function of the electrode potentials. A negative potential was established on the grid and the current specific to the fission fragments was determined. Measurements of the coefficients of electron emission when fission fragments escaped from a $U_3O_8$ layer with a thickness of 0.1 mg/cm$^2$ and when these fragments bombarded the polished surface of a stainless steel collector yielded values of $570 \pm 30$ and $370 \pm 20$, which are in accordance with the data of [1].

Two main groups of vacuum fission chambers can be distinguished in respect of design: with a cylindrical and with a plane-parallel system of electrodes. The simplest is a system of two coaxial cylinders [3, 4]. Electron emission occurs both during the escape of a fission fragment from the surface of the radiator and during bombardment of the opposite electrode. Therefore, in order to attain the highest possible sensitivity, it makes sense to deposit a fissionable coating on the working surfaces of both electrodes. Depending on which electrode

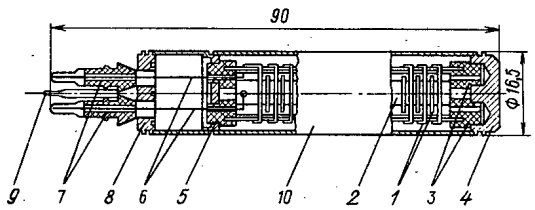


Fig. 1. Construction of KNV-1 vacuum fission chamber: 1) 15 pairs of disks; 2) support; 3) insulators of high-alumina ceramic; 4, 5, 8) flanges; 6) current-carrying conductor; 7) cermet connection joint; 9) exhaust tube for evacuating device; 10) 16-mm tube with 0.3-mm walls.

Translated from Atomnaya Énergiya, Vol. 47, No. 2, pp. 108-109, August, 1979. Original article submitted November 11, 1976.



0038-531X/79/4702-0636 $07.50 

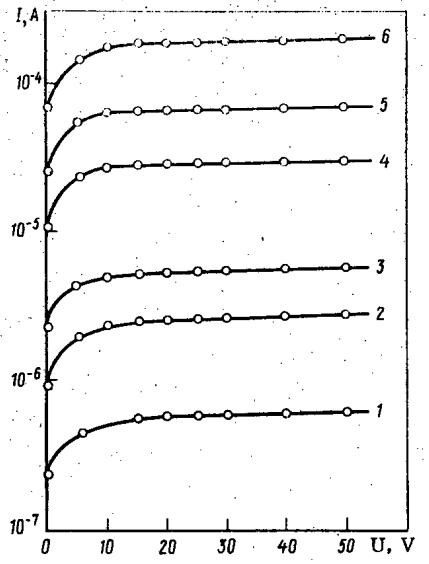


Fig. 2

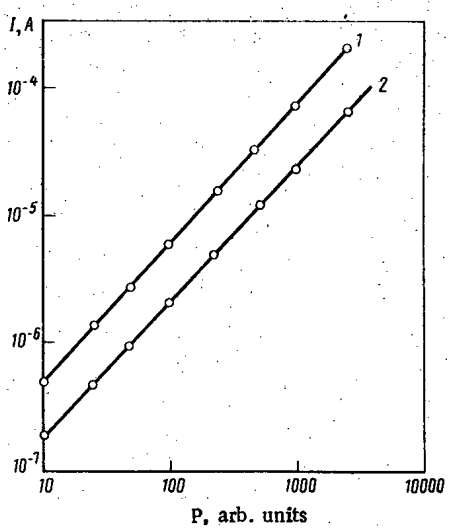


Fig. 3

Fig. 2. Current–voltage characteristics of KNV-1 chamber: 1-6) reactor power of 10, 50, 100, 500, 1000, and 2500 arb. units, respectively.

Fig. 3. Load characteristics of KNV-1 chamber: 1) at supply voltage of 24 V; 2) in short-circuit mode.

has the positive voltage applied to it to ensure saturation of the emission current, i.e., whether it is the central ($N_1$) or outer ($N_2$) electrode, we can write the following expressions for the sensitivity:

$$N_1 = eR(\delta_2 + \delta_{12}m + \delta_2' s); \quad (1)$$

$$N_2 = meR(\delta_1 + \delta_{21}(1-s)), \quad (2)$$

where R is the number of fission reactions in the outer electrode per unit neutron flux density; e, electronic charge (C); m, ratio of the amount of fissionable material on the central and outer electrodes; $\delta_1$ and $\delta_2$, coefficients of electron emission during the escape of fission fragments from the surface of the central and outer electrodes, respectively; $\delta_{12}$ and $\delta_{21}$, coefficients of emission under bombardment of the surface of the opposite electrode by fission fragments (the first subscript refers to the radiator of fission fragments and the second, to the electron emitter); and $\delta_2'$, coefficient of electron emission in the outer electrode under the effect of the fraction s of fission fragments which formed in the outer electrode and flew past the central electrode.

In practice, m is proportional to the ratio r of the radii of the respective electrodes,

$$m = kr. \quad (3)$$

The maximum sensitivity $N_1$ is obtained for

$$r = \sqrt{1-(2\delta_2'/\pi k\delta_{12})}. \quad (4)$$

Usually, k = 1, which yields $r \approx 0.8$. Obviously, an increase in k gives an increment in sensitivity but at the same time the optimal interelectrode gap decreases, and this results in constructional difficulties in detector design. On the other hand, the requirements on the vacuum diminish at small interelectrode gaps.

Measurement of small signals is frequently limited by the leakage currents through the insulators, e.g., when the detector is operating at elevated temperature. In such cases it is desirable to introduce a protective electrode, the role of which can be played by the grounded casing of the detector. The introduction of a protective electrode, especially when the interelectrode gas is small, is constructionally much simpler for the plane-parallel system of electrodes. Moreover, with the plane-parallel system of electrodes practically the entire volume of the detector casing is utilized, making it possible to increase the specific sensitivity of the detector.

Figure 1 shows the construction of a KNV-1 vacuum fission chamber with a plane-parallel system of electrodes. One of the electrodes is coated on either side with a layer of $U_3O_8$ (90% $^{235}U$) with a thickness of 0.5 mg/cm$^2$. The total area of the coating is 22 cm$^2$. At a supply voltage of 24 V the sensitivity of the KNV-1 chamber, as measured in an F-1 reactor, is $1 \cdot 10^{-18}$ A/neutron/cm$^2$ · sec. In the short-circuit mode the sensitivity is roughly five times smaller. Measurements of the sensitivity to $^{60}Co$ $\gamma$ rays in an ÉPGU-200 apparatus at a voltage of 24 V gave a value of $1 \cdot 10^{-15}$ A/R · h$^{-1}$. The operating temperature of the chamber is up to 400°C. In the case of long use in high thermal-neutron fluxes the detector electrodes may be coated with a mixture of nuclides, which makes it possible to compensate for the reduction in sensitivity because of burn-up of the radiator [4, 5]. For monitoring fast neutrons it is necessary to use coatings containing $^{232}Th$, $^{237}Np$, or $^{238}U$. The chamber capacitance is 30 pF.

Figure 2 gives the current–voltage characteristics of the chamber as obtained at various reactor powers. A distinctive feature of these characteristics is the fact that the beginning of their plateau is independent of the radiation intensity. Figure 3 gives the operating characteristics, both of which are linear in the range measured. The limit of linearity of the operating characteristic of a vacuum chamber with plane-parallel electrodes can be found from

$$i = 2{,}33 \cdot 10^{-6} U^{3/2} S/d, \qquad (5)$$

where U is the supply voltage of the chamber (in V); S, area of the electrode (in cm$^2$); and d, distance between electrodes (in cm).

The linearity limit for the KNV-1 chamber when d = 0.08 cm, S = 22 cm$^2$, and U = 24 V is about 0.5 A. The fact that vacuum fission chambers are practically inertialess allows them to be used to monitor not only steady-state but also pulsed neutron and $\gamma$-ray fluxes.

## LITERATURE CITED


1. J. Anno, J. Appl. Phys., 33, No. 5, 1678 (1962).
2. F. Jamerson et al., 36, No. 2, 70 (1965).
3. E. K. Malyshev et al., At. Energ., 27, No. 4, 37 (1969).
4. A. B. Dmitriev and E. K. Malyshev, Neutron Ionization Chambers for Reactor Engineering [in Russian], Atomizdat, Moscow (1965).
5. O. I. Shchetinin, A. B. Dmitriev, and E. K. Malyshev, At. Energ., 28, No. 2, 164 (1970).
6. Z. A. Al'bikov, A. I. Veretennikov, and O. V. Kozlov, Detectors of Pulsed Ionizing Radiation [in Russian], Atomizdat, Moscow (1978), p. 34.


# PHASE DIAGRAMS OF SYSTEMS OF URANIUM TRIFLUORIDE WITH FLUORIDE OF ALKALI METAL

V. A. Volkov, I. G. Suglobova, and D. É. Chirkst

UDC 546.791:541.49

In the development of new salt compositions for use as a reactor fuel it is necessary to have information about the phase diagrams of systems with uranium fluorides and about the character of the interaction of the components. The phase diagrams of the systems $UF_3$–LiF and $UF_3$–NaF have already been published [1] whereas in the case of $UF_3$–MF systems (M = K, Rb, Cs) only partial x-ray diffraction analysis has been carried out [2], serving as a basis for the execution of complete differential-thermal and x-ray phase analysis of these three systems (Figs. 1-3, Table 1).

Uranium trifluoride was obtained [3, 4] by sintering stoichiometric mixtures of uranium tetrafluoride and metallic uranium in nickel crucibles in a vacuum. The specimens were kept at 1030-1050 and 1010-1030°C for 2 h. Finely dispersed metallic uranium was obtained by decomposing the hydride. Uranium tetrafluoride

Translated from Atomnaya Énergiya, Vol. 47, No. 2, pp. 110-112, August, 1979. Original article submitted May 15, 1978.



0038-531X/79/4702-0638$07.50 

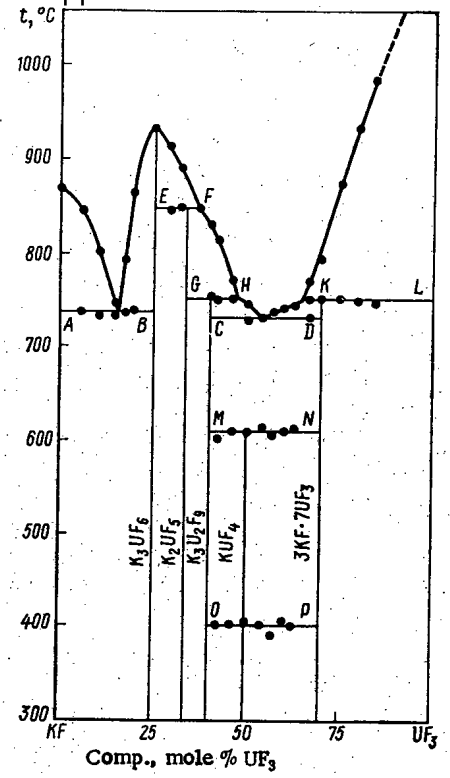


Fig. 1. Fusion diagram of $UF_3$–KF system.

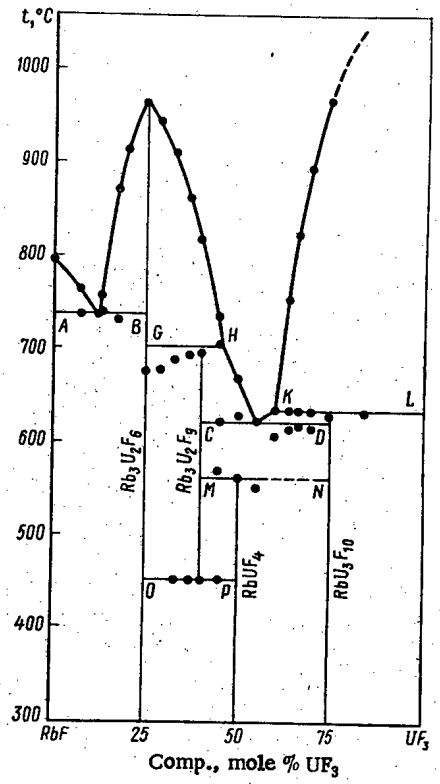


Fig. 2. Fusion diagram of $UF_3$–RbF system.

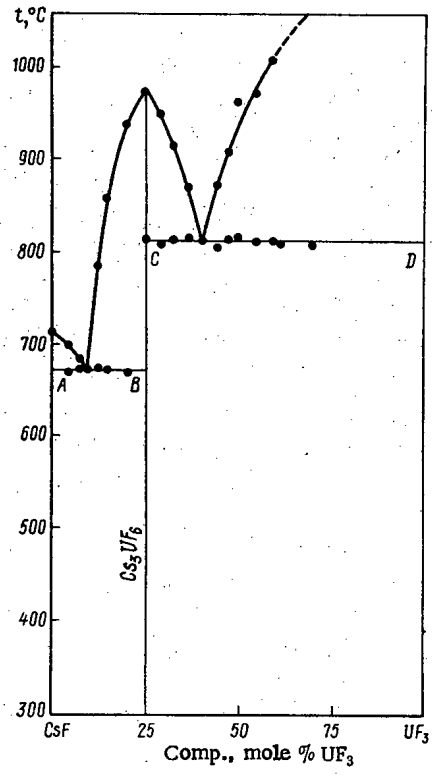


Fig. 3. Fusion diagram of $UF_3$–CsF system.

precipitated from the aqueous solution was dried in a vacuum at 400°C in a molybdenum test tube and was purified by double sublimation at 1100°C. Thermal analyses were performed with an FRU-64 light-beam recorder with a platinum–platinum-rhodium thermocouple by a method with no reference. The specimens were placed

TABLE 1. Phase Equilibrium in $UF_3$–MF Systems

| Equilibrium | M = K | | M = Rb | | M = Cs | |
|---|---|---|---|---|---|---|
| | t, °C | mole % $UF_3$ | t, °C | mole % $UF_3$ | t, °C | mole % $UF_3$ |
| Eutectic AB | 735 | 15 | 736 | 12 | 671 | 9 |
| Eutectic CD | 730 | 54 | 622 | 55 | 810 | 40 |
| Peritectic EF (formation of $K_2UF_5$) | 848 | 37 | — | — | — | — |
| Peritectic GH (formation of $M_3U_2F_9$) | 750 | 48 | 700 | 46,5 | — | — |
| Peritectic KL (formation of $MF \cdot nUF_3$, n = 2.3–3) | 750 | 66 | 632 | 60 | — | — |
| Formation of $MUF_4$ by solid-phase reaction MN | 608 | 50 | 560 | 50 | — | — |
| Phase formation OP | 401 | 50 | 450 | 40 | — | — |
| Dystectic $M_3UF_6$ | 932 | 25 | 962 | 25 | 972 | 25 |

TABLE 2. Parameters of Structures of Fluoro-uranates (III) of Alkali Metals

| Compound | System | Type of Structure | a, Å | c, Å | N | $d_{x\text{-ray}}$, g/cm³ |
|---|---|---|---|---|---|---|
| $K_3UF_6$ | Tetragonal | β-$K_3YF_6$ [10] | 9,45±0,02 | 9,57±0,02 | 4 | 3,62 |
| $Rb_3UF_6$ | Ditto | β-$K_3YF_6$ [10] | 9,58±0,01 | 9,88±0,01 | 4 | 4,43 |
| $Cs_3UF_6$ | Ditto | β-$K_3YF_6$ [10] | 10,10±0,02 | 10,70±0,02 | 4 | 4,54 |
| $K_2UF_5$ | Cubic | $CaF_2$ | 6,62±0,01 | — | 1,6 | 3,74 |
| $K_3U_2F_9$ | Ditto | $CaF_2$ | 6,00±0,01 | — | 0,8 | 4,67 |
| $RbUF_4$ | Hexagonal | $KYF_4$ [11] | 8,54±0,01 | 10,72±0,02 | 6 | 5,84 |
| $3KF \cdot 7UF_3$ | Cubic | $CaF_2$ | 5,94±0,01 | — | — | — |
| $RbU_3F_{10}$ | Hexagonal | $NH_4Er_3F_{10}$ [12] | 8,26±0,01 | 13,39±0,01 | 4 | 5,01 |

in thin-walled copper microcrucibles, set in quartz jackets which were vacuum-sealed. X-ray diffraction analysis was carried out by the polycrystal method on a URS-50I diffractometer in filtered copper radiation.

Congruently, melting hexafluorouranates (III) have cryolitelike structures (Table 2). The other fluoro-uranates (III) crystallize in fluoritelike lattices. In the potassium system, cubic phases of the fluorite type are common; only $KUF_4$ has an ordered low-symmetry structure, as a result of which its x-ray diffraction pattern is not indexed. In the rubidium system, as the difference in the sizes of the atoms of uranium and the alkali metal increase, ordering of the uranium and rubidium atoms occurs and the cubic lattice is distorted. The compounds $RbU_3F_{10}$ and $RbUF_4$ have hexagonal lattices which are derivatives of the fluorite structure. As a result of a further increase in the difference in the size of the atoms of uranium and alkali metal, fluorite-like phases are not realized in the cesium system.

Thus, as a result of the isodesmic structure of fluorouranates (III) with a $UF_3$ content above 25 mole%, in this range of compositions there is a reduction in the number of forms of tetragonal compounds, from four in the potassium system, to two in the rubidium system, and further to zero in the cesium system. At the same time, there is ordering of the structure and reduction of the thermal stability (temperature of incongruent melting or solid-phase decomposition) of the ternary compounds which form. This is at variance with the well-known Gromakov law [5], according to which the number of forms increases and the thermal stability of the complex compounds diminishes.

Two groups of exceptions to the Gromakov law can be distinguished.

1. In systems of ternary compounds with isodesmic structure complete reversal of the Gromakov law is observed ($UF_3$–MF).

2. In systems with an anisodesmic structure of the products of interaction, the law may be reversed for one of the forms of ternary compounds, as manifested in the congruous form of complexes considered in [6] ($UBr_3$–MBr [7]).

Reversals of the Gromakov law are characteristic of salt systems on the basis of fluorides of actinides and lanthanides, which play a significant role in nuclear fuel chemistry. It is precisely in these systems that

phases with isodesmic structures are common. The interatomic distances and ionic radii may serve as a quantitative characteristic for predicting the possibility of isodesmic phases being realized. The U–F distances in uranium trifluoride are $5 \times 2.36 + 6 \times 2.70$ Å, the mean being 2.55 Å [8]. The radius $r_{U-F}$ in $M_3UF_6$ can be taken to be equal to (1/4)c and calculations then give a mean value of 2.51 Å. Assuming a fluorine radius of 1.33 Å after Belov and Bokii [9], we can take the ionic radius of U(III) to be 1.20 ±0.02 Å. Thus, the sum of the radii, $\Sigma R_{U,F}$, is close to $\Sigma R_{K,F} = 2.66$ Å, which leads to the formation of a large number of isodesmic ternary compounds in which $r_{U,K-F}$ has an intermediate value of 2.59 ±0.02 Å (calculated from the parameters of the lattices of $3KF \times 7UF_3$ and $K_3U_2F_9$). It can be seen from the data obtained that with a difference of $\Delta R_{E,M}$ between the radii of the alkali metal and the complexing agent within the limits 0.2-0.4 Å, ordered fluoritelike phases are formed in $EF_3$–MF systems and compounds destabilize in the range of compositions from 25 to 50 mole % $EF_3$, while at $R_{E,M} > 0.4$ Å ternary compounds with an isodesmic structure are not formed.

## LITERATURE CITED


1. W. Grimes and D. Cuneo, Molten Salts as Reactor Fuels, in: Reactor Handbook, C. R. Tipton (editor), Interscience, New York, Vol. 1, 2nd. edition (1960).
2. R. Thoma, H. Friedman, and R. Penneman, J. Am. Chem. Soc., 88, No. 5, 2046 (1966).
3. H. A. Friedman, C. F. Weaver, and W. R. Grimes, J. Inorg. Nucl. Chem., 32, No. 9, 3131 (1970).
4. C. E. Bamberger, R. G. Ross, and C. F. Baes, J. Inorg. Nucl. Chem., 33, No. 2, 767 (1971).
5. S. D. Gromakov, Some Laws of Equilibrium Systems [in Russian], Kazan. Univ. (1961).
6. I. G. Suglobova and D. É. Chirkst, Radiokhimiya, 20, No. 3, 352 (1978).
7. V. M. Vdovenko et al., Radiokhimiya, 16, No. 3, 369 (1974).
8. J. Laveissère, Bull. Soc. Franc. Minèral. et Crist., 90, No. 3, 304 (1967).
9. G. B. Bokii, Crystal Chemistry [in Russian], Nauka, Moscow (1971).
10. H. Bode and E. Voss, Z. Anorg. Allg. Chem., 290, No. 1, 1 (1957).
11. M. P. Borzenkova, G. H. Kuznetsova, and A. V. Novoselova, Izv. Akad. Nauk SSSR, Neorg. Mater., 7, No. 2, 242 (1971).
12. N. V. Podberezskaya et al., Zh. Struk. Khim., 17, No. 1, 147 (1976).


# CALCULATION OF PARAMETERS OF SCINTILLATION DETECTORS FOR LOW-ACTIVITY γ RAYS

I. F. Lukashin

UDC 551.46.084:539.107.43

Measurements of low concentrations of radioactive nuclides in natural media are made from the peaks of the total absorption of γ rays. This pertains to both sources of monoenergetic radiation ($^{40}K$, $^{7}Be$, etc.) and cascade γ-ray emitters ($^{39}Cl$, $^{176}Lu$, $^{24}Na$, etc.). In the first case, the total-absorption peak is determined from the general γ-ray spectrum and in the second case, from the radiation spectrum obtained by selecting coincident γ rays recorded by two detectors simultaneously.

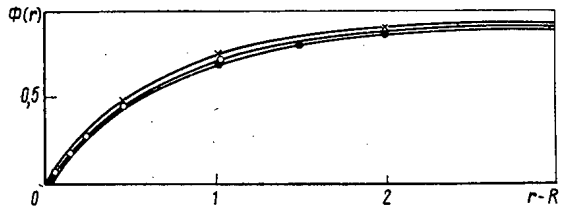


Fig. 1. Dependence of relative γ-ray flux on size of the radiating volume: ×) R = 2.0; ○) R = 1.0; ●) R = 0.5.

Translated from Atomnaya Énergiya, Vol. 47, No. 2, pp. 112-113, August, 1979. Original article submitted May 15, 1978.

0038-531X/79/4702-0641$07.50  

The construction and use of systems of apparatus for the study of hydrogeophysical processes by means of fields of nuclear tags requires knowledge of such parameters as the efficiency of registration of $\gamma$ rays by a detector recording the flux of $\gamma$ rays which effectively irradiate the volume of the medium.

Following [1], we replace the cylindrical NaI(Tl) crystal customarily used with a spherical detector of radius R of the same volume.* Then, in accordance with [2], the expression for the $\gamma$-ray flux in the detector from a spherical layer $\Delta r$ is of the form

$$\Delta\Phi(r)=\pi A\mu^{-3}\int_{R}^{r+\Delta r}d\xi\,\xi\int_{\xi-R}^{\sqrt{\xi^2-R^2}}e^{-\xi}(\xi^2\rho^{-2}-R^2\rho^{-2}-1)\,d\rho, \tag{1}$$

where A is the activity of the medium (in $\gamma$-ray quanta/min·liter) and $\xi$ and $\rho$ are the variables of integration.

Introducing the quantities $\alpha=R\sqrt{\left(\frac{r}{R}\right)^2-1}$ and $\beta=R\left(\frac{r}{R}-1\right)$ and bearing in mind that

$$\mathcal{E}_n(\varkappa)=\int_1^\infty e^{-\varkappa u}u^{-n}\,du,$$

Eq. (1) can easily be rewritten as

$$\Delta\Phi(r)=2\pi A\mu^{-3}r\,[R\mathcal{E}_2(\beta)+\mathcal{E}_3(\alpha)-\mathcal{E}_3(\beta)]\,\Delta r \tag{2}$$

(tables of the integroexponential function $\mathcal{E}_n(\varkappa)$ of the n-th order are given in [3]).

The probability of a $\gamma$-ray quantum, formed at a distance r from the detector, appearing in the volume of the detector is

$$\varphi(r)=(2r)^{-1}\Psi(R,\alpha,\beta), \tag{3}$$

where $\Psi(R,\alpha,\beta)=R\mathcal{E}_2(\beta)+\mathcal{E}_3(\alpha)-\mathcal{E}_3(\beta)$.

The total flux of unscattered radiation in the volume of the detector or in the cavity out of the medium by the detector is determined by integrating Eq. (2) with respect to r between the limits R and r:

$$\Phi(r)=\pi A\mu^{-3}R^2\left\{1+\frac{2}{R^2}[(e^{-\beta}-e^{-\alpha})-3(\mathcal{E}_5(\beta)-\mathcal{E}_5(\alpha))]-2\frac{r}{R}(\beta)\right\}. \tag{4}$$

In the limit as $r\to\infty$ the expression in braces in Eq. (4) becomes unity and the expression for the total radiation flux in the space R in the radiating-absorbing medium $\mu$, A becomes

$$\Phi(\infty)=A\pi R^2\mu^{-3}. \tag{5}$$

Equation (5) was first obtained in [4] by independent methods.

Inside the isolated cavity the $\gamma$-ray field is uniform and isotropic and, therefore, the radiation flux in a detector $R_0$ located in the cavity R is equal to

$$\Phi_0=A\pi R^2\mu^{-3}\pi R_0^2/\pi R^2=A\pi R_0^2\mu^{-3} \tag{6}$$

and, as was pointed out in [5], does not depend on the dimensions of the protective jacket of the detector, i.e., on the dimensions of the cavity. The efficiency of the detector is found from the formula [2]

$$\varepsilon=1-[1-\exp(-2\lambda)]\,(2\lambda)^{-1}, \tag{7}$$

where $\lambda = R\mu_0/\mu$ (here $\mu_0$ is the linear coefficient of absorption of $\gamma$ rays by the material of the detector).

*Here and henceforth the unit used for measuring the linear dimensions is $1/\mu$, where $\mu$ is the linear coefficient of attenuation of radiation in the medium.

The effective volume of the medium radiating $\gamma$ rays into the detector is found from Eq. (4). Figure 1 shows the plot of the relative radiation flux [expressed in braces in Eq. (4)] intersecting detector R versus the thickness of the radiating-absorbing layer of the medium $(r - R)$ for various R. The relative flux depends weakly on the detector size, to the extent of no more than 10% for R from 0.1 to 2. The contribution of the spherical layers of thickness 0.5, 1, and 3 to the total flux is $>50$, $\sim 75$, and $>95\%$, respectively. Thus, the effective radiating volume of the medium for unscattered $\gamma$ rays is bounded by two or three mean free paths of a $\gamma$-ray quantum and practically does not depend on the detector size; the periphery makes a negligible contribution to the total radiation flux.

In order to calculate the parameters of registration of cascade radiation by a system of two detectors of radius R placed in an isotropic radiating-absorbing medium at a distance of $2l$ from each other, we use Eq. (3). For two cascade $\gamma$-ray quanta with uncorrelated direction of emission the fact that they both enter both detectors comprises independent events. The probability of detection of a cascade formed at a point at distances r and r' from the centers of the detectors, therefore, is given by

$$\varphi_{\gamma\gamma}(r, r') = 4(rr')^{-1}\Psi(R, \alpha, \beta)\Psi(R, \alpha', \beta'). \quad (8)$$

and the counting rate of coincidences of cascade radiation in an active medium A [pairs of $\gamma$-ray quanta/min·liter] is

$$\Phi_{\gamma\gamma} = Ae_{\gamma\gamma}\int_V \varphi_{\gamma\gamma}(r, r')\,dV. \quad (9)$$

It thus follows that the efficiency of a detector of cascade radiation is

$$\varepsilon_{\gamma\gamma} = \varepsilon^2. \quad (10)$$

Numerical calculations performed according to Eq. (8) show that the highest counting rate for coincidences occurs when $l/R = 1$. The effective radiating volume of the medium is considerably greater than in the case when monoenergetic radiation is being recorded. The contribution to the cascade-radiation flux from various spherical volumes of the medium with radii 0.8, 2.0, and 3.6 was 25, 50, and 75%, respectively. Equations (9) and (10) make it possible to get an idea of the activity of a medium from the measured coincidence-counting rate.

## LITERATURE CITED

1. C. Sybesma, Measurements of Continuous Energy Distribution $\gamma$-Rays in a Scattering Medium, Amsterdam (1961).
2. Yu. A. Sapozhnikov, V. A. Lopatin, and V. P. Ovcharenko, At. Energ., 40, No. 3, 246 (1976).
3. V. I. Pagurova, Tables of Integroexponential Functions [in Russian], Moscow (1959).
4. G. I. Kosourov, Prib. Tekh. Eksp., No. 5, 95 (1962).
5. A. S. Vinogradov, Morskie Gidrofiz. Issled., No. 3 (49), 191 (1969).

# RELEASE OF HYDROGEN FROM 0Kh16N15M3B STEEL ON HEATING

A. G. Zaluzhnyi, D. M. Skorov,
A. G. Zholnin, V. D. Onufriev, I. N. Afrikanov,
V. S. Tsyplenkov, V. G. Vladimirov, and V. P. Kopytin

UDC 543.51

Measurements have been made on the release of hydrogen from 0Kh16N15M3B steel during uniform heating at 20 deg C/min over the range 100-1000°C with a high-vacuum mass-spectrometer system similar to that previously described [1].

The system was continuously evacuated by a NORD-100 pump, which was connected to the system by a pipe having a throughput of 1.28 ± 0.13 liter/sec for air or 4.8 ± 0.5 liter/sec for hydrogen. The use of this pipe of capacity much less than the pumping rate of the pump allowed us to estimate the gas release from the specimen. The total pressure in the working volume was recorded by a VIT-1A gauge, while the partial pressures of the individual gases were recorded with an IPDO-2A mass spectrometer. Each specimen was composed of foil, dimensions 13 × 13 mm, thickness 0.05-1.0 mm.

If a specimen is not saturated with hydrogen, there is a single peak (Fig. 1) at 350-400°C, and the exact position of this is dependent on the nature of the material (a similar peak is observed in uniform heating of technically pure specimens of tungsten, molybdenum, tantalum, cobalt, nickel, or chemically pure iron or platinum, as well as graphite, ceramic, and glass). The height of the peak is very much dependent on the surface cleanliness (degreasing with alcohol, electropolishing, or vacuum annealing) but not on the thickness of the specimen.

All the gases were recorded during the heating, not merely hydrogen; the hydrogen peak was accompanied by peaks at masses 12, 16, and 15. The peak at mass 12 characterizes the yield of CO, while the peaks at masses 16 and 15 correspond to methane [2]. We determine the amounts of hydrogen and CO released at this temperature together with the total pressure in the working volume; the main components of the gas released were hydrogen and CO, while the amount of methane was less by an order of magnitude.

These results indicate that the hydrogen peak is related to the dissociation of hydrogen compounds at the surface of the specimen; this is indirectly confirmed by results [3] on the effects of adsorbed hydrocarbons on the desorption of hydrogen.

When the specimens were saturated with hydrogen by electrolysis, uniform heating under vacuum gave a peak below 300°C (Fig. 2), whose position was dependent on the thickness. The height of the peak also in-

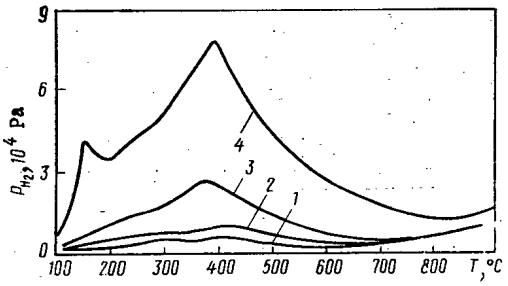


Fig. 1. Release of hydrogen from 0Kh16N15M3B steel during uniform heating: 1) specimen previously heated under vacuum to 1000°C; 2) electropolished specimen; 3) degreased specimen; 4) specimen without degreasing.

Translated from Atomnaya Énergiya, Vol. 47, No. 2, pp. 113-114, August, 1979. Original article submitted May 15, 1978; revision submitted January 15, 1979.



0038-531X/79/4702-0644 $07.50 

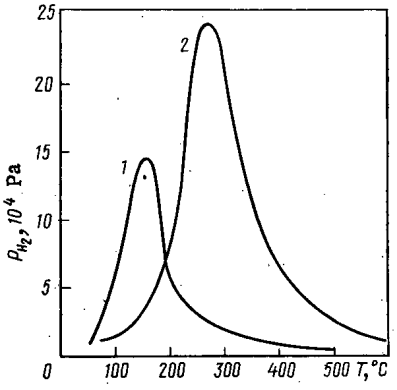


Fig. 2

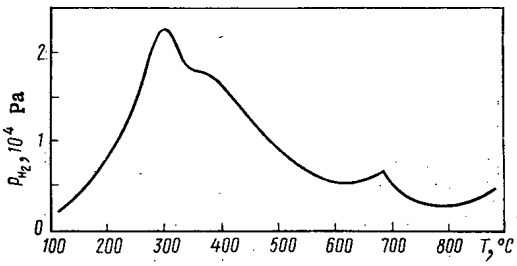


Fig. 3

Fig. 2. Curves for release of hydrogen from specimens of 0Kh16N15M3B steel of thicknesses (mm): 1) 0.2; 2) 1.0, saturated electrolytically with hydrogen and uniformly heated.

Fig. 3. Release of hydrogen from 0Kh16N15M3B steel bombarded by $H_2^+$ ions of energy 18 keV to a dose of $10^{18}$ ions/cm$^2$.

creased with the hydrogenation time. This peak is clearly related to release of gas from the bulk of the specimen. The surface is cleaned by the electrolytic saturation with hydrogen [4], so the peak at 350–400°C is absent.

Particular interest is attached to the release of hydrogen from 0Kh16N15M3B steel saturated with hydrogen on an accelerator by bombardment with $H_2^+$ ions of energy 18 keV to a dose of $10^{18}$ ions/cm$^2$. Figure 3 shows a typical curve, where there is a peak in the hydrogen release at 650–700°C, which is different from that for unexposed specimens. The release of hydrogen is not accompanied by the rapid release of any other gas. It is found that about $2 \cdot 10^{15}$ hydrogen atoms are released. This peak is also observed on heating the specimen a few days after the bombardment or several months later. It seems likely that the bombardment produces additional hydrogen traps.

## LITERATURE CITED

1. D. M. Skorov et al., in: Nuclear Science and Engineering, Series Fuel and Constructional Materials [in Russian], No. 2(5), Izd. TsNIIatominforma, Moscow (1976), p. 23.
2. G. L. Saksaganskii (editor), Ultrahigh Vacua in Instruments for Radiation Physics [in Russian], Atomizdat, Moscow (1976).
3. B. E. Nieuwenhuys et al., Surface Sci., 59, No. 1, 155 (1976).
4. S. Ya. Grilekes, Metal Degreasing, Etching, and Polishing [in Russian], Mashinostroenie, Leningrad (1977).

# BACKSCATTERING COEFFICIENTS OF ELECTRONS

G. B. Radzievskii

UDC 539.12.124

The backscattering coefficient, or the number albedo $\varepsilon(Z, E_0, \theta_0)$, for saturation conditions is the ratio of the number of electrons scattered from a thick flat target to the number of electrons incident on the target. Here Z is the atomic number of the target material, $E_0$ is the initial energy, and $\theta_0$ is the angle of incidence of the electrons. At the present time relatively complete and reliable information on the function $\varepsilon(Z, E_0, \theta_0)$ exists in the literature for wide ranges of Z and $E_0$ values only for normal incidence of the beam ($\theta_0 = 0$) [1], while data for oblique incidence of an electron beam are sparse and relate mainly to low $E_0$ (tens of kiloelectron volts).

The simplest way to obtain the missing values of $\varepsilon$ is to use the geometric similarity of the fields of scattered electrons for certain combinations of Z and $E_0$. Harder [2] showed analytically that for moderate values of $E_0$ (~0.1 MeV) solutions of the transport equation have similarity properties for fixed Z and variable $E_0$, and for high $E_0$ (~5-30 MeV) for fixed $E_0/Z$. It was pointed out earlier [3] that for high $E_0$, $\varepsilon$ depends only on $E_0/Z$. According to Harder [2], the scaling length in similar fields is the mean range $R_0$. The similarity of the fields of scattered electrons was shown in [4] by geometric arguments and also empirically. The combination of those points $Z_i$, $E_{0i}$ for which the conditions of approximate similarity of fields are satisfied was shown explicitly in the form of so-called isolines, and arguments were presented indicating that the scaling length is not quite proportional to $R_0$.

It follows from [4] that for fixed values of $\theta_0$ and those combinations of Z and $E_0$ which lie on one isoline the values of $\varepsilon$ and a number of other characteristics of the radiation field must be equal to one another. Thus, knowing the function $\varepsilon(Z, E_0, \theta_0)$ for a certain value $E_0 = E_{0n}$ (and many values of Z), the values of this function can be found for other values of $E_0$ (and a number of Z values). It is most suitable to apply this method of estimating the characteristics of an electron radiation field for small values of $E_{0n}$.

By using values of $\varepsilon$ from [5-11] for a wide range of values of $\theta_0$, data can be obtained for the most interesting range of small $E_0$ (~0.01-0.1 MeV) [6, 7], where $\varepsilon$ is practically independent of $E_0$ [1]. We denote such stationary values of $\varepsilon(Z, E_0, \theta_0)$ for $E_0$ of the order of 10 keV by $\varepsilon_0(Z, \theta_0)$. In [5] smooth relations $\varepsilon(E_0)$ were measured in the 0.4-1.4 MeV range for a number of values of $\theta_0$ and Z = 13, 29, and 73, and by extrapolating them $\varepsilon_0(Z, \theta_0)$ can be calculated.

Stationary values of $\varepsilon_0(Z, \theta_0)$ [5-7] are shown in Fig. 1a. Since they refer to particular values of Z, and for subsequent calculations the values of $\varepsilon_0(Z, \theta_0)$ are required for any values of Z, we approximate the data of Fig. 1a by the empirical relation

$$\varepsilon_0(Z, 0_0) = [1 + a(Z)\, X(\theta_0)^{\gamma(Z)}] \exp[-\alpha(Z)\, X(0_0)];$$
$$\gamma = 3.008 Z^{-0.053}, \qquad (1)$$

where $X(\theta_0) = 1 - 2\theta_0/\pi$, and $\alpha(Z)$ and $\gamma(Z)$ are shown in Fig. 2. The choice (1) takes account of the fact that $\varepsilon \to 1$ as $\theta_0 \to \pi/2$ [12].

The function $a(Z)$ is related to the albedo for normal incidence: $a(Z) = \varepsilon_0(Z, 0) \exp\alpha - 1$. Taking as $\varepsilon_0(Z, 0)$ a function averaged over data from [4-11], we obtain the curve $a(Z)$ in Fig. 2. The values of $\varepsilon_0(Z, \theta_0)$ calculated by Eq. (1) are shown by the open curves of Fig. 1a for the corresponding values of Z. They are not in bad agreement with the published values of $\varepsilon_0(Z, \theta_0)$. The mean-square deviation of the calculated values from the published data is ~12%.

According to [4] the albedo for any value of $E_0$ and any Z (so long as these Z and $E_0$ values are included in the family of isolines) can be estimated from the relation $\varepsilon(Z, E_0, \theta_0) \approx \varepsilon_0(Z', \theta_0)$, where Z' is the value of the atomic number for which the points $(Z, E_0)$ and $(Z', 0)$ lie on one isoline. The function $\varepsilon(Z, E_0, \theta_0)$ can be estimated by Eq. (1) by using Z' instead of Z.

---

Translated from Atomnaya Énergiya, Vol. 47, No. 2, pp. 114-116, August, 1979. Original article submitted May 15, 1978.



0038-531X/79/4702-0646$07.50 

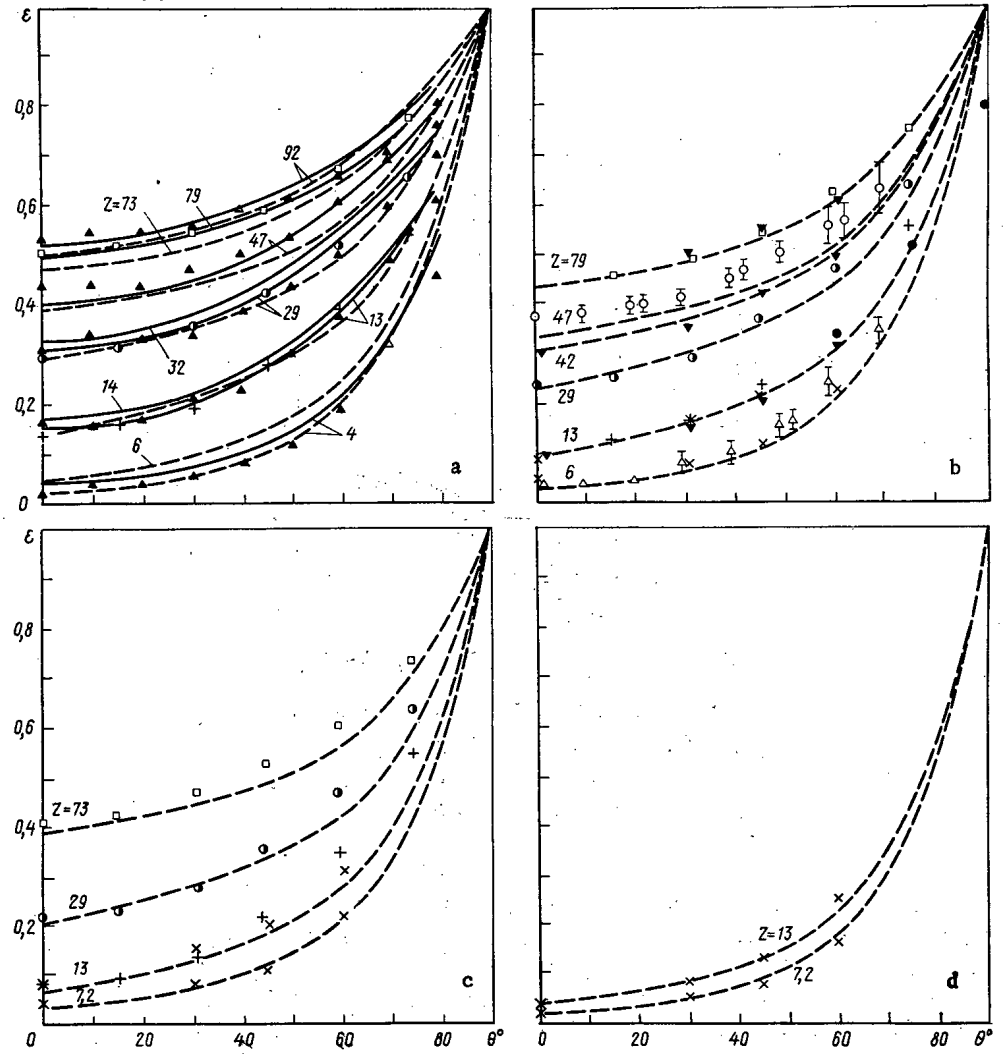


Fig. 1. Backscattering coefficients: a) $\varepsilon_0$, ▲, calculated by the Monte Carlo method [7] for $E_0$ = 20 keV and Z = 4, 13, 29, 47, 92; ——, experiment [6] for $E_0$ = 25 keV and Z = 4, 13, 14, 29, 32, 47, 79, 92; +, ◑, □, $\varepsilon_0$ for Z = 13, 20, 73, respectively [5]; b) ε(1 MeV), +, ◑, □, ε for Z = 13, 29, 73, respectively [5]; Δ, ○, for Z = 5, 6, and 47 [10]; ▼ for Z = 13, 42, and 79 [11]; × for Z = 7.2 and 13 [8]; ● for Z = 13 [9]; c) ε (1.4 MeV), +, ◑, □, for Z = 13, 29, 73 respectively [5]; × for Z = 7.2 and 13 [8]; d) ε (4 MeV), ×, for Z = 7.2 and 13 [8].

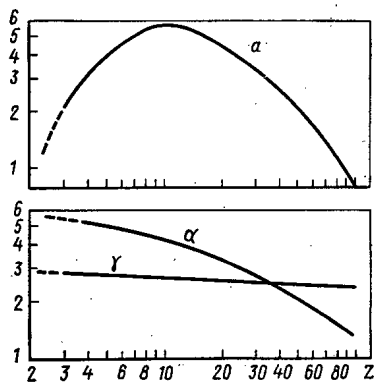


Fig. 2. The functions $a(Z)$, $\alpha(Z)$, and $\gamma(Z)$ appearing in Eq. (1).

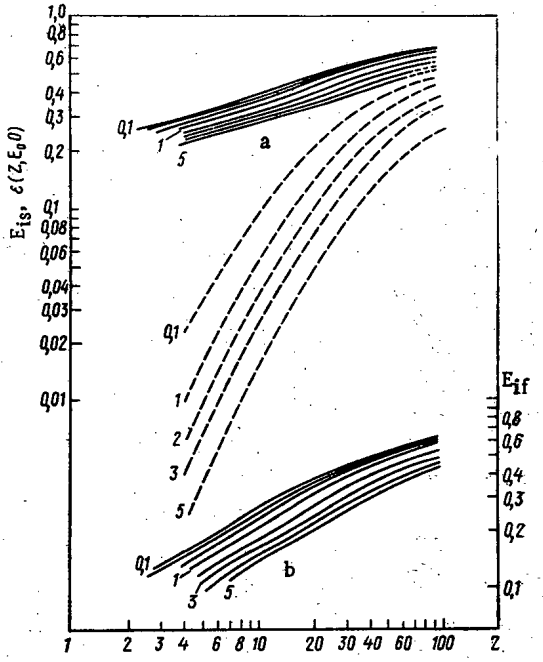


Fig. 3. Albedo for a) an isotropic source $\varepsilon_{is}$, and b) an isotropic flux $\varepsilon_{if}$ for $E_0 \leq$ 0.1, 0.2, 0.5, 1, 2, 3, 4, and 5 MeV; ———, $\varepsilon$ for $\theta_0$ and $E_0 \leq$ 0.1, 1, 2, 3, and 5 MeV [4].

The results of such estimates of $\varepsilon$ are shown in Fig. 1b ($E_0$ = 1 MeV), 1c ($E_0$ = 1.4 MeV), and 1d ($E_0$ = 4 MeV). The functions $\varepsilon(Z, E_0, \theta_0)$ calculated by Eq. (1) (open curves) are compared with sparse experimental values [5, 10, 11] and the values of $\varepsilon$ calculated by the Monte Carlo method [8, 9] for oblique incidence of an electron beam. Agreement of the values calculated from Eq. (1) and the published data here is approximately the same as in Fig. 1a (the mean square deviation for Figs. 1b, c, and d is ~14%). The use of similarity properties (family of isolines) does not introduce further errors into the values of $\varepsilon$, and this certainly can be considered another confirmation of the conclusions of [4].

The determination of the albedo when the electron flux incident on a thick target is not monoenergetic or monodirectional reduces to the integration of the functions $\varepsilon(Z, E_0, \theta_0)$ with respect to $E_0$ and $\theta_0$. In particular, it is easy to calculate the albedo for an isotropic source ($\varepsilon_{is}$) and an isotropic flux ($\varepsilon_{if}$):

$$\varepsilon_{is} = \int_0^{\pi/2} \varepsilon(Z, E_0\theta_0) \sin\theta_0 \, d\theta_0;$$
$$\varepsilon_{if} = 2\int_0^{\pi/2} \varepsilon(Z, E_0, \theta_0) \sin\theta_0 \cos\theta_0 \, d\theta_0. \qquad (2)$$

The results of the calculations are given in Fig. 3.

## LITERATURE CITED


1. T. Tabata et al., Nucl. Instrum. Methods, 94, No. 3, 509 (1971).
2. D. Harder, in: Proc. Second Symp. on Microdosimetry, Stresa (Italy), Oct. 20-24 (1969), p. 567.
3. H. Frank, Z. Naturforsch., 14a, No. 3, 347 (1959).
4. G. B. Radzievskii, At. Energ., 45, No. 2, 126 (1978).
5. A. Frederickson and E. Burke, IEEE Trans. Nucl. Sci., NS-19, No. 6, 160 (1972).
6. H. Drescher et al., Z. Angew. Phys., 29, No. 6, 331 (1970).
7. L. Reimer, Optik, No. 27, 86 (1968).
8. V. F. Baranov, Dosimetry of Electron Radiation [in Russian], Atomizdat, Moscow (1974).
9. M. Berger, Methods in Computational Physics, B. Alder et al. (editors), Vol. 1, Academic Press, New York (1963).

10. F. Titus, Nucl. Instrum. Methods, 89, 93 (1970).
11. A. Cohen and K. Koral, NASA Report TND-2782 (1965).
12. V. I. Boiko et al., At. Energ., 40, No. 3, 221 (1976).

# MEASUREMENT OF WATER AND STEAM FLOWS IN A SEALED VESSEL

V. N. Maidanik, L. N. Mitrakov,
A. P. Proshutinskii, A. G. Tolmachev,
Yu. A. Favorin, and V. K. Shanin

UDC 621.039.534.44

Few results have been published [1-7] on the nonstationary escape of water below the boiling point, and flow-rate measurements have been reported only in [7]. So far as we are aware, no combined studies have been performed on the escape of coolant and the condensation of steam in a closed vessel.

A testbed has been built (Fig. 1) at the Énergiya production organization. The drum contained a metal baffle of height 1.5 m together with dry condensers, which were composed of ceramic rings. The effects of the drum walls on the condensation of the steam were minimized by insulating the wall with a layer of foam plastic and an outer plastic case. A fast valve opened the full area of the exit pipe for the water within 0.01-0.02 sec. Tubes of diameters $D_y$ of 6, 10, and 15 mm and length 318 mm were installed in such a way that the inlets were directly in the pressurized section and the outlets were in the mixing chamber.

The initial conditions were provided by an electric heater within the pressurized tank. The flow of escaping liquid was determined with strain-gauge balances from the mass $M(\tau)$ as a function of time.

Measurements were made of the pressure and temperature in the pressurized tank and drum as functions of time, and also of the temperatures of the ceramic rings within the baffle section. The error of measurement for the pressure was not more than 3%, while that for the temperature was not more than 2%. The overall relative error in measuring the escaping mass at the start ($\tau$ = 2.5 sec) was 11%, while it was not more than 5.5% over the rest of the range. The measurements were made with an initial pressure of 12 MPa

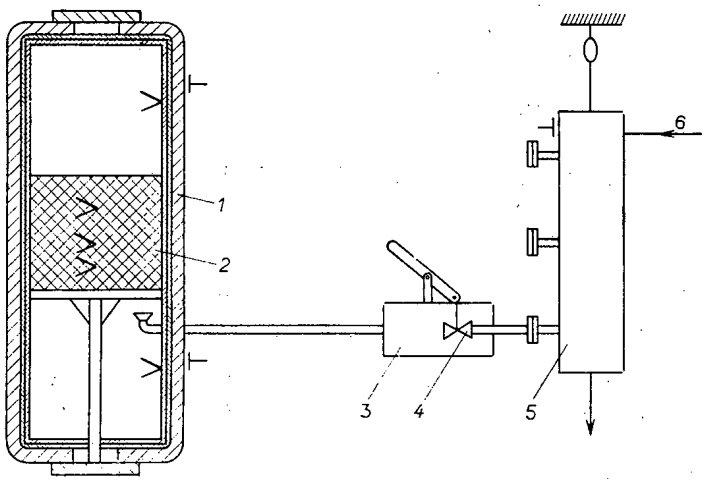


Fig. 1. The system: 1) receiving drum of volume 3.4 $m^3$; 2) dry-condenser baffle; 3) expansion chamber of volume 20 liters; 4) fast valve; 5) pressurized vessel of volume 80 liters; 6) feed water (P = 12.5, t = 104°C).

Translated from Atomnaya Énergiya, Vol. 47, No. 2, pp. 117-118, August, 1979. Original article submitted June 5, 1978.

0038-531X/79/4702-0649$07.50 

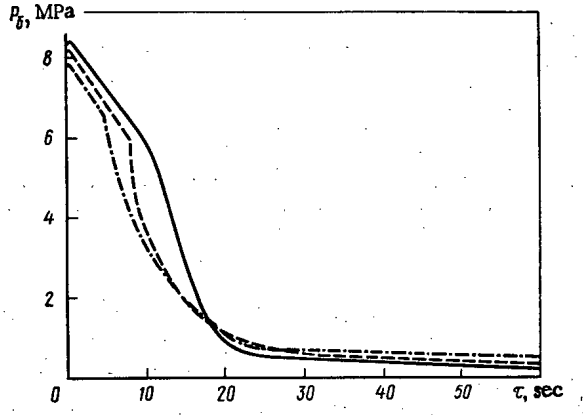


Fig. 2

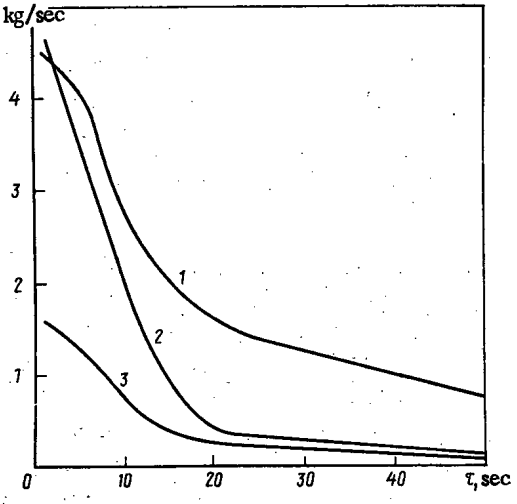


Fig. 3

Fig. 2. Pressure change in pressurized drum for $t_0$ = 300°C, $P_0$ = 12 MPa, and $D_y$ = 15 mm for tube in the lower position (solid line), middle position (broken line), and top position (dot–dash line).

Fig. 3. Flow of steam–water mixture at $t_0$ = 300°C and $P_0$ = 12 MPa; 1) flow of saturated water calculated from [10]; 2) our experiments; 3) flow of dry saturated steam calculated from [11].

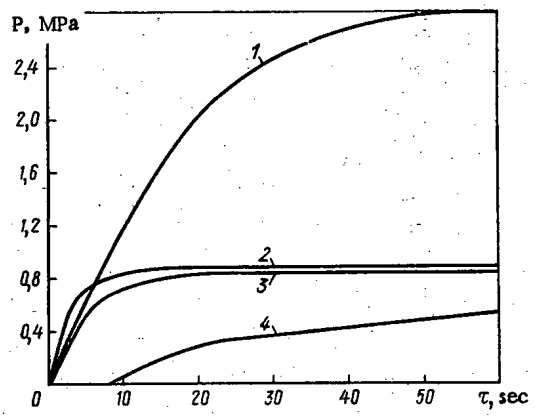


Fig. 4. Pressure as a function of time in the receiving drum for $P_0$ = 12 MPa and $t_0$ = 300°C.

and a temperature of 200-300°C for three positions of the escape tube within the pressurized drum. The difference between the working temperature and the saturation point was 25-125°C in the various runs.

Figure 2 shows the time course of the pressure in the drum for a fixed tube diameter and identical initial water temperatures but various positions of the holes. At the start of escape, the pressure falls below the saturation pressure for the given working temperature, because there is some delay in the boiling, which is metastable. In all cases, there was a characteristic kink in the curve relating the pressure to the time, after which the absolute value of the pressure gradient increased. This form of behavior has been reported previously [1, 8].

There is a clear-cut interface between the heat carrier and the water–steam mixture, as is clear from the measurements on $p(\tau)$ and $M(\tau)$. In the case of escape from a tube at the bottom, the kink in $p(\tau)$ appeared before the level fell to that of the tube. This evidently occurred because the rising steam flux breaks up the water. The $M(\tau)$ curves show that the amount of material escaping increases with the tube diameter.

The observed $G(\tau)$ derived from the $M(\tau)$ curves may be compared with the flow rates for saturated water calculated by the method [9] and also with the critical flow rate for dry saturated steam in a pipe [10] (Fig. 3).

At the start of the escape, the measured flow rate for the saturated water agrees satisfactorily with the calculated value; as time passes, the steam content at the inlet increases, and then the measured flow rates become much less than the calculated values. It is impossible to estimate the effects of the input steam content on the flow rate for saturated water because no measurements were made on the steam content in the vessel. The curves approach those calculated for dry saturated steam with the passage of time, which indicates an increasing steam content. Calculation of the steam condensation rate requires a knowledge of the flow rate on entry to the sealed vessel, which was determined from the heat balance on the assumption that the process is equilibrium and of isoenthalpic type, whereupon the observed $M(\tau)$ and $p(\tau)$ can be used.

Figure 4 shows the time course of the pressure in the drum; the experiments were performed under identical initial conditions. Curve 1 shows the pressure change on flow into an empty vessel from the middle of the pressurized vessel, while curve 3 is for entry to a drum containing ceramic rings. This filling substantially reduces the maximum pressure in the drum (from 0.28 MPa excess to 0.08 MPa). The evidence thus points to additional condensation of the steam as the ceramic rings are heated.

Curves 2-4 (Fig. 4) show the pressure variation in the drum for the given temperature and for pipe diameters of 15, 10, and 6 mm respectively. The delay in the start of pressure rise (particularly noticeable for $D_y$ = 6 mm) is related to the heating of the pipe.

## LITERATURE CITED


1. B. A. Dement'ev, V. L. Kuznetsov, and B. A. Ionov, Tr. Mosk. Energ. Inst., No. 81, Moscow Power Engineering Institute (1971), p. 100.
2. B. A. Dement'ev, V. L. Kuznetsov, and B. A. Ionov, Tr. Mosk. Energ. Inst., No. 200, Moscow Power Engineering Institute (1974), p. 74.
3. B. G. Gordon and B. K. Mal'tsev, Teploenergetika, No. 8, 62 (1975).
4. G. Leisther, B. Rudiger, and M. Zimmerman, Atomwirtschaft, 15, No. 5, 235 (1970).
5. G. Ashorth and D. Barton , Nucl. Eng., 7, No. 75, 313 (1962).
6. A. V. Alferov, V. V. Fisenko, and A. D. Shcherban', At. Energ., 41, No. 6, 413 (1976).
7. B. G. Gordon, B. K. Mal'tsev, and S. N. Bogdan, Teploenergetika, No. 10, 81 (1975).
8. B. G. Gordon, B. K. Mal'tsev, and S. N. Bogdan, ibid., No. 2, 22 (1977).
9. A. A. Avdeev et al., ibid., No. 4, p. 28.
10. M. E. Deich, Engineering Gas Dynamics [in Russian], Énergiya, Moscow (1963).

# NONDESTRUCTIVE METHOD OF MEASURING THE ACTIVITY DISTRIBUTIONS OF SOURCES

V. N. Groznov, V. M. Kotov,
V. V. Paramonov, B. V. Sorokin,
and Yu. S. Cherepnin

UDC 621.039.546:543.52(0.88.8)

Measurements of the activity distributions of various sources by nondestructive methods are necessary in solving many practical problems of reactor and radiation engineering, radiology, and well radiometry. The application of $\gamma$ scanning with a collimated detector without allowance for the "inleakage" component and the shape of the distribution of the activity under measurement was described in [1]. When the inleakage is taken into account, it becomes necessary to solve a Fredholm integral equation of the first kind. In [2] Timonov and Tanana considered the method of reproducing the detailed distribution of the activity from the measured intensity of the $\gamma$ rays by finding an approximate solution of the Fredholm integral equation on the basis of the regularization method of Tikhonov [3]. Implementation of this method necessitates choosing a regularization parameter, simulating the process of recording, and calculating trial variants.

In the present paper we propose a method of transforming the Fredholm equation by writing the kernel of the equation in the form of a matrix of contribution coefficients which can be determined experimentally for a known source geometry with an accuracy that is sufficient for obtaining a steady-state solution in most cases.

Let us consider the measurement of the height component of the distribution of $\gamma$-ray activity in a cylindrical source. The relation between the specific activity $Q(z')$ of the source and the recorded $\gamma$-ray intensity $N(z)$ is written in the form of a Fredholm equation

$$N(z)=\int_0^H K(z, z')\,Q(z')\,dz', \tag{1}$$

where H is the height of the source and $K(z, z')$ is the detection efficiency for $\gamma$ rays created at the point $z'$ by a detector set up at the point z.

The integral of Eq. (1) will be rewriten as

$$N_i=\sum_{j=1}^{n} K_{ij}Q_j, \quad i=1, \ldots, n, \tag{2}$$

where $Q_j=\int_{(j-1)h}^{jh} Q(z')\,dz'$ is the activity of the j-th section when the source is divided into n parts, $h=H/n$; $K_{ij}=\frac{1}{Q_j}\int_{(j-1)h}^{jh} Q(z')\,K(z, z')\,dz'$ is the contribution coefficient which represents the detection efficiency for $\gamma$ rays from the j-th section when the detector measures the radiation intensity of the i-th section of the source.

The activity distribution over the source is found by solving the system of linear equations (2) which has $n^2$ coefficients $K_{ij}$. If the detection efficiency $K(z, z')$ depends only on the distance between the points z and $z'$, which is the case when the material of the source is symmetric about the axis of the collimator and uniform with respect to $z'$, then the number of different contribution coefficients is reduced to n. In practice, the number of significant coefficients is usually less than n, which substantially facilitates solution of the system (2). The contribution coefficients can be found experimentally by using a source with a known activity distribution and with the same $\gamma$-ray transfer characteristics as in the source under study.

---

Translated from Atomnaya Énergiya, Vol. 47, No. 2, pp. 118-119, August, 1979. Original article submitted June 20, 1978; revision submitted December 11, 1978.



0038-531X/79/4702-0652$07.50 

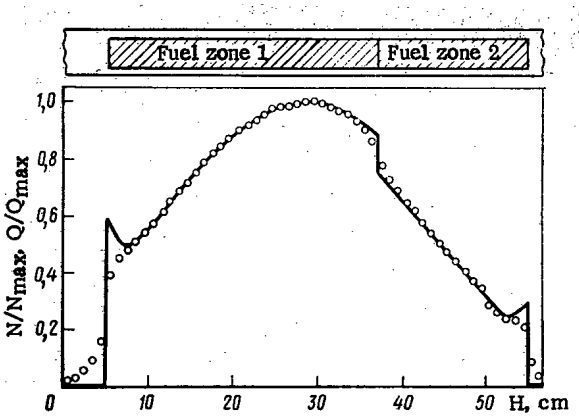


Fig. 1. Energy distribution over height of fuel channel: O) measured, ——) calculated by contribution method.

The method described here was used in practice in studying the energy distribution over the length of the fuel channels of a reactor. The contribution coefficients were determined with the aid of fuel channels with demountable fuel sections, one of which was irradiated in the uniform flux of the reactor. The counting rate for determining the contribution coefficients was measured near the interface between the irradiated and unirradiated sections of the fuel channel.

In the investigations it was possible to quite accurately determine the boundaries of the active zone of the fuel channel, to reveal the characteristic features of the energy distribution at the boundaries of the active zone resulting from the existence of end-type reflectors, and to more accurately determine the jump in the energy distribution at the boundary of zones with different concentrations of fissionable isotopes (see Fig. 1). The proposed method of establishing the distribution of activity by experimental measurements of the contribution coefficients is implemented quite simply in computer calculations and can be employed in solving a broad range of problems.

In conclusion, the authors thank V. M. Talyzin for assistance in discussions on the technique and results of measurements.

## LITERATURE CITED

1. V. V. Bychenkov et al., At. Energ., 38, No. 5, 299 (1975).
2. A. A. Timonov and V. P. Tanana, At. Energ., 43, No. 1, 49 (1977).
3. A. N. Tikhonov, Dokl. Akad. Nauk SSSR, 151, No. 3, 501 (1963).

# RADIAL MOTION OF PLASMA FILAMENT IN TOKAMAK THERMONUCLEAR MACHINE

V. S. Manuilov

UDC 621.039.623

One of the central problems in building tokamak thermonuclear reactors at the present time is that of ensuring insulation of the plasma filament from the walls of the discharge chamber. This problem is being tackled by developing a special system for stabilizing the parameters of the plasma filament. A system of this kind cannot be designed without an analysis of the dynamic properties of the individual elements comprising the thermonuclear reactors, including the plasma filament itself.

In [1-3], which dealt with the problems of the dynamics of plasma filaments, use was made of similar models of the plasma filament which were based on the following system of relations.

1. The equation of the balance of forces acting on the plasma filament in the horizontal plane.

2. The relation between the discharge current i and the major radius r of the plasma filament [$i_2 = i_1(r_2/r_1)^{\mu}$ for $-1 \leq \mu \leq 0$] is a consequence of the condition of the conservation of the poloidal magnetic flux through the circuit formed by the plasma filament.

3. The ratio between the major and minor radii, r and $a$, of the plasma filament [$a_2 = a_1(r_2/r_1)^l$ for $l = 0.5$] is a consequence of the condition of the conservation of the toroidal magnetic flux in the plasma filament. (Subscripts 1 and 2 refer to different states of the plasma filament.)

Furthermore, the system of relations was taken to include the balance equation for voltages in some structures of the machine and account was taken of the mutual inductive coupling of these structures. In this case the interaction of the plasma-filament current with the vertical component $b_V$ of the magnetic field was considered.

The plasma filament model based on the above relations is correct for plasma filaments with a small slope ($a/r \ll 1$). The relations listed above do not take account of the ohmic resistance present in the filament and the total poloidal magnetic flux setting up an eddy-current emf in the circuit of the plasma filament. The purpose of the present paper is to study the properties of the plasma-filament model.

Equations of Plasma-Filament Dynamics. Linearization of the Equations. Schematic Diagrams of Plasma Filaments. The equation of balance for voltages in the plasma-filament circuit is of the form

$$\frac{d\Psi_i}{dt} + U = \frac{d\Psi_e}{dt}, \tag{1}$$

where $\Psi_i = L_i$ is the flux linkage due to its inductive properties, $\Psi_e$ is the flux linkage of the plasma filament as the result of currents flowing in the elements of the machine construction, $U = U(i)$ is the voltage drop across the active resistance of the plasma filament, the magnitude of this drop depending on the discharge arc current,

$$L_i = \mu_0 r \left(\ln \frac{8r}{a} - 2 + \frac{l_i}{2}\right) \tag{2}$$

is the inductance of the plasma filament [4], $l_i$ is the internal inductance of the plasma filament, hereafter assumed to be constant, and $\mu_0 = 1.256 \cdot 10^{-6}$ (H/m).

The equivalent electrical circuit of the plasma filament, shown in Fig. 1, corresponds to Eq. (1). The result of linearization of Eq. (1) with allowance for Eq. (2) and $\Psi_e = \Psi_e(r, t)$ with subsequent application of the Laplace transform is of the form

Translated from Atomnaya Énergiya, Vol. 47, No. 2, pp. 119-122, August, 1979. Original article submitted June 20, 1978.



0038-531X/79/4702-0654$07.50 

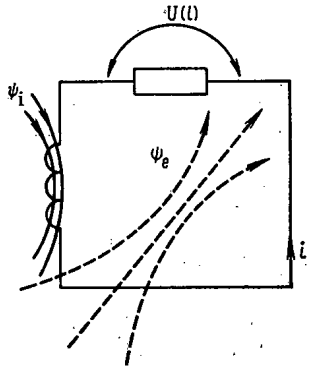


Fig. 1. Equivalent electrical circuit of plasma filament.

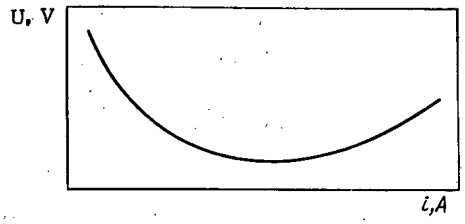


Fig. 2. Current–voltage characteristic of active resistance of plasma filament [$R_d^0 = (\partial U/\partial i)^0$].

$$\delta i = [k_1/(\tau_1 p+1)]\,[k_2\delta a+(k_3-k_4)\,\delta r+\delta\Psi_e(r^0,\ t)]\,p, \tag{3}$$

where $\delta i$, $\delta r$, $\delta a$, and $\delta\Psi_e(r^0, t)$ are the increments of the corresponding variables, $k_1 = 1/R_d^0$, $k_2 = \Psi_i^0/(w^0 a^0)$, $k_3 = (\partial\Psi_e/\partial r)^0 = 2\pi r^0 b_V^0$, and $k_4 = (1 + 1/w^0)\Psi_i^0/r^0$ are the coefficients of the transforms, $\tau_1 = L^0/R_d^0$ is the electrotechnical time constant of the plasma filament, $w^0 = \ln(8r^0/a^0) - 2 + l_i/2$, $R_d^0 = (\partial U/\partial i)^0$ is the dynamic resistance, which is determined by the slope of the current–voltage characteristic of the active resistance of the plasma filament at the operating point (Fig. 2), and $p = d/dt$. (The superscript 0 denotes the parameters of the plasma filament in the equilibrium state, relative to which the linearization is carried out.)

The balance equation for the forces acting on the plasma filament in the horizontal plane is of the form

$$M\frac{d^2r}{dt^2} = \frac{\mu_0 i^2}{2}z - 2\pi r i b_V\ , \tag{4}$$

where $M = 2\pi^2 r_L a_L^2$ Nm is the mass of the plasma filament; m, molecular mass of the gas; $z = \ln(8r/a) + \beta + (l_i - 3)/2$; N, concentration of molecules of the original gas in the liner; $\beta$, ratio of the mean gas-kinetic pressure in the plasma filament to the pressure of the poloidal magnetic field of the discharge current; and $r_L$ and $a_L$, major and minor radii of the liner. Henceforth, $\beta$ will be assumed to be constant.

The first term on the right-hand part of Eq. (4) represents the radial forces, which increase the major radius of the plasma filament [4], while the second term represents the force of the interaction of the plasma-filament current with the vertical component $b_V$ of the external magnetic field.

The distribution of the vertical component of the magnetic field in the XY plane (Fig. 3) is described approximately by

$$b_V = b_V^0\,(r/r^0)^n, \tag{5}$$

where $n < 0$ is the coefficient of decay of the vertical magnetic field.

Linearization of Eq. (4) with account for Eq. (5) with the subsequent application of the Laplace transform leads to

$$\delta r = (\tau_2^2 p^2+1)^{-1}\,(k_5\delta b_{VL} - k_6\delta i + k_7\delta a), \tag{6}$$

where $\delta b_{VL}$ is the increment in the vertical magnetic field at the center of the liner, $\tau_2 = (Mr^0/F^0|G|)^{0.5}$ is the time constant of the plasma filament owing to its mass, $k_5 = r^0/(1 + |n|\Delta^0/r^0)b_V^0 G$, $k_6 = r^0/i^0 G$, $k_7 = r^0/a^0 z^0 G$ are the transform coefficients, $b_V^0 = \mu_0 i^0 z^0/4\pi r^0$ and $F^0 = 2\pi r^0 i^0 b_V^0$, $G = -n - 1 + 1/z^0$ and $\Delta^0 = r^0 - r_L$.

Equation (6) was obtained with the assumption that the inequality $(r^0 - r_L)/r^0 \ll 1$ is satisfied.

The condition for the conservation of the toroidal magnetic flux in the plasma filament is of the form

$$b_T a^2 = \text{const}, \tag{7}$$

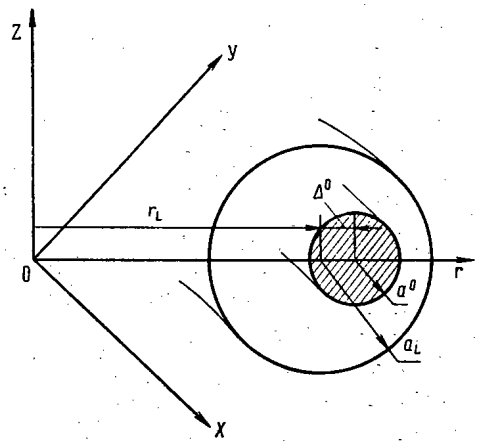


Fig. 3. Coordinate system.

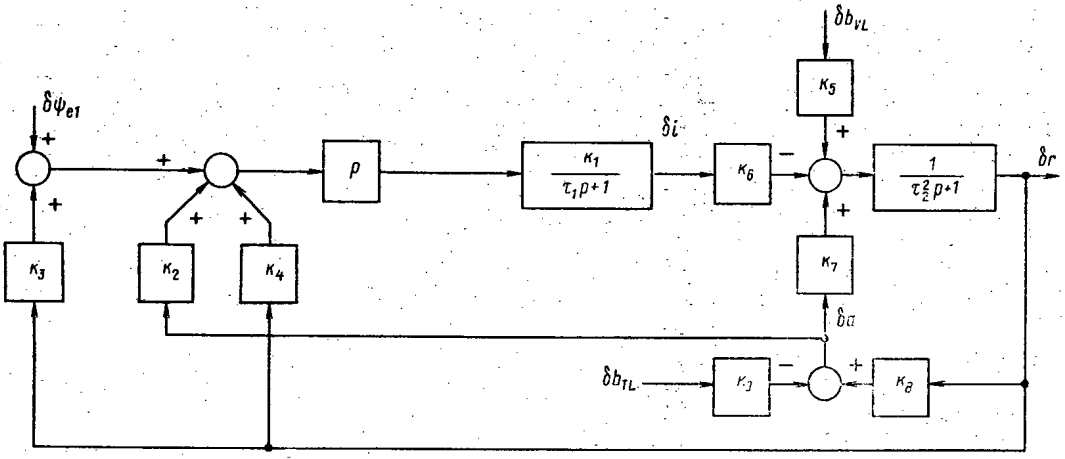


Fig. 4. Block diagram.

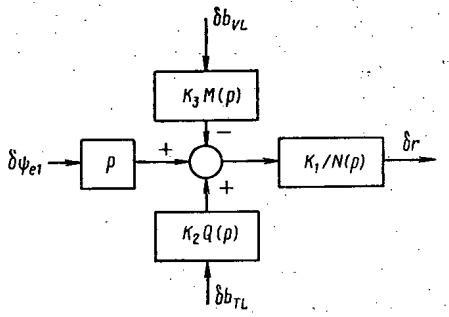


Fig. 5. Transformed block diagram of plasma filament.

where $b_T$ is the value of the induction of the toroidal magnetic field at the center of the cross section of the plasma filament.

When the well-known relation $b_T = b_{TL} r_L / r$ Eq. (7) after linearization can be rewritten as

$$\delta a = k_8 \delta r - k_9 \delta b_{TL}, \tag{8}$$

where $k_8 = a^0/2r^0$ and $k_9 = a^0/2b_T^0$.

The block diagram of the plasma-filament model, with account for Eqs. (3), (6), and (8), is shown in Fig. 4.

Analysis of Plasma-Filament Stability. Reaction of Plasma Filament to Perturbations. Solving the system of Eqs. (3), (6), and (8) for $\delta r$, we get

$$\delta r = [K_1/N(p)]\,[K_2 Q(p)\,\delta b_{TL} - K_3 M(p)\,\delta b_{VL} + p\delta\Psi_{e1}], \tag{9}$$

where

$$K_1 = -k_1k_6/(1-k_7k_8);\quad K_2 = k_7k_9/k_1k_6;$$
$$K_3 = k_5/k_1k_6;$$
$$N(p) = A_3p^3 + A_2p^2 + A_1p + 1;$$
$$M(p) = \tau_1 p + 1,\quad Q(p) = bp + 1;$$
$$A_1 = \tau_1 + (k_3 - k_4 + k_2k_8)\,k_1k_6/(1-k_7k_8);$$
$$A_2 = \tau_2^2/(1-k_7k_8);\quad A_3 = \tau_1\tau_2^2/(1-k_7k_8);$$
$$b = \tau_1 - k_1k_2k_6/k_7.$$

The block diagram corresponding to Eq. (9) is shown in Fig. 5.

It can be shown that the stability condition for this expression, in accordance with the Hurwitz criterion, consists in satisfaction of the inequalities

$$n > -1 + 1/(2z^0); \tag{10}$$
$$R_d^0 > 0; \tag{11}$$
$$(\partial\Psi_s/\partial r)^0 < 0, \tag{12}$$

where $\Psi_S = \Psi_e - \Psi_i$.

Condition (10) is much the same as that obtained in [1]. Condition (11) means that the stability of the plasma filament is possible only on that branch of the current–voltage characteristic of its active resistance which has a positive slope. Condition (12) means that for the stability of the plasma filament it is also necessary that the resulting flux linkage $\Psi_S$ through the plasma-filament circuit diminish with an increase in the major radius of the filament.

In the approximation of $\omega \gg \sigma_1$ and $\omega \gg \sigma_2$ the change in the major radius of the plasma filament under a jump increment in the vertical magnetic field, $\delta b_{VL} = kf b^0_{VL} h(t)$, is of the form

$$\delta r(t) \approx \delta r_\infty [1 + (-1+R)\,e^{-\sigma_1 t} - R\,e^{-\sigma_2 t}\cos\omega t], \tag{13}$$

where kf is a coefficient specifying the increment $\delta b_{VL}$, $h(t) = 0$ for $t < 0$ and $h(t) = 1$ for $t \geq 0$ is a unit step function, $\delta r_\infty = -kf b^0_V K_1 K_3$ is the steady-state value of the increment in the major radius of the plasma filament, $\omega$ is the angular velocity of the natural oscillations of the plasma filament, $R = \tau_1/\omega^2 A_3$ is the normalized amplitude, and $\sigma_1$ and $\sigma_2$ are the attenuation factors for the aperiodic and periodic components, respectively, of the transient process.

Numerical Estimates. Analysis of the Plasma-Filament Motion. Below are numerical estimates of the expressions obtained above, as calculated for the nominal operating modes of two machines:

| | Tuman-3 | T-10M |
|---|---|---|
| $i^0$, kA | 170 | $1.6\cdot10^3$ |
| $r^0$, m | 0.55 | 2.3 |
| $a^0$, m | 0.24 | 0.75 |
| $l_i^0$ | 0.5 | 1 |
| $\beta$ | 0.36 | 1 |
| $U^0$, V | 2.5 | 1 |
| $b^0_{TL}$, T | 1 | 3.5 |
| $n$ | 0.5 | —0.5 |
| $k_1$, $\Omega^{-1}$ | $0.68\cdot10^5$ | $1.61\cdot10^6$ |
| $k_2$, Wb/m | 0.489 | 6.2 |
| $k_3$, Wb/m | 0.216 | 3.24 |
| $k_4$, Wb/m | 0.461 | 5.46 |
| $k_5$, m/T | $-0.19\cdot10^4$ | —52.48 |
| $k_6$, m/A | $-0.698\cdot10^{-3}$ | $-0.762\cdot10^{-5}$ |
| $k_7$ | —245 | —5.11 |
| $k_8$ | 0.218 | 0.163 |
| $k_9$, m/T | 0.120 | 0.107 |
| $A_1$, $\sec_4$ | 0.175 | 16.0 |
| $A_2$, $\sec^2$ | $0.124\cdot10^{-10}$ | $0.109\cdot10^{-10}$ |

| | | |
|---|---|---|
| $A_3$, $sec^3$ | $0.676 \cdot 10^{-12}$ | $0.866 \cdot 10^{-10}$ |
| $K_1$, m/V | 0.872 | 6.69 |
| $K_2$, V/T | 0.619 | $0.446 \cdot 10^{-1}$ |
| $K_3$, V/T | 40.0 | 4.28 |
| $\sigma_1$, $sec^{-1}$ | 5.71 | $0.624 \cdot 10^{-1}$ |
| $\sigma_2$, $sec^{-2}$ | 6.33 | $0.320 \cdot 10^{-1}$ |
| $\omega$, $sec^{-1}$ | $0.509 \cdot 10^6$ | $0.430 \cdot 10^6$ |
| $R$ | 0.311 | 0.494 |
| $\tau_1$, sec | $0.544 \cdot 10^{-1}$ | 7.91 |
| $\tau_2^2$, $sec^2$ | $0.676 \cdot 10^{-9}$ | $0.2 \cdot 10^{-10}$ |

From these data as well as from Eq. (13) for the transient process it is seen that the motion of the plasma filament from one equilibrium position to another is advisably considered to consist of two stages: a practically instantaneous transposition of the plasma filament to an intermediate position with a relative amplitude R and a relatively slow transposition, accompanied by oscillations, to a new equilibrium position with a relative amplitude equal to unity.

The initial transposition R, as well as the attenuation factors $\sigma_1$ and $\sigma_2$, characterizing the degree of inertia of the plasma filament, are highly dependent on its initial parameters.

Conclusions. The present paper gives the results of the elaboration of a mathematical model of the radial motion of the plasma filament in tokamak thermonuclear machines with account for its ohmic resistance as well as the total flux linkage of the circuit formed in the plasma filament. At the same time, no account was taken of the effect of the metallic structures of the machine on the radial motion of the plasma filament. A significant limitation on the applicability of this model is the requirement of a small slope for the plasma filament ($a/r \geq 1$). Under these conditions it has been shown that the motion of the plasma filament from one equilibrium position to another under a change in the vertical magnetic field is of a complex nature. The parameters of the elements of the motion depend markedly on the initial characteristics of the plasma filament.

Analysis of the plasma-filament model for stability led to easily interpreted conditions, one of which had been known earlier. For present-day tokamak machines whose plasma filament has a high slope ($a/r \geq 1/3$) the results of the study can be rather of a qualitative than a quantitative character. In the case of experimental confirmation of the properties, however, it is desirable to use the present model in designing systems for stabilizing the parameters of the plasma filament and in modern tokamak thermonuclear machines.

## LITERATURE CITED

1. J. Hugill et al., Nucl. Fusion, 14, 611 (1974).
2. M. Fugiwara et al., J. Appl. Phys., 14, No. 5, 675 (1975).
3. U. Sudzuki et al., JAERI-M-6050, Tokai, Ibaraki.
4. V. D. Shafranov, Problems of Plasma Theory [in Russian], Vol. 2, Gosatomizdat, Moscow (1963).

# OPTIMAL FLATTENING OF TWO-DIMENSIONAL ENERGY DISTRIBUTION

R. A. Peskov

UDC 621.039.51

We consider a cylindrical reactor of radius $R-\delta$ and height $2(H-\delta)$, where $\delta$ is the augmentation distance. The initial equations are of the form

$$\Delta\varphi+\varkappa^2\varphi=0; \quad \varkappa^2=k^\infty-1; \qquad \varphi(-z, r)=\varphi(z, r); \quad \varphi(H, r)=\varphi(z, R)=0, \tag{1}$$

where z, r are the cylindrical coordinates measured in units of neutron migration length (z = 0, r = 0 is the center of the reactor), and $\varphi(z, r)$ is the one-group neutron flux. It is assumed that the material parameter $\varkappa^2$ and the neutron-multiplication factor $k^\infty$ depend on the coordinates whereas the transport cross section and the neutron migration length do not. The energy-distribution density $q = k^\infty\varphi$ is determined by profiling $k^\infty$. The problem consists in finding the function $k^\infty(z, r)$, with the constraint $k^\infty \le k^\infty_m$, which minimizes the coefficient of volume nonuniformity of the energy distribution:

$$K_v=(R-\delta)^2(H-\delta)\max_{z, r} q(z, r)\Big/\int_0^{R-\delta}\int_0^{H-\delta} 2rq(z, r)\,dz\,dr. \tag{2}$$

We consider the case of separation of variables:

$$\varkappa^2(z, r)=\lambda_1^2(z)+\lambda_2^2(v); \quad \varphi(z, r)=\psi_1(z)\psi_2(r); \tag{3}$$

$$\frac{d^2\psi_1}{dz^2}+\lambda_1^2\psi_1=0; \qquad \left.\frac{d\psi_1}{dz}\right|_{z=0}=\psi_1(H)=0; \tag{4}$$

$$\frac{d^2\psi_2}{dr^2}+\frac{1}{r}\frac{d\psi_2}{dr}+\lambda_2^2\psi_2=0; \qquad \psi_2(R)=\left.\frac{d\psi_2}{dr}\right|_{r=0}=0, \tag{5}$$

where $\lambda_i^2\Psi_i$ is, respectively, the component of the material parameter and the neutron flux distribution with respect to the i-th coordinate (i = 1 ~ z, i = 2 ~ r). In this case, the energy distribution can be written as:

$$q(z, r)=f_1(z)f_2(r)W(z, r); \quad W=1-\lambda_1^2\lambda_2^2/(k_1^\infty k_2^\infty); \tag{6}$$

$$k_i^\infty=1+\lambda_i^2; \quad f_i=k_i^\infty\psi_i; \quad i=1, 2, \tag{7}$$

TABLE 1. Continuous and Two-Step Optimal Profiling of One-Dimensional Reactors (R = H = 7; $\delta$ = 1.2)

| i | $k^\infty_{i,m}$ | Continuous | | Two-step | | |
|---|---|---|---|---|---|---|
| | | $b$ | $g_i^0$ | $b_{i,1}$ | $k^\infty_{i,1}$ | $g_i^0$ |
| 1 | 1,16 | 4,02 | 1,072 | 3,52 | 1,02 | 1,123 |
| | 1,12 | 3,50 | 1,110 | 2,99 | 1,02 | 1,148 |
| | 1,08 | 2,41 | 1,188 | 2,11 | 1,02 | 1,212 |
| 2 | 1,28 | 4,54 | 1,091 | 4,01 | 1,05 | 1,190 |
| | 1,20 | 3,77 | 1,192 | 3,28 | 1,05 | 1,266 |
| | 1,16 | 3,06 | 1,304 | 1,64 | 1,05 | 1,361 |

Translated from Atomnaya Énergiya, Vol. 47, No. 2, pp. 122-123, August, 1979. Original article submitted July 4, 1978.

0038-531X/79/4702-0659$07.50 

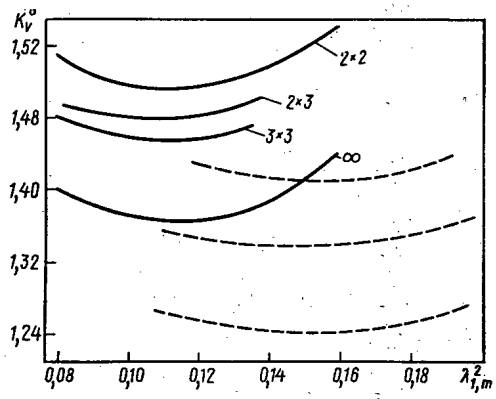


Fig. 1. Dependence of $K_V^0$ on $\lambda^2_{1,m}$ for various cases of synthesis of flattened two-dimensional energy distribution (R = H = 7, $\delta$ = 1): ∞) continuous profiling; $l_1 \times l_2$) number of zones over height ($l_1$) and over radius ($l_2$), $l_1$ = 2, 3, $l_2$ = 2, 3; ——) $k^\infty_m$ = 1.33; – – – –) $k^\infty_m$ = 1.42.

where $f_1(z)$ and $f_2(r)$, respectively, are the energy-distribution curves in the plane problem (4) and radial problem (5) with multiplication factors $k_1^\infty(z)$ and $k_2^\infty(r)$.

If $k^\infty \leq 1.33$, then $1 - W \leq 0.002$ and with an accuracy acceptable for practice it can be assumed that W = 1 and $K_V = g_1 g_2$, where $g_1$ and $g_2$, respectively, are the coefficients of nonuniformity of energy distribution over the height and radius (to be more precise, over the base), obtained in problems (4) and (5). In the case of separation of variables, flattening q(z, r) requires flattening of the distributions $f_1(z)$ and $f_2(r)$. The minimized value $g_i^0$ of the coefficient $g_i$, i = 1, 2, is determined with a given method of profiling the largest $k^\infty_{i,m}$ of the coefficient $k^\infty_i$, or, what amounts to the same thing, $\lambda^2_{i,m} = k^\infty_{i,m} - 1$. The limitation $k^\infty_m = 1 + \lambda^2_{1,m} + \lambda^2_{2,m}$ (the equivalent $k^\infty_{1,m} + k^\infty_{2,m} = k^\infty_m + 1$) indicates that the coefficient of nonuniformity, $K_V^0 = g_1^0 g_2^0$, is a function of, e.g., only $\lambda^2_{1,m}$ (or $k^\infty_{1,m}$).

A distinction is made between continuous and stepped (zonal) optimal profiling of the multiplication factor. In the problems under consideration, a continuous distribution of the energy release with a maximum value constant over the central region of the reactor corresponds to the first case. In the second case, the flattened energy distribution curve $f_1(z)$ or $f_2(r)$ suffers a discontinuity at the zone boundaries where, as a rule, it has the same maximum density of energy distribution as at the center. With continuous flattening, the relations $k_1(z)$ and $k_2(r)$ within the limits of the central region are of the form

$$k_i^\infty(x) = [1 - y_i(x)(1 - 1/k^\infty_{i,m})/y_i(b)]^{-1}, \quad x \leqslant b;$$

$$\text{plate} \quad -i = 1,\ y_1(x) = \operatorname{ch} x, \quad x = z;$$

$$\text{cylinder} \quad -i = 2,\ y_2(x) = I_0(x), \quad x = r,$$

where $I_0$ is a zeroth-order modified Bessel function. The coordinate b is determined by the condition of criticality which is obtained from the requirement of continuity of the neutron flux and current at the boundary of the region ($x \geq b$, $k^\infty_i(x) = k^\infty_{i,m}$). The results of calculations on the flattening of a one-dimensional energy distribution are given in Table 1, where $b_{i,1}$, $k^\infty_{i,1}$ ($i \leq 2$) are, respectively, the coordinate of the outer boundary and the multiplication factor of reactor zone 1 of type i.

The case of the separation of variables makes it possible to examine a large number of two-dimensional fields q(z, r), synthesized in terms of the flattened one-dimensional fields $f_1(z)$ and $f_2(r)$ in accordance with Eqs. (4)-(7). Examples of the dependence of the coefficient of volume nonuniformity, $K_V^0 = g_1^0 g_2^0$, on the height component of the material parameter of the outer "corner" zone ($\varkappa^2_m = \lambda^2_{1,m} + \lambda^2_{2,m} = \text{const}$) are given in Fig. 1 for various methods of profiling a cylindrical reactor of infinite height. An increase (decrease) in $\lambda^2_{1,m}$ leads to a decrease (increase) in $g_1^0$ and is accompanied by opposite changes in $\lambda^2_{2,m}$ and $g_i^\infty$, respectively, which explains the presence of the minimum in $K_V^0(\lambda^2_{1,m})$. A reduction of $k^\infty_m$ makes the optimum more distinct. For a minimum at H/R = 0.95 ± 0.05 (using the example of several reactors) the following relations were found:

$$\lambda^2_{1,m} = \lambda^2_{2,m}/2; \quad k^\infty_{1,m} = k_m/3 + {}^2/_3, \quad k^\infty_{2,m} = 2k^\infty_m/3 + {}^1/_3.$$

They make it possible to find the profiling law $k^{\infty}(z, r) = k_1^{\infty}(z) + k_2^{\infty}(r) - 1$ and to synthesize the optimal two-dimensional energy distribution in terms of the tabulated solutions of one-dimensional flattening problems.

# X-RAY FLUORESCENCE ANALYSIS OF URANIUM IN WATER WITH RADIOISOTOPIC $\alpha$ SOURCES

S. M. Brodskii, S. V. Mamikonyan, and V. I. Filatov

UDC 543.422.8.002.5

X-ray fluorescent analysis of uranium in solutions with the excitation of photon radiation has a sensitivity of $10^{-3}$-$10^{-4}$% [1]. In the present paper we consider the use of radioisotopic $\alpha$ sources to determine the uranium content in water in the range of concentrations from $10^{-5}$ to $10^{-3}$%. The energy of the $\alpha$ particles from the sources does not exceed 5-6 MeV and the external flux is $10^8$-$10^9$ particles/sec. With such parameters of the exciting radiation high sensitivity can be attained only in analysis by the M series of the characteristic radiation of uranium [2].

The experimental apparatus is shown in Fig. 1. The measurements were carried out in a chamber filled with helium at a pressure close to atmospheric. Four sources based on $^{210}$Po with a total activity of 50 mCi excited characteristic radiation in the target, 1 cm from the active surface of the sources. The average energy of the $\alpha$ particles which traverse the hermetic film of the source is 4.9 MeV. All of the parts of the device on which $\alpha$ particles can impinge were made of Plexiglas. In order to reduce the background. The x radiation of the target was recorded with a Si(Li) detector with a beryllium window that was 8 $\mu$m thick and had a sensitive area of 12.5 mm$^2$. The distance between the target and the sensitive area of the detector was 2 cm. The detector and the spectrometric channel ensured an energy resolution of 170 eV at the 5.9-keV line. The x-ray spectra accumulated in the memory of a multichannel analyzer were processed on a computer. The pulse-height distribution was approximated by Gaussian functions and a fifth-degree polynomial. A program written in FORTRAN IV made it possible to find the number of pulses in each photopeak of the characteristic radiation. The time taken to process one spectrum on an ES-1033 computer was no longer than 20 sec. The relative intensity of the genuine spectral lines of the M series of uranium (Fig. 2) was determined on the basis of this program. The ratios of the intensity of the $M_\beta$, $M_\gamma$, and $M_\zeta$ lines to the intensity of the $M_\alpha$ line are 0.59, 0.06, and 0.05, respectively, without allowance for the detector efficiency.

The spectrometer was calibrated with solutions of uranyl nitrate $UO_2(NO_3)_2$ in distilled water. The analyzed targets were prepared by evaporating 1 ml of solution from a Dacron-type film 1 $\mu$m thick. The surface from which evaporation took place was in the form of a disk with an area of 1 cm$^2$. The uranium concentration in the water was chosen to be 0.5 to 10 $\mu$g/ml, which corresponds to a uranium content of $5 \cdot 10^{-7}$ to $10^{-5}$ g/cm$^2$ on the surface of the target. With a channel width of 40 eV in the multichannel analyzer this ensured the necessary accuracy in processing spectra in 2000 sec. The number of photons, $N_U$, in the peaks of the characteristic radiation of the uranium M series, recorded by the detector when $\alpha$ particles traverse a target containing $M_U$ g uranium/cm$^2$, can be calculated from

$$N_U = (6.02 \cdot 10^{23}/A_U)\,(\Omega/4\pi)\, n\sigma_U \omega_U \varepsilon_U M_U, \quad (1)$$

where $A_U$ is the mass number; $\sigma_U$, total ionization cross section (cm$^2$); $\omega_U$, fluorescence yield for the M shell of uranium; $\varepsilon_U$, registration efficiency of the detector; and $\Omega$, solid angle between the target and the detector. It is assumed that the distribution of the analyzed substance over the surface of the target is uniform and that the absorption of characteristic radiation in it can be neglected. The experimental dependence of $N_U$ on the uranium concentration is given in Fig. 3. The considerable scatter of the points about the linear calibration curve predicted by Eq. (1) indicates nonuniformity of the uranium distribution over the surface of the target. An effective way of taking account of the influence of the nonuniformity of the target is by means of the internal-standard method which is often used in x-ray fluorescence analysis with excitation by a proton beam [3, 4]. Sulfur was chosen as the element for the internal standard. The same quantity of a water-soluble sulfur com-

Translated from Atomnaya Énergiya, Vol. 47, No. 2, pp. 123-125, August, 1979. Original article submitted August 7, 1978.

0038-531X/79/4702-0661$07.50  

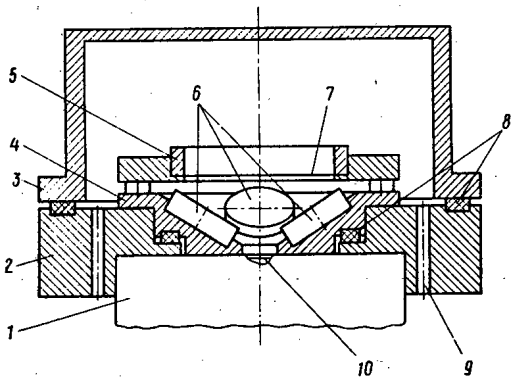


Fig. 1

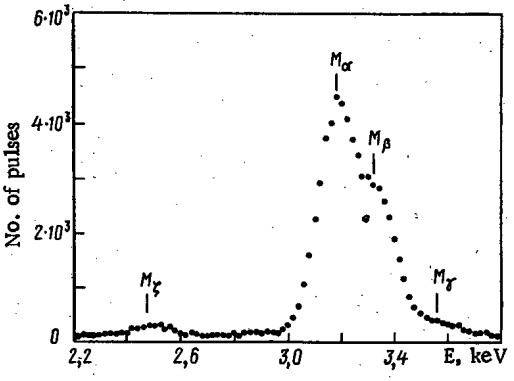


Fig. 2

Fig. 1. Diagram of measuring chamber: 1) head part of detector cryostat; 2) chamber base; 3) chamber cover; 4) source holder; 5) target holder; 6) alpha sources; 7) target; 8) hermetic seal; 9) helium inlet port; 10) detector window.

Fig. 2. Spectrum of characteristic M series radiation of uranium.

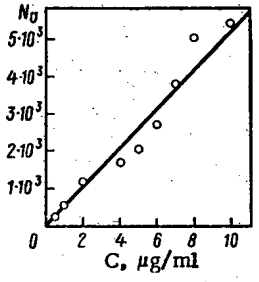


Fig. 3

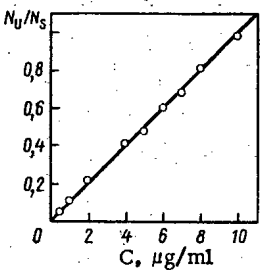


Fig. 4

Fig. 3. Dependence of number of pulses in uranium M-series peaks on the uranium concentration: O) experiment.

Fig. 4. Dependence of ratio of number of pulses in uranium M-series peaks to the number of pulses in the K-series peak of sulfur on the uranium concentration: O) experiment.

pound was added to all the solutions analyzed, the sulfur concentration being 1.16 μg/ml. Figure 4 shows the dependence of the ratio of $N_U$ to the number of pulses $N_S$ in the peak of the characteristic K-series radiation of sulfur on the uranium in solutions. The mean relative deviation of the experimental points from the calibration curve was reduced by a factor of about 10.

The unknown uranium content in the target can be found, if the ratio $N_U/N_S$ is known, from the formula

$$N_U = k\,(N_U/N_S)\,M_S, \tag{2}$$

where $M_S$ is the quantity of sulfur in the target. When account is taken of the fact that an expression similar to Eq. (1) is valid for $N_S$, we have

$$k = (A_U\sigma_S\omega_S\varepsilon_S)/(A_S\sigma_U\omega_U\varepsilon_U).$$

The cross sections were calculated for ionization by 4.9-MeV α particles of the K shell of sulfur in the Born approximation [5] and of the M shell of uranium in the momentum approximation [6]. For uranium, $\sigma$ = 35,520 b, $\omega$ = 0.045, $\varepsilon$ = 0.932 [7, 8], whereas for sulfur these values are 21,470, 0.0818, and 0.819, respectively. Substituting these values in Eq. (2), we get k = 7.19. The measured value of k is 8.75 ± 0.13. The divergence between the calculation and experiment is explained by the inaccuracy of the theoretical cross sections for ion-

TABLE 1. Uranium Content in Water, μg/ml

| Uranium concentration | | Potassium concentration | Uranium concentration | | Potassium concentration |
|---|---|---|---|---|---|
| given | meas. | | given | meas. | |
| 2,0 | 1,61 | 0,5 | 8,0 | 9,99 | 1,0 |
| 3,0 | 4,66 | 0,5 | 2,0 | 3,02 | 2,0 |
| 6,0 | 7,57 | 0,5 | 6,0 | 7,63 | 2,0 |
| 2,0 | 2,70 | 1,0 | 10,0 | 9,72 | 2,0 |
| 5,0 | 4,26 | 1,0 | | | |

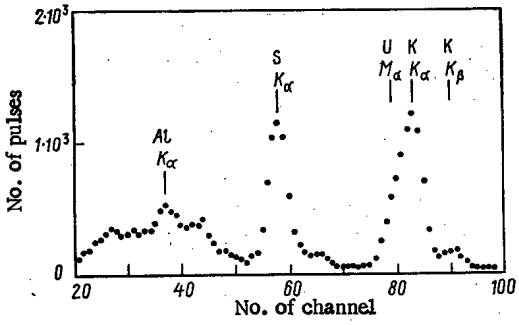


Fig. 5. X-ray spectrum of target containing 6 μg uranium and 2 μg potassium (the K peak of aluminum arises from the scattering of characteristic radiation by the hermetic seal of the source).

ization. Equation (2) does not contain the number of α particles which have traversed the target and, therefore, there is no need to introduce a correction for the decrease in the activity of the sources in view of the short half-life of $^{210}$Po.

One of the main advantages of the excitation of characteristic radiation by α particles in comparison with photons is the absence of a background of scattered radiation, thus making it possible to obtain high sensitivity of analysis. The sensitivity threshold, defined as the uranium content in the target at which the number of pulses in the Mα and Mβ peaks is equal to three times the rms error of measurement of the background under these peaks, is $6 \cdot 10^{-8}$ g/cm$^2$. Increasing the activity of the sources to 450 mCi will make it possible to reduce the sensitivity threshold by a factor of three. The main contribution to the background radiation comes from bremsstrahlung due to secondary electrons knocked out by α particles from shells of atoms in the target and from Compton scattering of γ rays of the $^{210}$Po decay products. With the assumption that the distribution of the scattered γ rays in the energy range from 3 to 6 keV does not depend on the energy, the contribution of bremsstrahlung due to secondary electrons is equal to 60% according to our estimates. The bremsstrahlung background can be reduced by choosing a thinner material for the substrate of the target.

The presence of admixtures of some elements in the water worsens the sensitivity and accuracy of the analysis because of the superposition of the peaks of characteristic radiation from these elements and uranium. A study was made of the effect of such contents of an interfering element, potassium, at which the ratio of the K peaks of potassium to the M peak of uranium is less than 5. The x-ray spectrum of one specimen is shown in Fig. 5. The energy difference between the Mβ line of uranium and the $K_\alpha$ line of potassium is 24 eV and the uranium and potassium can be separated by processing only if the relative intensity of the M-series lines of uranium is given. The uranium content in the water containing a potassium admixture was determined by the internal-standard method from Eq. (2) with k = 8.75 (see Table 1). The mean relative error of the measurements did not exceed 30%.

## LITERATURE CITED

1. R. Larsen and T. Karttunen, Adv. X-Ray Anal., 18, 62 (1975).
2. R. Hight and C. Foster, Adv. X-Ray Anal., 18, 333 (1975).

3. J. Campbell et al., Anal. Chem., 47, 1542 (1975).
4. K. Ishii et al., Phys. Rev., A11, 119 (1975).
5. G. Basbas et al., A7, 983 (1973).
6. J. Garcia et al., Rev. Mod. Phys., 45, 111 (1973).
7. W. Bambynek et al., 44, 716 (1972).
8. K. Ishii et al.. Nucl. Instrum. Methods, 126, 75 (1975).

# COMPARISON OF INCOMPLETE FACTORIZATION WITH VARIABLE DIRECTIONS IN SOLVING A ONE-GROUP TWO-DIMENSIONAL REACTOR EQUATION

P. N. Alekseev, N. I. Buleev, S. M. Zaritskii, V. A. Stukalov, and L. N. Usachev

UDC 539.125.52:621.039.51.12

Numerical calculations on the neutron physics of a multiparameter reactor model require optimization of the techniques for solving systems of linear algebraic equations of the form

$$\hat{A}\varphi = \mathbf{f}. \tag{1}$$

Numerical studies have shown [1] that the variable-directions method is one of the most effective iterative methods of solving (1) when the matrix $\hat{A}$ is symmetrical, and it is therefore desirable to compare that method with incomplete factorization, which is rapidly developing at the present time.

The basis for incomplete factorization [2, 3] is as follows. The initial equation is put as

$$(\hat{A}+\hat{B})\varphi = \mathbf{f}+\hat{B}\varphi. \tag{2}$$

Matrix $\hat{B}$ is selected such that $(\hat{A}+\hat{B})$ can be represented as the product

$$(\hat{A}+\hat{B}) = \hat{K}\hat{S}_1\hat{S}_2, \tag{3}$$

where $\hat{S}_1$ and $\hat{S}_2$ are matrices whose structure is simpler than that of $\hat{A}$, and which have unit elements on the principal diagonals; $\hat{K}$ is a diagonal matrix. Then (2) is replaced by the system

$$\begin{aligned} \hat{S}_1\mathbf{z} &= \hat{K}^{-1}[\mathbf{f}+\hat{B}\varphi]; \\ \hat{S}_2\varphi &= \mathbf{z}, \end{aligned} \tag{4}$$

which is solved by successive approximation.

There were no difficulties in using (4) when the shape of the two-dimensional or three-dimensional region is arbitrary and any boundary conditions are imposed on the function; it is only necessary to consider the difference approximations for the boundary conditions as independent equations on the same basis as equations of the type of (1) for internal nodes. In that respect, the incomplete-factorization method has advantages over the various forms of the variable-direction method, since the use of the latter becomes difficult if the boundary of the region is not parallel to the lines in the net.

The representation of (3) is possible for reactor problems for $\hat{B} = 0$ and if $\hat{S}_1 = \hat{S}_2^T$ (Kholetskii expansion [4]) we get a direct inversion of A. However, direct methods require large store volumes, and iterative methods are often preferable in practical cases. In incomplete factorization $\hat{B}$ can be put as $\hat{B} = \hat{D} - \hat{H}$, and the norm can be minimized by choosing $\hat{S}_1$ and $\hat{S}_2$, where that choice uniquely defines $\hat{D}$, or by choosing $\hat{H}$; if the latter is a diagonal matrix, we get diagonal compensation, whereas we get peripheral compensation if $\hat{H}$ differs from diagonal.

Translated from Atomnaya Énergiya, Vol. 47, No. 2, pp. 125-127, August, 1979. Original article submitted August 16, 1978.

 0038-531X/79/4702-0664$07.50 

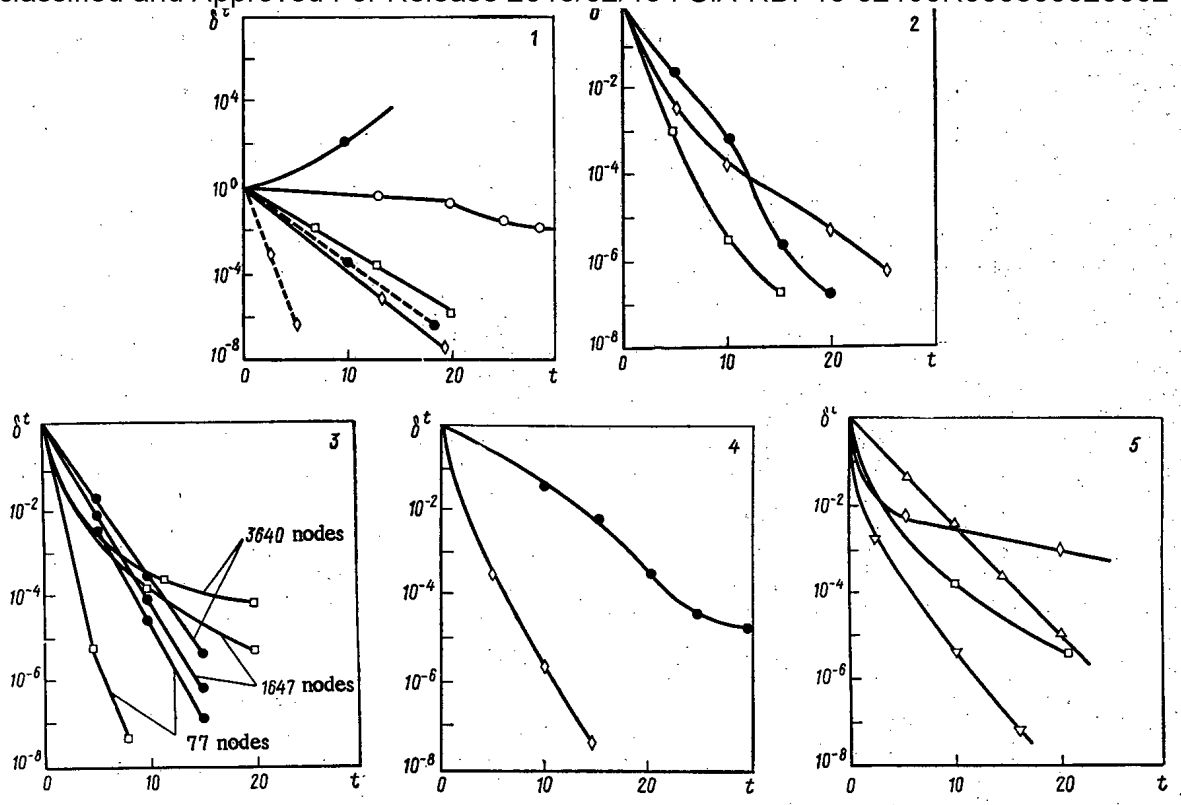


Fig. 1. Change in the error $\delta^t$ in the iterative process (t is the number of the iteration): ○) variable directions, accelerating parameters in decreasing order; ●) variable directions, accelerating parameters ordered by Lebedev's method; ◇) incomplete factorization, diagonal compensation; △) incomplete factorization, diagonal compensation, acceleration scheme of (5); ▽) incomplete factorization, diagonal compensation, Chebyshev acceleration; □) incomplete factorization, peripheral compensation; 1) BFS assembly (broken line – first model, 272 nodes; solid line – second model, 420 nodes, substantially nonuniform grid); 2) oxide breeder reactor (1887 nodes); 3) cell (various numbers of working nodes); 4) artificial model (361 nodes); 5) cell with 1647 nodes, effect of acceleration in accordance with (5).

A method has been given [5] for accelerating two-pass methods analogous to those based on (4) by formal application of extrapolation to each equation as follows:

$$\begin{aligned} z^{t+1} &= \omega_z [\hat{S}_1^{-1} \hat{K}^{-1} (f + \hat{B}\varphi^t)] - (\omega_z - 1) z^t; \\ \varphi^{t+1} &= \omega_\varphi [\hat{S}_2^{-1} z^{(t+1)}] - (\omega_\varphi - 1) \varphi^t, \end{aligned} \tag{5}$$

where t is the number of the iteration and $\omega_z$ and $\omega_\varphi$ are acceleration parameters, which are calculated from the empirical formula $\omega_z = \omega_\varphi = 1.19/(1.19 - 0.19\rho)$, where $\rho$ is the spectral radius of the iteration matrix for (5) for $\omega_z = \omega_\varphi = 1$.

The performance of the variable-directions method and of various forms of incomplete factorization has been examined on the following models, which have been described in detail elsewhere [1]: 1) one of the BFS critical assemblies; 2) on the same BFS assembly, in the center of which was a zone with a much smaller step in the finite-difference net; 3) a model for a fast reactor with oxide fuel producing 1000 MW; 4) a model for a cell in (x, y) geometry with strong coupling between the spatial variables; and 5) an artificial model that describes an operator with widely separated spectral boundaries: $\lambda_{max}/\lambda_{min} \sim 10^6$. Models 1, 2, 3, and 5 were calculated in (r, z) geometry. A method of numerical comparison for iterative methods for one-group problems has been described elsewhere [1].

Figure 1 shows some of the results, where we indicate the error $\delta^t = \max_{i,j} |\delta^t_{i,j}|$, where (i, j) is the number of the node in the finite-difference net.

The conclusions are as follows: 1) if the number of nodes is small (about 300), then incomplete factorization is always more effective than variable directions; 2) if the boundary conditions are of the second kind and the number of working parameters is more than 1000, then the convergence rate for incomplete factorization decreases considerably as the number of iterations increases; 3) in all the cases considered, incomplete factorization is more effective than variable directions in the first 5-10 iterations; 4) incomplete factorization is less sensitive to the spectral features of operator A than is the variable-direction method; and 5) the scheme of (5) gives an increase in the asymptotic rate of convergence of incomplete factorization with diagonal compensation. We have to note however that matrix $\hat{D}$ in incomplete factorization with diagonal compensation differs from the same with peripheral compensation.

These results indicate ways of improving incomplete factorization: optimization of the choice of $\hat{S}_1$, $\hat{S}_2$ and $\hat{H}$ and use of various acceleration methods. For example, the convergence rate at the start of the iteration can be increased considerably in the case of diagonal compensation of the acceleration (by Chebyshev's method), by permutation of the acceleration parameters, as has been suggested by Lebedev (the same applies in the asymptotic case), while for model 4 the same scheme reduces by a factor 2-3 the number of iterations required to reduce the error by a factor $10^3$ from that of the initial approximation (by comparison with incomplete factorization with peripheral compensation). It may prove promising to combine various methods, e.g., in multigroup calculations, where the one-group equations are solved by the incomplete factorization method in the first 5-7 iterations, after which the variable-direction method is applied.

## LITERATURE CITED

1. P. N. Alekseev, P. A. Bolobov, S. M. Zaritskii, and L. K. Shishkov, Papers on Programs and Methods for Physics Calculations on Fast Reactors [in Russian], COMECON, Dimitrovgrad (1975), p. 15.
2. N. I. Buleev, in: Numerical Methods in the Mechanics of Continuous Media [in Russian], Vol. 6, No. 3, Izd. Sib. Otd. Akad. Nauk SSSR (1975), p. 18.
3. N. I. Buleev, in: Numerical Methods in the Mechanics of Continuous Media [in Russian], Vol. 9, No. 1, Izd. Sib. Otd. Akad. Nauk SSSR (1978), p. 5.
4. J. H. Wilkinson and C. Reinsch, Linear Algebra, Vol. 2, Springer-Verlag (1971).
5. Z. Woznicki, in: Reactortagung Dusseldorf, Bonn (1976), p. 83.

# EXPERIMENTAL INVESTIGATION OF EFFECT OF LEAD AND BISMUTH MULTIPLICATION ZONES ON NEUTRON PARAMETERS OF MODEL OF LIQUID-SALT BLANKET OF THERMONUCLEAR REACTOR

V. M. Novikov, S. B. Shikhov, V. L. Romodanov, V. A. Zagryadskii, and D. Yu. Chuvilin

UDC 621.039.512.2

The principal purpose of blanket zones of thermonuclear reactors (TNR) is to utilize the energy of the thermonuclear neutrons as well as to produce tritium for "pure" TNR or tritium and fissionable nuclides for hybrid and symbiotic TNR systems. The choice of coolant and structural materials for the blankets of TNR determines their neutron-physical parameters. Melts of fluoride salts of lithium, beryllium, and heavy elements are among the promising working media for such blankets. Such liquid-salt blankets are under consideration for both "pure" [1] and hybrid TNR [2, 3].

For liquid-salt blankets, however, the contribution of the reaction $^7$Li(n, n')T to the total neutron balance is small. This is due to the substantial "softening" of the neutron spectrum as the result of inelastic scattering on fluorine nuclei. Thus, for a pure TNR with a liquid-salt blanket the coefficient of tritium production per thermonuclear neutron, $K_T$, can be only slightly greater than unity [2]. In order to compensate for this effect as well as to ensure additional production of fissionable nuclides in hybrid TNR multiplication zones can be introduced into the blanket. Such a zone is put behind the vacuum wall of the TNR, thus making it possible to use the fission of $^{232}$Th and $^{238}$U in the spectrum of thermonuclear neutrons or efficient multiplication of neutrons in the (n, 2n) reaction on such elements as beryllium and lead [4].

Translated from Atomnaya Énergiya, Vol. 47, No. 2, pp. 127-128, August, 1979. Original article submitted September 1, 1978; revision submitted December 27, 1978.

 0038-531X/79/4702-0667$07.50 

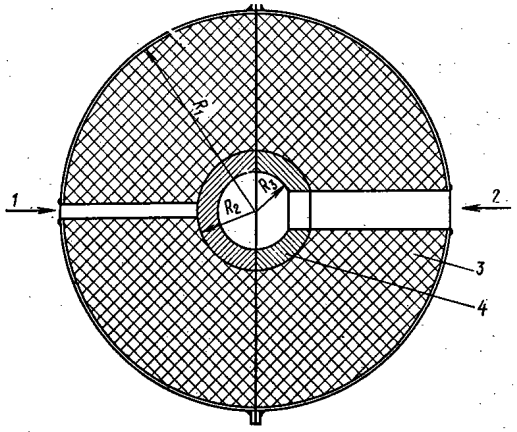


Fig.1. Structural model of liquid-salt TNR blanket: 1) experimental port; 2) port for source; 3) flibe; 4) lead or bismuth insert; $R_1$, $R_2$, $R_3$ have values of 200, 60, and 37 mm, respectively.

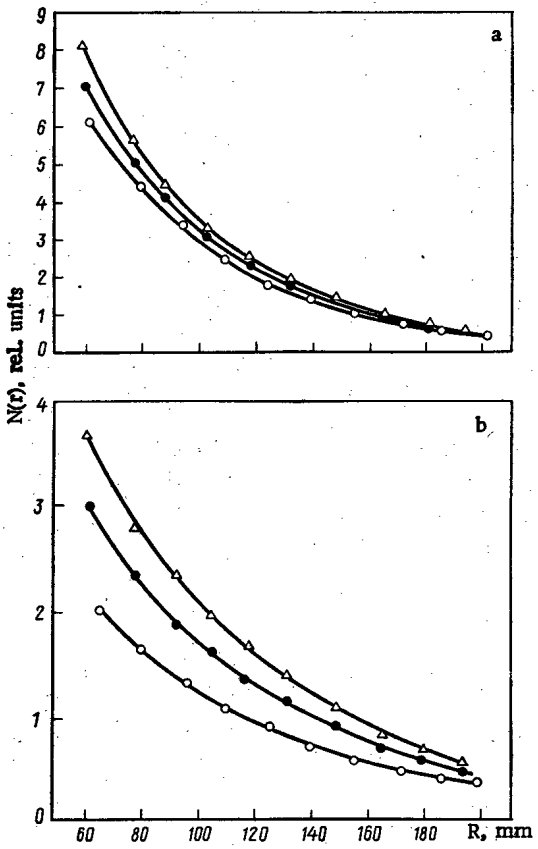


Fig. 2. Spatial distribution of fission rates of a) $^{232}Th$ and b) $^{235}U$: ○) salt; ●) salt–lead; △) salt–bismuth.

The present paper is the first of a series outlined in the substantiation of the program of research on a model of a liquid-salt TNR blanket on the T-20 device [5].

The experimental model of the liquid-salt blanket (Fig. 1) was a sphere of diameter 400 mm, filled with flibe (a eutectic mixture of fluorine salts of lithium and beryllium, LiF and $BeF_2$, in a 50:50 ratio in molar percent). The effect of the lead and bismuth multiplication zone on the neutron-physical parameters of the blanket model was studied in the experiment. The lead and bismuth multiplication zones were set up in the inner region of the model. The source of 14-MeV neutrons was a neutron generator making use of the D-T reaction.

The energy of the accelerated deuterons was 140 keV and the current in the target was 500 $\mu$A. The neutron yield was $\sim 10^{10}$ neutrons/sec. The titanotritium target had a diameter of 45 mm.

Small KNT-2 and KNT-5 pulsed fission chambers, containing $^{232}$Th and $^{235}$U, respectively, served as the neutron detectors. The source strength was calibrated by counting concomitant $\alpha$ particles; this made it possible to compare the results of experiments in a homogeneous sphere and in a sphere with multiplication zones.

The technique employed to study the blanket model consisted of measuring the $^{232}$Th and $^{235}$U fission rates, reduced to one neutron-source strength. The pertinent results are given in Fig. 2. As is seen from the plots, the introduction of multiplication zones results in an increase in the $^{232}$Th and $^{235}$U fission rates, with bismuth having a more pronounced effect than lead. The error of the fission-rate measurements at each point in space did not exceed 0.5%.

The experimental results were compared with calculations according to the BLANK program in a spherical geometry for a point source [6]. An analysis was made of the spatial distribution of the fission rate for a homogeneous salt moderator and for a salt–lead system. The fission rate was normalized to the corresponding value of the fission rate at a point in the center of the salt layer. The normalized point is least subject to the harmful effect of perturbations caused by the boundaries of the salt layer and its distance from the neutron source reduces the effect of its being an extended source.

Comparison of the calculation and experiment showed that there is satisfactory agreement of results at points which are quite far from the neutron source. At distances of less than 100 mm, however, the results differ appreciably. The probable cause of this divergence is that the neutron source and the fission chambers are extended and not pointlike.

By the method described in [7] a correction was made to the results of the experiment for the extended nature of the neutron source. Although the corrected results are much closer to the calculated values, the difference could not be compensated completely.

Besides the spatial distribution we also compared the relative contribution of the lead multiplication zone to the $^{232}$Th and $^{235}$U fission rates. The contribution of the lead multiplication zone was defined as the ratio of the fission rates of thorium and uranium in the salt–lead system to the corresponding fission rates in the homogeneous model. Comparison of the spatial relations of these ratios, measured in the experiment and calculated according to the BLANK program, shows the results to be close to each other. The absolute values of these ratios, however, are different. For $^{235}$U the experimental values are below the calculated values by 10%, on average, whereas for $^{232}$Th they are higher by 15%, on average. The possible reason for the difference may lie in the inaccuracy of the constants used. In order to arrive at the final conclusion it is necessary to perform a series of experiments with neutron detectors providing more detailed information about the neutron spectrum. Activation indicators could be used as such detectors.

## LITERATURE CITED

1. Fusion Power Technology at ORNL, Report ORNL (1974).
2. V. L. Blinkin and V. M. Novikov, Nucl. Fusion, 18, 893 (1978).
3. L. M. Lidsky, Nucl. Fusion, 15, 151 (1975).
4. S. S. Rozhkov and G. E. Shatalov, in: Proc. Symp. on Fusion–Fission Reactors, Livermore (1976), p. 143.
5. V. A. Glukhikh, I. A. Monoszon, and T. F. Churakov, NIIÉFA Preprint B-0319, Leningrad (1976).
6. S. V. Marin, G. E. Shatalov, and D. V. Markovskii, Preprint IAÉ-2832 (I. V. Kurchatov Institute of Atomic Energy), Moscow (1977).
7. J. Wade, Nucl. Sci. Eng., 4, 12 (1958).

# SEVENTIETH BIRTHDAY OF NIKOLAI NIKOLAEVICH BOGOLYUBOV

The eminent Soviet theoretical physicist and mathematician Academician Nikolai Nikolaevich Bogolyubov was born in Nizhni Novgorod (now the city of Gorki) on Aug. 21, 1909. His scientific activity began at an early age; at the age of 13, in Kiev, he began to work in a seminar directed by Academician N. M. Krylov, and in 1924 he wrote his first scientific paper. His early work, which was carried out jointly with Academician N. M. Krylov, was distinguished by a high degree of talent and mathematical depth, and one of his original works on the development of direct methods for solving extremal problems was honored by the award of a prize by the Bologna Academy of Science.

Starting in 1932 N. N. Bogolyubov (in collaboration with Academician N. M. Krylov) began to develop a new area of mathematical physics – the theory of nonlinear oscillations – which they called nonlinear mechanics. Nikolai Nikolaevich overcame fundamental mathematical difficulties in creating an apparatus which was able to effectively describe the behavior of general nonconservative systems, and developed new asymptotic methods of nonlinear mechanics on the basis of a rigorous mathematical foundation. He succeeded in applying to statistical mechanics the ordinary methods of perturbation theory which were developed in nonlinear mechanics, and obtained results which determined the subsequent development of this science. In his monograph Several Statistical Methods in Mathematical Physics, Nikolai Nikolaevich considered the general problem of formulating a stochastic Markov process in a dynamical system and showed that it is possible to apply the methods of the theory of Markov processes for large-scale times. He showed that depending on the choice of a time scale in the appropriate approximations, one and the same random process could be considered either as dynamic, Markovian, or as a certain non-Markov process. It was here that for the first time the idea of a hierarchy of time in statistical physics was expressed and realized, with which are associated the subsequent developments of the statistical theory of irreversible processes.

N. N. Bogolyubov created the most effective method in the statistical mechanics of classical systems. This is the method of chains for the distribution functions of complex particles, known in the world literature as the method of Bogolyubov–Born–Green–Kirkwood–Ivon. The method of solving chains of equations for distribution functions is based on the idea of a hierarchy of relaxation times. For example, in the case of low density or the Coulomb interaction, the solutions are in the form of expansions in powers of small parameters – the density or the reciprocal Debye radius. Under certain conditions of synchronization of the distribution functions, the chain of equations decouple and the kinetic equations can be derived to any approximation with respect to the density. If the Boltzmann kinetic method is based on the assumption of molecular chaos, the basis of the Bogolyubov method lies in taking into account the possibility of the existence of correlations and also the higher expansions in powers of the density. N. N. Bogolyubov showed that in the evolution of the distribution functions over times much larger than the mean free time, such a hydrodynamic stage sets in when the time dependence of the single-particle distribution function enters only through macroscopic parameters: the mean particle density, the mean velocity, and the mean internal energy. For this stage, the hydrodynamic equations can be constructed directly from the Liouville equation, omitting the kinetic energy. This idea had a great influence on the subsequent development of the theory of nonequilibrium processes.

N. N. Bogolyubov also obtained important results in the field of quantum statistical mechanics. The method of constructing the kinetic equations was generalized by him to the case of quantum systems. He applied the method of deriving the hydrodynamic equations to construct the hydrodynamics of superfluids.

Nikolai Nikolaevich developed a method of approximate second quantization in order to determine the energy spectrum of weakly excited states of quantum systems. In particular, the new methods made possible the discovery of an extremely important physical phenomenon – the stabilization of the condensate in nonideal systems at temperatures close to zero. N. N. Bogolyubov showed that correlated pairs of particles with oppositely directed momenta play an important role in the formation and stabilization of the ground state of a Bose system. Using a special transformation of the Bose amplitudes now widely known as the Bogolyubov transformation, Nikolai Nikolaevich constructed the mathematical apparatus best suited to the phenomenon.

---

Translated from Atomnaya Énergiya, Vol. 47, No. 2, pp. 129-130, August, 1979.

0038-531X/79/4702-0669$07.50  

This work, which was brilliant in its obvious simplicity and in its precision of physical understanding, served as the basis for the construction of the microscopic theory of superfluids, systematically describing the energy spectrum of the system and explaining the relation between the superfluid and normal states. Nikolai Nikolaevich showed that the elementary excitations in a Bose gas (correlated pairs of particles with opposite momenta and spins) also exist in superconductors. This led to the explanation of superconductivity as the superfluidity of the electron gas caused by the interaction of the electrons with the lattice phonons. The development of the concept of superconductivity as the superfluidity of a Fermi system led N. N. Bogolyubov in 1958 to the discovery of a new fundamental effect – the superfluidity of nuclear matter. At the present time, the concept of superfluidity in nuclear matter is the basis of modern nuclear theory.

N. N. Bogolyubov is responsible for the proof of the important theorem of quasiaverages, which shows that the density of the momentum distribution of particles in superfluid systems in the vicinity of zero momentum tends to infinity no slower than the reciprocal of the square root of the momentum. This theorem, which is known as the Bogolyubov theorem of quasiaverages, is used in the theory of phase transitions in which the ground state is unstable with respect to small excitations. He showed how it is possible to remove the quasidegeneracy and apply ordinary methods of perturbation theory to such systems. Nikolai Nikolaevich obtained a well-known inequality which culminated in an exceedingly simple but rigorous proof of the absence of ferro- or antiferromagnetism in one- and two-dimensional systems.

The ideas and methods developed by N. N. Bogolyubov and the fundamental results he obtained in statistical physics proved to be quite fruitful in the study of important problems of the quantum theory of fields; in particular, with regard to the degeneracy and stability of the vacuum. Since the 1950s, the quantum theory of fields has consistently remained one of his main scientific interests. He approached the formulation of the quantum theory of fields in a new way. He formulated the axioms and theorems from which the orderly structure of the S-matrix formalism is built. The Bogolyubov causality condition, which is expressed in the language of variational derivatives with respect to the field, has played a special role in the development of the S-matrix formalism. The axiomatic structure of perturbation theory has led to a clear understanding of the sort of mathematical objects one must be concerned with in quantum field theory. N. N. Bogolyubov showed that the source of the difficulties in field theory which are related to divergent integrals does not lie in the physics, but rather in the imperfect mathematical definitions with which theoretical physics works. N. N. Bogolyubov gave the correct method for defining the chronological product of field operators and a systematic procedure for eliminating divergences which has become known as the R-operation.

The creation of the axiomatic theory of perturbations is a great contribution to the development of field theory. Yet this is only part of the overall axiomatic approach. From an analysis of the causality and locality conditions, N. N. Bogolyubov drew the conclusion that they can be considered as the conditions that are im-

posed on the class of generalized functions which are permissible in quantum field theory. This made it possible to perfect the axiomatics and to prove the existence of dispersion relations within the framework of field theory. The rigorous proof of dispersion relations is based on the so-called "edge-of-the-wedge" theorem, which was discovered and proved by N. N. Bogolyubov and which bears his name. The rigorous mathematical approach to the construction of an axiomatic physical theory changed the style of physical thinking and became an important influence on the subsequent development of the theory.

The method of dispersion relations became essentially the only method for describing the strong interactions of elementary particles. It was used to describe the hadronic interactions at asymptotic energies, in the derivation of the dispersion sum rules, and in estimating the low-energy parameters of the scattering amplitude. The value of the method of dispersion relations consists in the fact that because it is based on the general axioms of local field theory, it can be a criterion for testing the correctness of the foundations of the theory.

N. N. Bogolyubov also obtained important results in the theory of the symmetry of elementary particles.

The abundance of his scientific results, his continuously expanding interests, the depth of his physical ideas, the wealth of the methods he developed in fundamental directions of theoretical physics, his pedagogical mastery and scientific generosity, and his personal charm all combined to create the favorable and necessary conditions for the formation and continuous growth of scientific schools in the areas of mathematics and modern theoretical physics. His students and successors carry on scientific work in mathematical physics and nonlinear mechanics in Kiev, and in quantum field theory in Moscow, Dubna, Serpukhov, Novosibirsk, and abroad.

N. N. Bogolyubov's scientific authority is remarkable. His work is translated into many foreign languages. N. N. Bogolyubov's scientific services have been acknowledged throughout the world by his being elected as a foreign member of the Academy of Arts and Sciences of the USA (1960), the Heidelberg Academy of Sciences of the Federal Republic of Germany (FRG) (1968), the National Academy of Science of the USA (1969), and the Bulgarian (1970) and Hungarian (1979) Academies of Science. He was elected a Corresponding Member of the Polish Academy of Science in 1962 and of the Academy of Science of the German Democratic Republic (GDR) in 1966. Academician N. N. Bogolyubov has received honorary doctorates in science from the University of Allakhabad (1959), Humbolt University in Berlin (1960), the University of Chicago (1967), the University of Turin (1969), the University of Wroclaw (1970), the University of Bucharest (1971), the University of Helsinki (1973), the University of Ulan-Bator (1974), and the University of Warsaw (1977). For his scientific achievements, N. N. Bogolyubov has received medals from the Helmholtz Academy of Sciences of the GDR (1969), from the Max Planck Institute of the FRG (1973), and from the Benjamin Franklin Institute of the USA (1974). He has received the Heinemann Award in mathematical physics (USA, 1966) and the Komandorskii Service Award (Poland, 1977).

Academician N. N. Bogolyubov is one of the leading members of scientific organizations. He is presently a member of the Presidium of the Academy of Sciences of the USSR and is the Academician-Secretary of the Mathematical Section of the Academy of Sciences of the USSR. He heads an extremely large international scientific center – the Joint Institute of Nuclear Research in Dubna.

Nikolai Nikolaevich devotes much effort and attention to public affairs. N. N. Bogolyubov is a deputy to the Supreme Soviet of the USSR and an active member of the Pugwash movement. His scientific and public-affairs activities have received high recognition. He is a laureate of the Lenin Prize, has twice been awarded the State Prize, and has been rewarded with four orders of Lenin and other orders and medals of the Soviet Union and other socialist countries. In 1969 he was conferred with the title of Hero of Socialist Labor.

On this important anniversary, we wish Nikolai Nikolaevich Bogolyubov good health and new creative success in his work.

## JOURNAL OF COLLABORATION

The First Conference of the section on Instruments and Nuclear Technology Facilities was held on Apr. 3-6, 1979, in Warsaw (Poland). The Section approved the technical assignment on correlometers and spectroanalyzers – instruments for measuring correlation functions and for determining the power density spectra for reactor diagnostics; plans for a program of development of collaboration between the member-nations of COMECON in the field of radiation technology up to 1985, and the overall technological requirements for radiation-technological facilities.

The section considered the methods developed for testing correlometers and spectroanalyzers, technical specification on the development of a reactimeter based on analog technology, the first plan for a procedure for determining the shielding efficiency of a $\gamma$-spectroscopic apparatus, the operating characteristics of semiconductor detectors for radiodiagnostic investigations were analyzed, and also proposals for their improvement and extension of their application.

The section heard information about the improvement of equipment for nuclear instrument manufacture for nuclear power stations up to 1985, about work on the implementation of plans for the development of COMECON standards for instruments and facilities of nuclear technology 1978-1979, etc.

The First Conference of the Scientific–Technical Council on Fast Reactors, of the COMECON Permanent Commission of Atoménergo, took place on Apr. 17-20, 1979, in Bucharest (Romania). The Council defined the most important problems of collaboration between the COMECON member-nations for the development of high-power reactor facilities in 1981-1985, heard a report on the results of a meeting of representatives of the delegations of the countries in the Commission for the preliminary agreement of plans of consent and a program of collaboration.

At the Conference, working plans were ratified, reports were discussed concerning work on the topic "General Questions of Safety, Assessment of the Probability of Accidents, and the Development of Safety Criteria of Nuclear Power Stations with Sodium-Cooled Fast Neutron Reactors." The Council noted that this work is of practical interest, and considered it appropriate to conduct a meeting of specialists in order to work out a plan for future joint work. The specialists of Czechoslovakia and the Soviet Union reported on the work on the theme "Material Studies for the Problem of Fast Reactors." The participants in the Conference listened with great attention to a report on the operation of the BN-350 reactor and noted that the steady and reliable work, and also the accumulated experience, have created prerequisites for extending the investigations on fast reactors.

Reports were heard from the Hungarian and GDR specialists on their work on the theme "Development of a System of Combined Vibroacoustic Diagnostics of Fast Reactors and Plant."

Reports by the GDR and Soviet specialists were heard, concerning the preparation for signing contracts on the development and testing of measuring instruments for monitoring the oxygen and hydrogen content in the sodium circuits of fast reactors, and concerning the investigation and development of acoustic methods and instruments for detecting water leakage into the sodium, and boiling in fast reactors.

The First Conference of the Scientific-Technical Council on Radiation Safety took place on Apr. 23-27, 1979, in Havana (Cuba). The Council considered the results of the Seminar held in Cuba on Radiation Safety, in connection with the development of nuclear power generation in Cuba, ratified the plan of a program for comparing methods of dosimetry of $\beta$ radiation and mixed $\beta-\gamma$-radiation fields, and data were discussed associated with the development of a special medical inventory for use in work with radioactive substances and ionizing radiation sources. Data were heard, related with problems of the Council, resolutions of the Permanent Committee of COMECON Atoménergo, other COMECON organs, and other problems.

A conference of specialists of COMECON member-nations on the preparation of specific proposals for collaboration in the field of thermonuclear research was held on Apr. 24-26, 1979, in Moscow. The participants in the Conference heard information from Soviet specialists about the realization of the decisions of the

Translated from Atomnaya Énergiya, Vol. 47, No. 2, p. 131, August, 1979.

 0038-531X/79/4702-0672$07.50 

Thirty-Fourth Meeting of the Permanent Commission of COMECON Atoménergo on controlled thermonuclear fusion, and also discussed proposals for collaboration in this field. Information was heard about the development of an international plan for the INTOR tokamak reactor.

The First Meeting of Section I on Reactor Science and Technology was held on Apr. 24-27, 1979, in Sofia (Bulgaria). Its participants heard a report on the results of investigations in the field of intrareactor measurements, the development of sensors and instruments for the VVÉR-1000 reactor, and the most important trends of collaboration in this field were defined. The state of work on the decision for the conclusion of agreements on the commissioning of power units with water-cooled/water-moderated reactors with a capacity of 1000 MW, and their further improvement, and also the results of a conference of representatives of the countries and international organizations for the preliminary agreement for plans of a program and agreement on collaboration in this problem were reported. The meeting considered the preparation of the starting data for the preparation of plans of agreement and plans of collaboration for the development of nuclear thermal power stations and AST for central heating.

The participants in the Conference ratified the proposals for the structure and content of a unified catalog, prepared to specification, of a testing base of the member-nations of COMECON for power-generating thermal reactors.

## SOCIALIST INTEGRATION OF NUCLEAR SCIENCE AND TECHNOLOGY

## Peaceful Atom in the Countries of Socialism. Collaboration between Member-Nations of COMECON *

Reviewed by E. V. Kulov

In connection with the passing in 1979 of the 30th year of the Council for Mutual Economic Aid (COMECON), Atomizdat has issued a jubilee handbook, representing the collective work of eminent scientists and engineers of the countries of socialist friendship, and reflecting the evolution and utilization of the achievements of nuclear science and technology in the national economy. The book broadly highlights problems and prospects for the future development of the different fields of nuclear science and technology, the fruitful collaboration of the COMECON member-nations within the scope of the Permanent Commission of COMECON on the utilization of atomic energy for peaceful purposes, and the activities of international scientific and economic organizations. Readers will find in the book information which convincingly confirms that under the conditions of a socialist government, the peaceful atom is an effective factor for accelerating scientific–technical progress and for serving the good of mankind.

Collaboration on the utilization of nuclear energy for peaceful purposes is developing in such directions as nuclear power generation, nuclear instrument design, nucleides and labeled compounds, radiation safety and shielding techniques, and the application of radioisotope methods and apparatus in the national economy.

The main attention in the work of the Permanent Commission is paid to nuclear power generation, as the greatest progressive trend of the utilization of nuclear energy. In accordance with this, the realization of a long-term special-purpose program is developing for collaboration in the fields of energy, fuel and raw materials, accepted by the Thirty-Second Session in 1978. The program has been calculated up to 1990. The execution of its legislative enactments will allow the demand for electric power in the European COMECON countries to be increased by a factor of $\approx 1.5$. The main trend of cooperation is the construction in the COMECON member-nations of nuclear power stations with a total capacity of 37 million kW, and also two nuclear power stations of 4 million kW each in the Soviet Union, the electric power from which will be supplied to the European COMECON member-nations.

A detailed account of the state and problems of nuclear power generation is given in an article by A. M. Petros'yants, inaugurating the handbook. In it, a retrospective and a prospective view is given on power-re-

*Atomizdat, Moscow, 256 pp., 8 figures, 80 kopecks (1979).

Translated from Atomnaya Énergiya, Vol. 47, No. 2, p. 133, August, 1979.

0038-531X/79/4702-0673$07.50 

actor construction in the COMECON member-nations. The advantages of socialist economic integration in this important field of international collaboration are shown. It is noted that the achievement of nuclear-power problems would be impossible without an enormous combination of complex and fundamental nuclear-physics research; mention of this is also made in the article.

A unique account of the state of affairs and successes in the field of the peaceful utilization of atomic energy is given in articles on this topic, described by specialists of Bulgaria, Hungary, GDR, Cuba, Poland, Romania, the Soviet Union, and Czechoslovakia. This group of articles sums up the generalizing paper of the specialists of the Secretariat Division of COMECON, showing what great and fruitful work has been achieved by the workers this international body.

In the field of vision of the compilers of the handbook, they were not able, of course, to dwell on the aspect of the work of the international organizations and bodies, set up within the framework of the "nuclear problem." This involves the temporary scientific-research body for conducting reactor-physics research on a critical assembly in Hungary, the international economical society "Interatominstrument" in Poland, for the organization of production cooperation, delivery of plant and rendering technical assistance in the construction of nuclear power stations "Interatoménergo" in the Soviet Union, and the Joint Institute for Nuclear Research in the Soviet Union. This group of articles gives a wide panorama of the joint work, from scientific-technical to practical work over all trends of the peaceful utilization of atomic energy.

The handbook concludes the news items of the work of the Permanent Commission. After dry lines of minuted records, the intense and many-sided activities are seen clearly.

The publication reviewed is unique. It shows how versatile and fruitful scientific international cooperation can be. And it is even more noteworthy that this is international socialist cooperation.

# SEMINAR ON PROCEDURAL PROBLEMS FOR INVESTIGATING THE RELIABILITY OF LARGE POWER-GENERATING SYSTEMS

T. A. Golubeva

A Seminar on the theme "State and Prospects for the Development of Methods of Calculating Reliability and Their Application for Solving Practical Problems," organized by the Siberian Power Institute, Academy of Sciences of the USSR, Siberian Branch, was held in March 1979 at Alma-Ata. About 100 specialists attended. Forty-five reports were heard on electric power generation, gas-, petroleum, thermal-, water-, and coal-supply systems. The main attention was paid to the development of the theory and procedures of investigating the reliability of power generation for planning and operating, reliability standardization, the creation of an authentic data base for solving problems of ensuring reliability, and the investigation of plant reliability.

The principal ones are the investigations of reliability at different levels of territorial-time hierarchy, the determination of its indices with a known computational scheme and the parameters of the system, taking account of optimization of the system structure. Attention was paid to the distinctive feature of the investigation within the framework of automatic dispatcher control at different levels of territorial-time hierarchy of control, the assessment of the values of the reliability index and the treatment of working solutions.

In standardizing reliability, problems are raised of working out standards, standard documents and their classification, consideration of damage by power supply breakdowns, development of procedures for planning the development and operation of power-generating systems, principles of agreement of standards between different levels of territorial-time hierarchy of control, and also with the requirements for plant reliability.

When setting up a data for solving problems on reliability, a collection of statistical operating data is required; investigations of the properties and presentation standards of this information; the development of automated collection systems, processing and analysis of data on the reliability of the plant of power generation systems, and reliability of power supply requirements.

When investigating plant reliability, the main attention is paid to the procedural aspects of its prediction and optimization for planning, choice of the characteristics of units and components, taking account of reliability and safety, optimization of fundamental schemes and emergency arrangements for new power facilities, the basis of a maintenance cycle at stages of planning, and methods of planning the reliability of means of shielding and control.

In the section "Nuclear Power Station Plan," two papers were heard. The paper by A. I. Klemin and E. F. Polyakov (NIKIÉT) reported on the treatment of guiding technical data, intended for the calculation of structural reliability indices of a nuclear power station unit, its part in individual systems, including safety systems at the planning stage. By structural is understood the reliability of the structural layout of a nuclear power station unit, its part or system with specified reliability indices of the component elements, known functional relations between them, and the assumed strategy of planned-precautionary repairs. Definitions, formulas, and recommendations of the calculation are contained in the processed data. Recommendations for calculating the reliability of such specific systems as control and safety rods, control and measuring instruments and automation equipment system, and also safety systems, are given separately. On the basis of the data, the analytical methods of the modern theory of reliability, using the device of minimum section of complex systems, are formulated. Calculation by this procedure allows, at the planning stage, the level of structural reliability to be estimated, weak points to be revealed, the most reliable standby plant to be selected, the requirements on reliability of nuclear power stations with respect to component elements to be assigned, and the reliability of the various alternatives of structural performance of nuclear power stations to be estimated.

The report of V. D. Mikhailov et al. (Nongovernmental Organization "Énergiya") considered the quality assurance and authenticity of data, which can be used in the future to estimate the reliability in planned devel-

Translated from Atomnaya Énergiya, Vol. 47, No. 2, pp. 133-144, August, 1979.

0038-531X/79/4702-0675$07.50  

opment, fabrication, maintenance and operation of nuclear power station plants. The first attempt to collect data showed the usefulness and timeliness of this work and the necessity for further development. The report also discussed the modernization and automation of the collection process, the accumulation and processing of data, and also prospects for their more efficient utilization.

The topics for further work were defined in the Section.

The proceedings of the seminar will be published.

## FOURTH ALL-UNION SEMINAR ON HIGH-TEMPERATURE POWER GENERATION

A. Ya. Stolyarevskii

The thematics and problems of this seminar, which took place at the end of March, 1979, at the I. V. Kurchatov Institute of Atomic Energy, were defined in the opening address by N. N. Ponomarev-Stepen, who remarked on the necessity for a purposeful study of the different scientific and engineering aspects associated with high-temperature gas-cooled thermal (VTGR) and fast (BGR) neutron reactors, plant, refinement of their characteristics in connection with the planning of the first experimental-industrial facilities.

The report by N. I. Tikhonov at the plenary session, concerning the construction, characteristics, and first stage of operation of the high-temperature helium reactor loop PG-100, started up in December 1978 at the I. V. Kurchatov Institute of Atomic Energy, was the most interesting. The loop, with a total power of 0.7 MW (0.3-MW fuel elements), was calculated to operate at temperatures up to 900°C and pressures up to 100 kgf/cm$^2$. Despite ~300 accessory units, 3000 welded joints, knife-edge sealing of the cover of the gas-blower, the helium leakage from the circuit amounted to 0.3%/day, which is considerably lower than planned.

The prospects and possibilities of using VTGR for heat supply were considered in a report by E. K. Nazarov et al. The reasons were analyzed which limit the feasibility of using nuclear heat supply sources in conjunction with the conventional systems for transfering thermal energy, means of overcoming these limitations were contemplated, due to the construction of nuclear stations for long-range heat supply with a capacity of 10-15 GW (thermal), with high-temperature reactors and chemicothermal systems for transferring the thermal energy with dispersed requirements to distances of up to 150-200 km. One of the most promising systems is based on the assimilation into the chemical industry in large-scale processes of the high-temperature (~800°C) catalytic conversion of methane. The results of the successful development of methanation catalysts for chemicothermal heating equipment will allow confidence in the provision of a high temperature level (up to 650-700°C).

The choice of the scheme and the capacity of the nuclear power-technological stations of different designation, based on VTGR, has shown that the optimum ratio in the generation of electric power and technological heat over a wide range of variable technicoeconomical parameters amounts to 1-2/1. The necessity for the uninterrupted supply of energy of individual users leads to the construction of industrial nuclear power-technological stations, consisting of not less than two units. For the individual units, the appropriate number of heat-transfer loops is from 4-8 up to 12, with a certain power reserve of individual loops.

The report of V. K. Ulasevich et al. was devoted to a plan for an experimental-industrial station based on a BGR with a capacity of 300 MW (electrical). Important characteristics of the BGR-300 reactor were noted, such as the integral grouping of the plant of the primary circuit in a high-pressure vessel of prestressed ferroconcrete, fuel-element rods with a high bulk energy intensity, turbine plant operating on standard high steam parameters (170 kgf/cm$^2$, 530°C), and high-pressure helium in the primary circuit (160 kgf/cm$^2$). In the case of total depressurization of the primary circuit, the use of a special protective shell is provided, calculated on a pressure of 3 kgf/cm$^2$, and an emergency core cooling system (4 × 50%). As investigations have shown, nuclear power stations with BGR-300 have advantages by comparison with those based on reactor-breeders of another type. A comparison of reactor-breeders based on helium, sodium and dissociating coolants have shown the importance of such characteristics as the specific charge and the specific annual requirement on plutonium (at the accelerated introduction stage), and the indices of production of surplus plutonium.

Construction of VTGR (31 reports). At the present time, the feasibility has been established of constructing gas-turbine facilities with a capacity of up to 10 GW (electrical); at the same time, according to tech-

nicoeconomic considerations, the practical limiting capacity of the turbocompressor units of these facilities amounts to ~2 GW (electrical). Experimental investigations have confirmed the feasibility of developing reliable and economical bearings and sealing units for helium gas-turbine facilities.

One of the most important units is the steam generator. In one of the reports, the results were given of experimental investigations of the thermohydraulic parameters of a steam generator in a single-tube model with natural values of the superheated steam ($P_{sup.st}$ ~ 170 kgf/cm$^2$, $T_{sup.st.}$ ~ 540°C). Comparative investigations of the thermohydraulic characteristics of a multientrance and modular versions revealed the efficiency of the modular version, as applicable to the VGR-50 facility. The lifetime of the evaporative element with the temperature conditions produced in the experiments of the helical coil in the zone of declining heat exchange, which amounted to ~$5 \cdot 10^4$ h, was estimated. The transition to testing the module of the steam generator on the helium test-bench with a capacity of 6-8 MW was noted. For the VGR-50 and the BGR-300, the use of a steam generator of the spiral type is recommended, with a coil diameter of 5-8 diameters of the pipes assembled from individual chains. The critical steam content on experimental facilities with sodium heating for spiral surfaces amounted to 0.9, which considerably exceeds the corresponding values for straight-tube surfaces (~0.6).

The backfilling mechanism of globular fuel elements was studied experimentally, the optimum geometry of the base of the core was determined with these fuel elements, and the velocity profiles of their movement for different configurations of the bounding surfaces, and ways of reducing the stresses of the insertion of the immersed compensating control and safety rods in the case of backfilling. As applicable to VTGR with circulating globular fuel elements it was shown experimentally that the radial smoothing of their movement profile contributes to an increase in the number of discharge openings, a reduction of the number of pylons protruding from the reflector in the core, and the formation on the inside surface of the reflector of hemispherical bulges, etc. It was established on the test rig with labeled dummy globular fuel elements that in the ducts between the pylons, stagnation zones are formed in which the velocity of motion of the fuel elements is less by comparison with the average for the core, by more than a factor of three.

The programmed experimental finishing of the fuel elements in the reactor channels formed possibly provides a more complete simulation of such parameters as the volume power distribution, burnup, stress, temperature, radiation damage, etc. The experimental dependences of the leakage of gaseous fission products were given as a function of the temperature and fuel burnup, and different models of their yield from the VTGR microfuel elements were verified. The best agreement with experiment is given by the defect-trap model. Based on the dynamics of the yield of $^{85,87-90}$Kr, it was determined that the main mechanisms are that of recoil nuclei (up to 800°C) and migration processes taking place in the cladding which are contaminated with fissile material (1000-1400°C).

Monitoring for the entry of water into the primary circuit in accident situations is of special importance because of the positive "water" reactivity coefficient of the VTGR. In the report by O. M. Traktuev, a unique method is given for indicating a sharp change of moisture of inert gases, and the results of tests on laboratory samples of indicators are given, using the principle of potentiometry of an electrochemical element with a solid electrolyte and with buffering of one detector. At 700-800°C, the recorded partial pressure of oxygen in the gas mixture amounted to $10^{-7}$ kgf/cm$^2$ and more.

The versions of the grouping of high-pressure vessels considered, e.g., such as integration, showed that the most economical and reliable is integral grouping with the arrangement of the main plant of the primary circuit in a single high-pressure vessel, the dimensions of which (diameter and height) may be 30 m or more. The cost of these vessels is approximately the same as the corresponding cost of metal vessels for reactor facilities with water coolant, taking account of operating costs and including monitoring. As applicable to nuclear power stations with BGR-300 reactors, individual problems of technology of the erection of reactor vessels of prestressed ferroconcrete were worked out on large-scale models. An original technology was suggested for the prestressing of cylindrical structures, the erection of a hermetically sealed shell for the multicavity vessel of the experimental-industrial nuclear power-technological VG-400 station. The operation of these reactor vessels was confirmed in the elastic region, including with cyclic loading in excess of 1000 cycles.

A part of the reports was devoted to high-temperature nuclear reactors, based on the use of a solid and liquid-salt coolant, in the gas phase, and also thermonuclear reactors.

Neutron-Physics Characteristics of High-Temperature Gas-Cooled Reactors (30 Reports). The characteristics of fast breeder-reactors with helium coolant and with rod-shaped fuel elements based on nitride fuel were given (U, Pu)$^{15}$N with a capacity of 4300 MW (thermal) and 1600 MW (electrical) (report of N. N. Pono-

marev-Stepen et al.). A structural solution similar to the BGR-300 was assumed. The nitride fuel, by comparison with oxide (U, Pu)$O_2$ fuel, is characterized by a higher density, a lower neutron moderation and absorption, and a higher thermal conductivity. The advantages of this fuel allows breeder-reactors to be constructed with a higher breeding factor ( ~1.85) and a fuel doubling time of ~3.5 years with a helium pressure in the primary circuit of ~16 MPa, and ~3 years with 25 MPa. M. F. Troyanov et al. reported on the experimental investigations on a fast gas-cooled reactor on the critical test rig KOBRA. In the majority of cases, good agreement between the calculated and experimental data is noted.

An analysis of the results of calculations of the principal physical characteristics of the VTGR fuel compositions by the NEKTAR program (USSR) and WIMS-D (Great Britain) showed that agreement between the calculations was noted for the thermal range of neutron energies. A procedure was described for determining the effective resonance integrals of capture in $^{238}U$ and fission in $^{235}U$, the distribution of the microelements according to mass was measured, and the effective integrals for microfuel elements with the most probable mass were measured. It was noted that the fuel cycles of VTRG with a ratio of moderator nuclei to fuel nuclei of ~350-400 and a high initial enrichment are the least sensitive to absorbing impurities. The possibilities of using a critical assembly for determining the composition of the VTGR globular fuel elements were investigated – the initial amount of fissile material in the fuel elements, burnup, the presence of the absorber (boron) in the absorbing elements, etc. It was noted that critical assemblies, based on beryllium or zirconium hydride moderators, can be constructed which will ensure the highest sensitivity for monitoring the composition of the globular fuel elements and the absorbing elements of VTGR. The experimental investigations on the critical assembly and the analysis of the errors permitted the limits of sensitivity of the proposed method to be established at the level of 20 mg $^{235}U$.

Thermophysics of VTGR (30 Reports). An analysis of the thermophysics at a given stage of development of the computational-theoretical and experimental work was given by V. N. Krymasov. In the report of E. G. Baryshev et al. the results were given of experimental investigations in which data were obtained about the thermal stabilization of the flow in the near-wall region and the generalized criterial relations for calculating the heat-transfer stabilization in reactors with globular fuel elements. S. V. Popov presented the results of numerical investigations of the thermophysics of VTGR with globular fuel elements, based on unique programs in R – Z geometry, and the effect of the geometry of the lower part of the core on the coolant velocity field, the helium temperature and the fuel. The temperature conditions in the meeting zone of the main coolant flow and the flow from the discharge channel of the fuel elements were considered, and the location and size of this zone were estimated. The effect of anisotropy of the fuel element material, the variability of the heat-transfer coefficient over the surface, various defects in the fuel elements were revealed on the basis of three-dimensional thermal calculations of a globular fuel element in R – $\varphi$ – $\theta$ geometry (report of A. L. Kalishevskii et al.).

On the whole, the reports (about 110) heard at the seminar demonstrated the increased level of work on the generalization of technical solutions established in plans of pilot plants, based on the high-temperature, gas-cooled reactor.

One of the most important questions for solving the problem of the construction of reactor facilities of a new type – the development of structure materials corresponding to the operating conditions of the primary circuit – was considered during a "round table." In particular, it was noted that the welding technology developed will ensure the necessary gastightness in the working temperature range of the corresponding VTGR components, and the leakage amounted to less than $5 \cdot 10^{-8}$ liter (NTP)/$\mu$m · sec, i.e., with the existing helium leak detectors, it was found to be below the sensitivity of the flow monitoring method. In the report of V. G. Markov the results were given of the assimilation and use of austenitic chrome–nickel steel, having adequate heat resistance, a high resistance to intercrystallite corrosion, and durability in a helium atmosphere. From the point of view of providing durability in a helium atmosphere, alloys alloyed with niobium have the best characteristics (lower depth of oxidation) by comparison with alloys alloyed with titanium. An interesting report was given by Yu. A. Dushin concerning an investigation of materials in helium with a controlled impurity composition. The theoretically important value of the testing of materials in a medium simulating the action of the reactor coolant was noted. The gas leakages, observed in a few cases, were due to the formation of an open channel because of microcracks, which were a consequence of a metallurgical defect. With prior monitoring of the material, no helium leakages were recorded in 50 cases out of 50 at 750°C on samples from 0.8 to 15 mm. The inertial nature of helium leads to the fact that it does not dissolve in metals and cannot diffuse through them. This physical fact is confirmed by the numerous Soviet and foreign experiments.

Academician A. P. Aleksandrov participated in the work of the Seminar. The proceedings of the Seminar will be published.

# INTERNATIONAL SYMPOSIUM ON THE THERMODYNAMICS OF NUCLEAR MATERIALS

V. V. Akhachinskii and A. S. Panov

The Symposium was held at the end of January – beginning February 1979 in Jülich (Federal Republic of Germany). Some 130 specialists from 27 countries participated in its work. Fifty-seven reports were presented, mainly from the USA (16), Federal Republic of Germany (FRG) (14), Great Britain (10), the Soviet Union (9), and France (5).

Of the less-numerous computational-theoretical papers, the report of L. Mainz et al. (Federal Republic of Germany (FRG)) should be mentioned, concerning the development of a thermodynamic model which is based on the existence in phases of variable composition of tetrahedral defects, consisting of oxygen vacancies and two positively charged metal ions. The thermodynamic properties and structural features of $PuO_{2-x}$ and $CeO_{2-x}$ are explained. S. Fenoiya and G. Sunderman (FRG), in order to calculate the interaction parameters in multicomponent systems, proposed correlation relations, based on assumptions concerning the linear relation between the solubility and activity in complex systems, and concerning the existence of a link between the thermodynamic activity and the interaction parameters for binary systems with similar magnitudes for ternary and more complex systems. M. Rand (Great Britain) reported on the significantly refined data concerning the specific heat of gaseous actinide elements at 1000-10,000°K, taking account of the additional contributions of unobserved electron levels in the statistical sum and its derivatives. G. March and R. Thorn (USA) considered the thermochemistry of nonstoichiometric oxides of uranium with the inclusion of data concerning the photoelectron spectroscopy of the 4f-, 5f-, and 2p-electrons. M. Rened, R. Akkerman, and E. Pouch (Great Britain, USA) cited mass-spectrometric data concerning the vaporization of $UO_2$ at 1813-2463°K, and the refined thermodynamic constants for the solid and gaseous phases. G. Chilton and D. Edwards (Great Britain) established that with increase of the content of plutonium, the negative oxygen potential of mixed oxide fuel $(U, Pu)O_{2\pm x}$ becomes less. M. Tetenbaum and R. Akkerman (USA) reported data on the vaporization, thermodynamic properties, and phase boundaries of $ThO_{2-x}$.

New data on the vaporization and thermodynamic constants of the silicides and halides of uranium and thorium were obtained by D. Sud et al. (India). Yu. V. Vamberskii et al. (Soviet Union) cited thermodynamic data for the systems U–V, U–Pd, U–Nb–(Mo, V), U–Nb–Zr, and V. V. Akhachinskii and L. F. Timofeeva (Soviet Union) for Pu–Al systems. V. Yamawaki and M. Kanno (Japan) studied the thermodynamic properties of alloys of Mo–Pd, Mo–Rh, and Mo–Pu–Pd, and K. Spier and T. Yurik (USA) studied the system Ti–B–N. Z. Mozer and R. Kastane (Poland, France) cited data on the thermodynamics of liquid solutions of the system Mg–Zn–Sn; T. Ryuts, F. Kozlov, et al. (GDR, Soviet Union) cited data on the thermodynamics of liquid sodium containing dissolved hydrogen and oxygen.

A large group of reports was devoted to the interaction of nuclear fuel with the claddings, coolant and fission products in fast reactors. P. Woodley and M. Adamson (USA), for the systems $ThO_2$–$UO_2$ and $ThO_2$–$PuO_2$, gave a review of the phase diagrams, thermodynamic properties and chemical interaction reactions with austenitic stainless steel, sodium, cesium, and a Na–K alloy, and noted that additions of $ThO_2$ reduce the partial pressure of oxygen, improve compatibility with the claddings, and reduce swelling of the fuel. M. Adamson, P. Potter, et al. (USA, Great Britain) considered the thermochemical aspects of the interaction of $UO_{2+y}$, $U_{1-x}Pu_xO_{2+y}$, and $U_{1-x}Ce_xO_{2+y}$ with the cladding, coolant (Na, K) and fission products (Cs, Te, etc.) during irradiation in a reactor. The conditions of formation of compounds causing swelling of oxide fuel were discussed. Great attention was paid to the corrosion of austenitic stainless steel in consequence of the formation of tellurides of Fe, Cr, and Ni. Noting the increase of the oxygen potential of the fuel during irradiation, as a result of the accumulation of fission products and the redistribution of oxygen under the conditions of a temperature gradient, the authors suggested use of the buffer mixture of Nb/NbO, V/VO, etc. for the protection of claddings from oxidation, K. Wilson (USA), for this same purpose, recommended for limiting the migration of oxygen the use of prestochiometric fuel or the introduction of getters of niobium and titanium. In this case the conditions of the disposition of the getters in the form of foil, coatings and sintered pellets were discussed.

R. Lorenzelli et al. (France) presented data about intrareactor investigations of the reactions of $UO_2$, $PuO_2$, and $UO_2$–$PuO_2$ with cesium, and data concerning the types of compounds formed. E. Korfunke, E. Westrum, D. Yakesh et al. (Netherlands, USA, Czechoslovakia) reported on the thermodynamic constants of uranates of stable existence of these compounds. U. Benedikt (FRG) showed the solubility mechanisms of fission products

in carbides and nitrides of uranium and plutonium, and on this basis explained certain special features of the phase composition of irradiated carbide, nitride and carbide–nitride fuel. A. Naomidis et al. (FRG) analyzed the behavior of fission products in irradiated microfuel elements of high-temperature, gas-cooled reactors with high burnup (up to 70%). The chemical state and migration of solid fission products in irradiated $UO_2$, $UC_2$, and ($UO_2$ + 10% $UC_2$) was discussed. Oxycarbide microfuel elements, in which to a lesser degree than in $UO_2$ the "amebic" effect is manifested, and to a lesser degree than in $UC_2$, are more stable, the claddings are attacked because of the discharge of rare-earth elements. T. Besman and E. Beecham (USA) carried out a thermodynamic analysis of the interaction processes of ThC with the canning materials, containing Fe, Cr, and Ni, and on the basis of the numerical and experimental results, optimized the compositions of the alloys. V. N. Zagryazkin et al. (Soviet Union), in order to reduce the rate of carbonization of metals during their interaction with UC, suggested alloying the fuel with additions of US.

A part of the reports was devoted to the controlled migration of oxygen into oxide fuel under temperature gradient conditions. M. Froman et al. (France) carried out intrareactor measurements of the redistribution of oxygen in $UO_{2+x}$ by the emf method, and verified the well-known fact of oxygen migration into hotter regions. In one of the reports, the results were given of direct measurements by the emf method, of the radial distribution of oxygen in irradiated prestochiometric fuel $U_{0.724}Pu_{0.236}O_{2-x}$ with a high burnup, and showed that oxygen migrates into colder regions, where the accumulation of fission products such as Cs, Ba, Te, etc. was also noted. G. Schuhmacher and co-workers (FRG), by the example of (U, Pd)$O_{2+x}$, discussed the mechanism of mass migration of oxygen under the conditions of a temperature gradient using the Seebeck effect.

In some reports, diagrams of phase equilibria of the actinide elements with metalloid components and fission products were discussed, as applicable to fast reactor fuel. P. Potter, M. Rand, K. Spier, and T. Hines (Great Britain, USA) analyzed the phase diagrams: U(Pu)–C–O; U(Pu)–N–O; U(Pu)–C–N; U(Pu)–C–Re(Te, Cr, Ni), as well as Tc–Mo; Tc–Rh; Tc–Pd; Mo–Tc–Rh; Mo–Tc–Pd, and Mo–Ru–Pd. The types of compounds formed were discussed and their regions of stable existence were noted. The results were given of a thermodynamic calculation of the phase diagrams of the system UC–UN (A. L. Udovskii and O. S. Ivanov, Soviet Union) and new data were given concerning phase equilibria in the system U–Cr–C (Z. M. Alekseeva and O. S. Ivanov, Soviet Union); the introduction of chromium increased the length of the region of homogeneity of UC from the side of the UC–$U_2C_3$ boundary.

The reports in which the phase stability of multicomponent alloys were considered in the case of prolonged high-temperature operation under reactor irradiation conditions were of special interest. D. Watkin and A. Midovnik (Great Britain) carried out a thermodynamic calculation of the effect of small additions of a fourth element (Nb, Ti, Al, Mo, Co, C) on the phase stability of the system Fe–Cr–Ni. The tendency of Mo, Nb, Ti, and Al to stabilize ferrite was verified, and the strong austenizing effect of the action of carbon was established. The process of the formation of deposits of $Ni_3Si$ from unsaturated solid solutions was discussed in the system Ni–Si under the action of irradiation, and the authors showed the role of local supersaturation as a result of the interaction of radiation defects with impurities, the driving force was calculated, and its relation with the neutron fluence was established. M. Koch and Yu. Chen (USA), by thermodynamic calculations and numerous experiments, showed the nature of the phases separating at 750-1350°C from austenitic stainless steel, including the contained impurities of niobium and titanium, and the temperatures and kinetics of formation were determined (NbN, NbC, TiN, TiC, and $Cr_{23}C_6$). K. Tilbert (FRG) showed by thermodynamical calculations that the vaporization and removal of $^{60}Co$ from the core, formed by irradiation of alloys of the nimonic and inconel type etc., cannot be avoided.

A large group of reports was devoted to the thermodynamics of aqueous solutions. P. Tremain (Canada) made a review of methods of calculating the high-temperature values of the free Gibbs energy for aqueous solutions, based on the data for room temperature. J. Fouget, D. Navratil, V. Medvedev, et al. (Belgium, USA, Soviet Union) carried out thermodynamic estimates of the actinide complexes in aqueous solutions. A. Strezov et al. (Bulgaria) considered the changes of thermodynamic functions with the formation of metal–ligand complexes. K. Musicas et al. (France) discussed the problem of aqueous complexes, which are formed by metal ions present in reprocessed nuclear fuel, with orthophenanthrolene and dibutyl phosphate ligands, and explained the types of complexes which are characteristic for the trivalent actinide metals. D. Lambert (France) considered the thermodynamics of the dissolution of magnetite in water in the presence of hydrogen.

Reports on the thermodynamics of the blanket zone materials of thermonuclear reactors were included in the program of the Symposium. In the review report of E. Velekis (USA) for three categories of materials – liquid lithium, solid lithium alloys, and lithium-containing ceramics – data were given about the P–C–T diagrams, activity coefficients, isotopic effects, Sieverts constants, free energy of formation, phase boundaries,

etc. The latest data on the solubility of $Li_3N$, $Li_2O$, and $Li_2C_2$ in liquid lithium were discussed, and the prospects of their removal by means of a cold trap were assessed. Kh. Ile et al. (FRG) presented the results of the experimental determination of the composition and vapor pressure over lithium oxide and with a solution of deuterium in lithium.

V. V. Akhachinskii (Soviet Union) determined the enthalpy of formation of the dihydride $YH_{1.994}$ and the nonstoichiometric trihydride of yttrium $YH_{2.799}$, equal to $-52.30 \pm 0.30$ and $-59.08 \pm 0.41$ kcal/mole, respectively. E. B. Boiko et al. (Soviet Union) presented data about the diffusion of hydrogen in the hydrides of the transition metals of Group IV and alloys based on them.

In two reports, the burial of radioactive wastes by vitrification was discussed. R. Odoy (FRG) established that the losses of alkaline fission products and glass components due to volatilization during solidification are quite significant, and depend on the temperature, time, and composition of the surrounding medium. The most stable compounds (e.g., $CsAlSi_5O_{12}$) were suggested. G. Matzke (FRG) considered the diffusion of actinides in nitrified wastes. The measured diffusion coefficients of the actinides in glass at 180-350°C are small ($10^{-16}$-$10^{-18}$ $cm^2 \cdot sec^{-1}$), whereas for flattening the concentration gradient resulting from the leaching out of the glass, they should be greater than the experimental values by more than a factor of $10^3$-$10^4$, which confirms the reliability of the use of glass and vitreous ceramics for burying the actinide elements.

A part of the reports was devoted to the analysis of accident situations during operation of reactors, and the determination for this of the necessary characteristics of the nuclear fuel. E. Fischer (FRG) cited the values of the constants occurring in the equation of state of nonstoichiometric $UO_2$ for a temperature of 3120-7500°K. G. Karov and M. Bober (FRG) reported the characteristic data obtained experimentally and by a numerical method, for saturated $UO_2$ vapor, existing in the state of a neutral gas, and a thermal plasma in the temperature range up to 5000°K, and also for Cs and Na in the region of the critical temperature. The emission coefficients of solid and liquid materials ($UO_2$, UC, $ThO_2$, and $Nd_2O_3$) were determined over the range 1500-4800°K. D. Benson and E. Bergeren (USA) described a series of experiments to measure the vapor pressure over nonirradiated and irradiated $UO_2$ under rapid heating conditions to 2560-5250°K. In the latter case the total vapor pressure amounted to 93-691 $kgf/cm^2$. R. Oze (FRG) with co-workers measured the vapor pressure of uranium carbides at a temperature up to 7000°K by means of pulsed laser heating. D. Power (USA) analyzed the effect of the formation of gases on the interaction of fused material of the core with concrete; the erosion and disintegration of concrete, the rapid release of a large quantity of heat and the discharge of gas were discussed.

The proceedings of the Symposium will be issued by IAEA.

## CONFERENCE ON CONTROLLED THERMONUCLEAR FUSION

É. I. Kuznetsov

In February 1979 in Zvenigorod, participants in research on high-temperature plasma physics and controlled thermonuclear fusion (CTF) assembled. A Conference was held here devoted to the 70th birthday anniversary of Academician L. A. Artsimovich (1909-1973), who over a period of many years was the acknowledged leader of research on CTF. About 200 Soviet and foreign specialists participated in the work of the Conference. Twenty review and 55 original reports were heard in four sections (closed magnetic traps, inertial plasma containment, pulsed systems, and open traps). On the opening day of the Conference, a memorial session was held, at which Academician B. B. Kadomtsev addressed a paper on the creative course of Academician Artsimovich. Soviet and foreign scientists spoke with recollections of the life of Lev Andreevich, his contribution to CTF and the effect on the development of world science.

The review reports of the Soviet physicists were devoted to experimental research on tokamaks (V. S. Mukhovatov), problems of theory (V. D. Shafranov), the nature of collapse instability (B. B. Kadomtsev), experiments on plasma compression in tokamaks (V. E. Golant), investigations on stellerators (M. S. Rabinovich), hf plasma heating in toroidal systems (K. N. Stepanov), recent research of open thermonuclear systems (D. D. Ryutov), systems of the plasma focus type (N. V. Filippov and V. A. Gribkov), investigations of the energy concentration of relativistic electron beams (L. I. Rudakov), the initiation of thermonuclear reactions by means of ion beams (A. A. Kolomenskii), plasma accelerators (A. I. Morozov), and the corpuscular method of plasma diagnostics (V. V. Afrosimov).

The American physicists spoke about the long-term program of work on CTF (D. Clark), investigations on the PLT tokamak (G. Foort), a tokamak with a superpowerful magnetic field IGNITOR (B. Koppi), and a program of research on open traps in Livermore National Laboratory (R. Post). Review reports of S. Mori and K. Takayama were devoted to the work on CTF conducted in Japan, investigations on the DITE toroidal facilities (Great Britain), FT (Italy) and TFR-600 (France) – reports of R. Bickerton, S. Segre, and D. Tashon.

The year 1978 was a fruitful year for tokamak research; the ion and electron temperatures were significantly increased, and the behavior of the plasma in the collisionless regime was studied (important from the point of view of operation of a thermonuclear reactor), as a result of reducing the concentration of impurities the range of the discharge parameters was extended with stable behavior of the plasma. Investigations were started on the large-scale facilities DOUBLET-III, ALCATOR-C (USA), FT (Italy), TFR-600 (France) and Tuman-3 (Soviet Union). As a result of using high-powered auxiliary (nonohmic) heating sources, the plasma parameters on certain operating facilities were improved by a factor of several. The results obtained on PLT proved to be interesting, where with a beam injection power of hydrogen atoms of 2.1 MW and a plasma density of $2.2 \cdot 10^{13}$ cm$^{-3}$, an ion temperature of ~5.5 keV was successfully achieved, which exceeds the D–T "ignition" temperature with an unlimitedly large plasma containment time. As the experiments showed, in the collisionless regime, the power containment time of the ions amounted to 25 msec, which corresponds to neoclassical thermal conductivity. On T-11 (Soviet Union) transition to the collisionless region was achieved at a considerably lower temperature (0.5 keV) and plasma containment time, and also proved to be in agreement with neoclassical theory. This means that in the operating conditions of a future power-generating tokamak reactor, no new types of instability will arise, preventing the construction of the reactor. As the electron thermal conductivity in the case of a high plasma density, according to experiments on ALCATOR and T-11, also approximates to neoclassical, sound predictions of the thermonuclear plasma parameters in the tokamak reactor will be possible. However, up to now the physical mechanism of the losses of the electron component at low density – increase of the coefficient of electron conductivity by two orders of magnitude by comparison with neoclassical – is still not clear. A possible reason for this phenomenon may be the breakdown of the magnetic field structure. In order to understand the process, accurate and sufficiently complete experimental data about the actual dependence of the coefficient of thermal conductivity on the electron temperature will be necessary. The majority of experiments have shown the anomaly of the diffusion of the plasma at the periphery of the plasma cord (in the high-temperature zone, diffusion approximates to neoclassical) and the impurities, which are not accumulated at the center of the cord, but drift away from the plasma with a velocity which is close to the diffusion velocity of the main plasma. It is precisely due to this phenomenon that the concentration of impurities in the plasma could be reduced by a factor of several and in the majority of facilities, where optimal methods of purifying vacuum chambers are used, the effective charge of the impurities in a hydrogen plasma approaches unity.

According to initial theoretical calculations, the value of $\beta$ (the ratio of the plasma pressure to the toroidal magnetic field pressure) in tokamaks cannot exceed 1-2%, which was a considerable drawback of the tokamak from the point of view of constructing an economically profitable reactor. Higher values of $\beta$ have been obtained on certain facilities. Thus, on T-11, due to operation in a regime with a reduced safety factor of the stability of the plasma cord ($q = 2$), the value of $\beta$ amounted to 5%. Recent theoretical work also confirms that $\beta$ can reach 8%.

There have been successes in plasma heating by ion-cyclotron and low-hybrid resonances and by means of Alfvén waves; however, in all experiments the power injected into the plasma still does not exceed the ohmic heating power. When heating up the plasma by adiabatic compression, an improvement of the plasma thermoinsulation is observed. Alternatives of heating are being considered, when the compression is combined with other methods – the injection of a beam of fast atoms and hf heating.

The conclusion can be drawn that on tokamaks of the next generation, in the next few years a plasma will be obtained with a thermonuclear temperature and density which will be maintained stable for a long time.

At the present time, more than ten different stellerators are operating in the world, and a further four large-scale facilities are being planned. Stellerators allow operation in both the tokamak regime (in the presence of a discharge current) and also in the nonconduction regime using nonohmic methods of heating. The latter regime is important first and foremost for investigating the nature of the anomalous electron thermal conductivity. It was shown recently that the previously observed short plasma containment time in stellerators in the tokamak regime, by comparison with tokamaks, was connected with an imperfect design of the magnetic systems. Therefore, the main efforts in studies of stellerator systems are directed now at the development of nonohmic methods of plasma heating, and to explaining the cause of the anomalous electron

thermal conductivity, and also to finding the optimum magnetic field configurations and stellerator designs, including with magnetic diaphragms and inverters (systems for the removal of impurities). It should be noted that already the advantage of spiral magnetic fields has been demonstrated for stabilizing collapse instabilities and for improving plasma thermal insulation.

From the moment when a stable plasma containment was obtained on the open magnetic trap 2XIIB (USA), at a pressure exceeding the magnetic field pressure, and also when Soviet physicists spoke about the idea of ambipolar magnetic traps, there has again been a sharp growth of interest toward open magnetic systems. In the Soviet Union and the USA, in the near future experiments are to be started to verify the plasma containment theory in ambipolar traps. These systems are the normal trap with magnetic plugs, but each plug is joined through yet another trap. Within the confines of the traps, a plasma is formed whose density exceeds the density in the central trap, and in consequence of this, a potential barrier originates and which contains the ions in the central trap. In this case the containment time can be increased by a factor of many tens by comparison with the normal open trap. In the case of positive results of the verification, the possibility will be revealed of constructing a power-generating reactor, which is structurally simpler by comparison with closed systems. Preliminary engineering development of reactors based on ambipolar systems is already being conducted in some countries.

Recent work on $\theta$-pinches has been devoted mainly to plasma heating in a longitudinal magnetic field by conventional methods and the injection of relativistic electron beams and colliding plasma bunches. A new method of heating in systems of this type (Soviet Union) has permitted, by the retardation of colliding plasma flows, an ion temperature of $\sim 1$ keV (as a result of thermalization of the energy of the bunches) to be obtained, with a plasma density of $\sim 10^{15}$ cm$^{-3}$. In one of these experiments (Soviet Union) it has been shown experimentally that in the small volume of a solenoid, a quite long field in the megagauss range can exist.

In experiments on plasma focusing (Soviet Union) it has been shown conclusively that this system represents a plasma inductive storage device with a plasma tripping device, and generates a beam of electrons and ions with a pulse duration of $\sim 10^{-8}$ sec (with a power of 1 TW). The number of accelerated ions reaches $10^{15}$-$10^{16}$ with an energy of 1-1.5 MeV. The electron streams are focused to a size of 1 mm, and this provides an energy flux density at the target of more than $10^{13}$ W/cm$^2$. By irradiating the plasma formed at the plasma focus at a defined instant of the compression phase with a laser, the maximum radiation absorption is observed, giving an increased neutron yield of a factor of 1.5-2.

The use of plasma accelerators for obtaining a high-energy plasma and for filling the magnetic traps is considered as one of the possible routes for building a reactor system. At the present time, an accelerator on a current of up to 0.5 MA (with a duration of 100 $\mu$sec) and an energy of 0.1 keV has been built (Soviet Union). At the same time, the various plasma accelerators, initially being developed within the framework of the CTF program, have now found a wide application as plasma engines for space vehicles, in the treatment of solids and in other fields of technology.

Work has been proceeding successfully on laser thermonuclear fusion. During recent years new experimental data have been obtained about the interaction of high-powered radiation (with an energy of $\sim 100$ J) with the plasma corona of a solid target, in the first place by absorption of laser energy fluxes with a density of $10^{13}$-$10^{16}$ W/cm$^2$. However, the heat-transfer process, the nature of the formation of fast particles, the generation of superpowerful magnetic fields, etc. are still not clear. The development of high-powered laser systems (neodymium and $CO_2$) with control automation has reached a high level, which has allowed facilities with a laser beam with an energy of up to 10 kJ to be constructed, and experiments on the irradiation of microtargets to be started at energies of $\sim 1$ kJ and higher.

Corpuscular diagnostics has proved to be a very effective means of measuring the parameters of the ion component of a high-temperature plasma, and has allowed information to be obtained about the heating and cooling processes of ions. At the present time, passive (analysis of the stream of particles from the plasma) and active (the injection of a sampling beam of atoms into the plasma with subsequent analysis of the atoms scattered by the ions of the plasma, and ions of the plasma which have been recharged by the beam) methods of corpuscular diagnostics are being used in many countires. In the Soviet Union multichannel analyzers with magnetic scanning have been developed, which will allow particles to be analyzed according to mass and energy during a single working discharge. They are being used successfully in several foreign facilities. Experiments have been carried out to determine the concentration of impurities (ions of oxygen and carbon) by a method based on recording the characteristic emission, which originates with the recharging of the impurity ions by atoms of the injected sampling beam. Methods of corpuscular diagnostics are finding extensive application in large-scale facilities of the next generation, for determining the local parameters of hydrogen ions and impurity ions.

# CONFERENCE ON MATERIALS FOR THERMONUCLEAR REACTORS

N. A. Makhlin

In the work of this Conference held on Jan. 29-31, 1979, in Miami (USA), scientists from Great Britain, Denmark, Canada, the Soviet Union, USA, Federal Republic of Germany (FRG), Switzerland, Sweden, and Japan participated. Some 226 reports were presented, of which 18 were reviews, and 8 sections worked: the use of materials in facilities and system analysis; the interaction of a plasma with the wall; radiation effects; problems of tritium and the compatibility of materials; materials for systems with inertial plasma containment; lifetime of walls; materials for special purposes, and economics and prospective materials.

The work agenda of the Conference provided for the presentation of original papers mainly as bench reports. Only review reports, a large part of which were presented by American scientists, were taken into account. The Director of the Division of Thermonuclear Research, Department of Energy, USA, E. Kintner, addressed the Conference; he made a review of the state of work on thermonuclear power generation.

In some reports, the state of affairs and prospects were highlighted, and also an attempt was made to formulate the principal requirements for materials in the various systems with magnetic and inertial plasma containment, and the specific properties of the material-behavior problem in hybrid reactors, etc. were discussed. In the conceptual designs of thermonuclear reactors, the tendency is marked to a certain increase of the neutron loading at the wall up to 2-4 $MW/m^2$, by comparison with 1 $MW/m^2$ provided for in designs of the middle 1970s. This was caused both by considerations of the economy of the reactors and by the expectations in solving material-behavior problems. As a result of this, the predicted lifetime of the first wall coresponds to a loading of 10-20 $MW \cdot yr/m^2$.

When considering the so-called surface effects, taking place by the interaction of the plasma with the wall, the main attention was paid to such phenomena as chemical and physical sputtering, blistering, peeling, capture, and reemission of implanted gas, secondary ion emission, and the charged state of reflected and atomized particles. In the reports of the American specialists, work was presented on the choice of limiters and wall screens, from the point of view of stability toward thermal shocks and thermal fatigue. In order to test materials with respect of stability toward thermal shocks and thermal fatigue, it was necessary to work out a special program of tests, standardization, criteria of comparison and sampling of the materials based on simulation tests. Investigations of the atomization of complex compounds with the predominant atomization of one (light) alloy component were of considerable interest. This, in conjunction with radiation-stimulated diffusion transfer of the light component from the body of the alloy to its surface, where equilibrium concentration is established, opens the path to the reduction of loading of the thermonuclear plasma with heavy impurities. The work of the American and other researchers gave the basis for supposing that in order to reduce the contamination of the plasma due to the different mechanisms of surface erosion, work in the field of development of materials with low atomic number should be continued: special grades of graphite, carbides, borides, composites with graphite, and also titanium coatings. Studies of the mechanism of the entry of impurities into the plasma as a result of the onset of unipolar arcs are being extended.

New results have been obtained of studies of the phenomenon associated with the capture and reemission of hydrogen isotopes. Special attention includes the study of titanium and its alloys, in which the considerable absorption and the weak reemission of hydrogen isotopes is observed, and also materials where isotopic effects are strong. Just as in respect of "surface" effects, so also with "volume" effects, the importance and necessity of a complex approach to the solution of material-behavior problems of CTF once again has appeared. Thus, the preliminary irradiation of samples with heavy ions has a significant effect on the reduction of reemission, leading to a large number of migrations in the atom. The interaction of structural materials with liquid metal coolants discussed, in essence has been reduced to the analysis of the lithium problem, and is also complex: the material-behavior aspects of technology associated with tritium; the development of traps, getter systems, efficiency of pumping systems, and other elements of the tritium circuit; compatibility and corrosion of materials in liquid lithium; corrosion inhibitors in lithium; the use of different lithium and sodium salts as a coolant, and the contamination of liquid lithium by impurities.

The reports and discussions once again confirmed that the problem of radiation stability is particularly acute for thermonuclear reactor materials. Special attention is paid also to such phenomena as radiation swelling and creep, structural and phase transformations under radiation, and change of mechanical properties (particularly high- and low-temperature embrittlement). Because of this, further extension of the work on determining the nature of radiation defects during the irradiation of materials by thermonuclear neutrons, and estimates of the buildup of helium and hydrogen will be necessary. Theoretical work on calculating the formation and growth of vacancy pores, gas bubbles, etc., including computer simulation are very important.

A large number of papers was devoted to the study of swelling of stainless steel, mainly SS 316, irradiated both in reactors and ion accelerators (simulation experiments). Specific, practically important results were obtained. For example, preliminary 20% cold straining reduces swelling of this steel during irradiation in HIFIR, under conditions of the buildup of a large amount of helium and a considerable number of migrations per atom (up to 60) at a temperature below 700°C. A significant reduction of swelling is observed also by alloying steel with silicon and titanium. From the data of the simulation experiments of other materials, the results obtained confirm the small swelling of titanium and especially its alloys with aluminum and vanadium, produced by a large radiation dose. However, data are required in corroboration with the results of reactor tests.

In some reports it was mentioned that radiation damage as a result of a large dose of radiation accelerates phase disintegration and leads to radiation-stimulated deposition of segregations. Helium has a strong but ambiguous effect on phase disintegration by accelerating the growth of one and slowing down the growth of other phases. Radiation creep is being studied intensively, which, in the opinion of many specialists may be one of the principal factors determining the construction, efficiency and economy of future thermonuclear reactors. For the first wall of the reactor, the position is aggravated in that, in consequence of the drop in temperature, over its thickness, nonuniform swelling and creep originates. Their interaction leads to the onset of an additional high stress, the value of which is increased with increase of the specific loading. It is significant that in this case, as the simulation tests have shown, the rate of radiation creep during irradiation in the pulsed regime is greater than for steady irradiation.

In studying the mechanical properties of possible materials for thermonuclear reactors, particular attention has been paid to the effect of large concentrations of radiation defects, helium and hydrogen on the characteristics of short-time tests, on cyclic fatigue, and deformation mechanisms. The dependence of the degree of embrittlement and hardening of certain materials and alloys on the neutron spectrum appears to be important. It is probable that here, on the one hand, the dependence of the $(n, \alpha)$ reaction cross section on energy is revealed, and on the other hand, it is the leading role of helium embrittlement. Because of this, works on dosimetry and experimental data on the buildup of helium in materials with a different content of elements, especially with a large value of the $(n, \alpha)$-reaction cross section, are interesting.

The results of the investigations of the nature of the primary radiation defects, originating by irradiation with high-energy neutrons and also by simulated radiation, showed the significant dependence of the structure of the radiation defects on the imparted energy spectrum. In certain cases, noncomparability of the experimental results obtained by different authors is observed. There is no agreement between the qualitative and quantitative characteristics of cascades and subcascades, damage functions, etc. when comparing the experimental results with the calculations on computers.

On the whole, the work of the Conference was very fruitful. It showed the importance and necessity of solving the problem of material-behavior for thermonuclear fusion, the extension of work in this direction, and at the same time the new problems and tasks formulated, the solution of which will contribute to the construction of reliable, economical and long-lived working facilities and thermonuclear reactors.

The proceedings of the Conference will be published in the "Journal of Nuclear Materials."

# INTERNATIONAL IAEA SYMPOSIUM ON THE BIOLOGICAL CONSEQUENCES OF THE DISCHARGE OF RADIONUCLIDES BY NUCLEAR INSTALLATIONS

Yu. I. Moskalev

The Symposium was held on Mar. 26-30, 1979, in Vienna. Some 240 Specialists from 33 countries attended, and also representatives of four international organizations, including the International Commission on Radiation Protection (ICRP). During the five working days 62 reports were heard and discussed, which were devoted to methods of estimating the radiation dosage to mankind by radionuclide discharge by nuclear power-generating facilities, the distribution, kinetics of exchange and the biological action of $^{238}$PU, $^{239}$Pu, $^{241}$Am, $^{244}$Cm, $^{232}$Th, $^{227}$Th, $^{58}$Co, $^{60}$Co, $^{54}$Mn, $^{224}$Ra, $^{226}$Ra, $^{90}$Sr, $^{3}$H, $^{14}$C, etc., their migration into the environment and through biological chains; the analysis of factors affecting the cleansing of skin from radionuclides; the role of decorporation in radiation protection; the effects of the combined action of internal emitters and other contaminants of the environment. Epidemological observations on personnel subjected to occupational irradiation were considered, observations for radionuclides in food products and the value of these data assessing radiation loads in man, radioecological and ecological parameters of the movement of radionuclides, the value of these factors for assessing the risk, and radiation monitoring. New scientific information on all the problems enumerated was discussed at the Symposium, and some data have important practical value.

At the opening of the Symposium, P. Bryant (Great Britain) gave a review report on radionuclides ejected by nuclear power-generating installations, and methods of estimating irradiation dosages to man. The report was constructed on the basis of the new recommendations of Publication No. 26 ICRP, the expected collective radiation dosage was estimated (man·rem/MW(el)·yr) for the thyroid gland and the bone marrow, due to the atmospheric and water migration route of radionuclides for light-water reactors. The prospects of developing nuclear power were considered, taking account of the use of new sources of nuclear fuel ($^{241}$Pu, $^{241}$Am, $^{231}$Th, and $^{231}$Pa). Because of the storage of radioactive wastes, attention was paid to carrying out investigations by modeling the environment (volcanic activity, mining operations).

The blastomogenic effect of $\alpha$ and $\beta$ emitters continued to attract attention. In contrast from intravenous injection, in the case of inhalation of microspheres of $^{238}PuZrO_2$ or $^{239}PuZrO_2$ with an activity of 8 to 100 nCi, for a significant part of animals pulmonary swellings developed. The optimum frequency of swelling was observed with an average dose of ~7.5 krd (R. Thomas and D. Smith, USA). An increase of the average duration of life of female rats was noted with the injection of a small amount of $^{241}$Am and $^{252}$Cf, giving an irradiation dosage to the osteoclast of 6-60 rd. The radiosensitivity of dogs was established to be greater by comparison with rats. With an identical, or near, tissue dose, dogs were found to be 4-6 times more sensitive than rats to osteocarcinogenic action of $^{241}$Am (Yu. I. Moskalev and coauthors, Soviet Union). After inhalation of aerosols of $^{238}$Pu, $^{239}$Pu, $^{241}$Am, and $^{244}$Cm, the risk of developing cancer of the lungs in rats was found to be within the limits of 0.0006-0.0029 per rad (Ch. Sanders and A. McGuffy, USA). In some reports, the possibility was noted of the development of leukemia with the incorporation of transuranic radionuclides. Leukemia resulted on the average 8 times more infrequently than osteosarcoma (D. Taylor, Great Britain).

It was noted that fission neutrons and $\alpha$ particles from $^{239}$Pu ( ~1 and 5.15 MeV, respectively) have an approximately identical mutogenic action by comparison with constant low-intensity $\gamma$ irradiation by $^{60}$Co quanta. The relative biological efficiency (RBE) of $\alpha$ radiation and fission neutrons is found to be within the limits from 13 for predominant lethal up to ~40 for reciprocal chromosome translocations (D. Gran and coauthors, U.S.A.).

A comparative analysis of the experimental data for the induction of swelling of the lungs by the inhalation of $\alpha$ and $\beta-\gamma$ emitters was the subject of a report of the American specialists.

With a low irradiation dosage, the RBE for soluble and insoluble compounds of $\alpha$ emitters by comparison with $\beta-\gamma$ emitters was estimated to be equal to 23 and 85, respectively. These estimates are provisional, but they show the validity of the ICRP solution concerning the change of quality factor for $\alpha$ radiation from 10 to 20.

Great attention at the Symposium was paid to tritium. Experiments on mice indicated that by comparison with low-intensity chronic $\gamma$ irradiation by $^{60}Co$ quanta during intrauterine and post-natal development, during 14 days the RBE of tritium oxide in the region of low-power dosage reaches 3 (R. Dobson, U.S.A.). In experiments on yeasts it was shown that the RBE of tritiated uracil by comparison with the action of $^{60}Co$ $\gamma$ radiation is less than unity, whereas in the case of tritiated water, the RBE is equal to 2.8. In cultures of cells of mammals, several factors can affect the value of the RBE of tritium. They include the position of tritium in the molecule used as a marker for DNA (the so-called position effect); the stage of the cell cycle, when damage occurs, as there is a "hot time" for mutagenesis during the cell cycle; the region of DNA which is damaged, as there are "hot positions" inside nuclear DNA for different genetic points (G. Burke and coauthors, U.S.A.).

The identical reduction of the amount of trunk cells by the action of $^{137}Cs$ $\gamma$ radiation and tritiated water was noted. Prolonged entry of tritium from drinking water to the amount of 3 $\mu$Ci/ml, creating approximately during 3 weeks a dose intensity of 0.69 rd/day, has an average expressed biological effect. This concentration is many orders higher than the content level of tritium in water, which may originate during operation of power reactors (A. Karsten and E. Kronkeit, U.S.A.). S. Apelgot (France) showed that the transmutation effect can be estimated only for radionuclides decaying inside DNA, and in the case of decay in other molecules, the radiation effect predominates, depending on the radiation dosage.

S. Cohen and coauthors (U.S.A.) investigated the metabolism of krypton in the human organism. Five periods of semiexcretion of krypton were noted (21.5 sec, 4.7 min, 0.33, 2.41, and 6.67 h). It is excreted slowest of all from the fatty tissue. S. Sundel-Bergman and K. Johanson (Switzerland) studied the frequency of DNA chain ruptures in fibroblasts of Chinese hamsters labelled with $^{14}C$. The RBE for the $\beta$ particles of $^{14}C$ was found to be close to unity. V. Sonntag (FRG) showed that with the incorporation of $^{239}Pu$, the maximum surface dosage in the bones of rats is 10 times higher than average. The report of N. Priest (Great Britain) was devoted to the refinement of the dosimetric model of the behavior of $^{239}Pu$ in bones. The results were used for calculating the permissible limit of the annual uptake of $^{239}Pu$, which was found to be a factor of 1.5-3 less inflexible than when using the ICRP model (1979).

F. Staizer and coauthors (Great Britain) showed that the ICRP pulmonary model used at the present time for estimating tissue dose can overestimate by at least a factor of 10 the quantity of plutonium entering the blood after inhalation. The greatest effect on its behavior was found to be sodium and potassium (with atomic ratios of M : Pu equal to 27-36), increasing the extrapulmonary deposition of $PuO_2$ by more than a factor of 400.

G. Methivier and coauthors (France) established that the intratracheal injection of benzpyrene prior to inhalation of $^{239}PuO_2$ has a synergic effect on shortening the life span and the frequency of development of cancer of the lungs. The modifying effect of benzpyrene on the induction of lung cancer shows the necessity for taking account of harmful habits (smoking) of occupational workers, which might increase the blastomogenic action of radionuclides. Ch. Mace (U.S.A.), based on investigations of European patients, living for more than 10 years after the intravenous injection of thorotrast, estimated the risk of the onset of cancer of the liver for people (300 cases in $10^6$ population per rad of $\alpha$ radiation). K. Pulheim (GDR) determined the period of semiexcretion of $^{60}Co$ from the human organism, equal to 230 days, and $^{54}Mn$ and $^{58}Co$ ~ 35 days.

According to the calculations of R. Rowland (U.S.A.), by the incorporation of 0.1 $\mu$Ci of $^{226}Ra$, the risk of developing osteosarcoma over 50 years (from 20 to 70 years) amounts to $2.7 \cdot 10^{-5}$, with a single intake of 44.5 nCi of $^{239}Pu$ (accumulation in the bones of 40 nCi) it is $\sim 189 \cdot 10^{-5}$, and the natural frequency among townsfolk in the U.S.A. is $33 \cdot 10^{-5}$. Thus, with the accumulation in the skeleton of 40 nCi of $^{239}Pu$, the development of approximately one case of osteosarcoma can be expected per 500 people.

The report by I. Omona and M. Sumia (Japan) assesses the consequences of contamination of sea products required by man, by radionuclides in the region of location of the nuclear power reactor "Tokai." The content of radionuclides in reservoir water in Japan is determined at a distance of 5 km from the discharge point. In the tissues of fish in the vicinities of the fuel reprocessing factory at Windscale (Great Britain), $^{238}Pu$, $^{239-240}Pu$, $^{241}Am$, and $^{242,244}Cm$ have been detected. The entry of the transuranic elements into the human organism from consumable fish does not exceed 0.01 of the values recommended by the ICRP (R. Pentreath, Great Britain).

Considerable attention at the Symposium was paid to consideration of the radioecological parameters of the mobility of radionuclides. Based on an analysis of the data, the range of values of the migration factors of radionuclides into milk and meat cortex was estimated and also the buildup of radionuclides in foodstuff and fodder agricultural cultures. The results of other investigations have shown that the Chamberlain model developed earlier for the absorption of aerosols by vegetation for grassy forms may be used for estimating the ab-

sorption of radionuclides by vegetables (beans, soya, bread cereals, and other nongrassy forms). F. Van Dorp and coauthors (The Netherlands) proposed a model which will allow the transfer of activity from soil to crops to be estimated.

The Symposium proceeded in a businesslike creative manner. The reports were discussed thoroughly and some of them developed into lively debates.

## URGENT PROBLEMS OF RADIATION PROTECTION

R. M. Aleksakhin

In March 1979, in Paris, a meeting of Committee 4 of the ICRP was held. Its task was to evolve rules, standards and recommendations for radiation protection and safety. Representatives from IAEA, World Health Organization (WHO), International Labor Organization (ILP), and several other international organizations participated in the Meeting.

The purpose of the Meeting was to consider questions of the practical application of the new proposals of Publication No. 26 of the ICRP, in which the basic concepts of radiation safety are discussed. The essence of the new concepts consists in the necessity for observing in practice three principles of radiation protection: justification (reasons) for the system of radiation protection measures used (the use of ionizing radiation in practical work is justified only in the case when it will ensure a "pure" advantage to be gained, i.e., the risk from radiation is less than the dosage received by man); optimization (radiation dosage is reduced by the optimum method, reaching the level when its further reduction is found to be unjustified, in consequence of the high cost of measures to ensure protection); and the introduction of systems for limiting the irradiation dosage (the individual irradiation dosage of occupational workers does not exceed the defined limits).

The practical introduction of these proposals, however, is associated with considerable difficulties. These include, in particular, a comparison of the permissible economic expenditure in providing radiation protection, expressed in monetary equivalents, on the one hand, and the accepted irradiation dosage due to this reduction, estimated as a collective dose (man · rem), on the other hand. If the system for limiting the individual irradiation dosage at the present time is sufficiently complete and scientifically justified, then for a collective and collective expected dose (for long-lived radionuclides such as $^{14}C$, $^{129}I$, $^{239}Pu$, etc.), the situation is found to be complicated. The gradation of the permissible dose, normalized in units of man · rem/kW · h of electric power generated in nuclear power stations, taking account of the complete nuclear fuel cycle, has not yet been evolved. There are also procedural difficulties in calculating the collective and collective expected dose.

In the light of the new concepts of radiation safety, radiation monitoring during the irradiation of occupational workers in the outside environment in the vicinity of nuclear power installations was discussed. The necessity for estimating the collective irradiation dosage of the population, residing in the neighborhood of nuclear establishments, introduces the problem of modelling the migration of the most radiation-hazardous nuclides into the natural environment. Radiation monitoring of the outside environment in the vicinity of nuclear power installations complicates the global radioactive fallout. The radiation dosage to the population, estimated in this way, because of the nuclear fuel cycle factories, must be considered in the combination of the effect on the surrounding environment of all the factories located in this region. Only in this case can the effect of the radiation factor and factors of some other nature on the environment and the population be estimated unambiguously.

The discussions dwelt on the use of proposals for normalizing the effect and the introduction of a system for limiting the dose load, contributed by the natural radiation background. The urgency of the problem was stressed by the rising technogenic enhancement in recent years of the natural background, in consequence of the intensification of the circulation of heavy natural radionuclides from the uranium and thorium families in the mining-extraction and processing industries, the use of structural materials with an increased content of natural radionuclides, the increased use of mineral fertilizers and chemical substances with a high concentration of uranium, thorium and their decay products in agriculture, etc. The estimation of the radiation dosage due to the decay products of radon for the population in houses in regions with an increased concentration of radium, and occupational workers in the mines, occupies a special place in the effect of the natural radiation background.

At the Meeting the principles and methods of the use of irradiation optimization as a part of a system for limiting the dose effect were discussed. The limitations concerned both external irradiation (optimization because of distance from the source and strengthening of physical protection) and also internal irradiation (improvement of ventilation, purification of the air, and distance from the source). An attempt has been made to estimate the expenditure on optimization of the irradiation dose limitation for various nuclear power installations from a calculation of the economic costs on protection and a reduction of the collective irradiation dosage.

Despite the difficulties defined for the practical achievement of the new concepts of radiation protection, the acceleration of their introduction will be facilitated by a more rigorous assessment of the radiation consequences of the transition of power generation to a nuclear basis for the population and the environment.

## SEVENTH SEMINAR ON COMPUTER SIMULATION OF RADIATION AND OTHER DEFECTS IN SOLIDS

Yu. V. Trushin

In December 1978 at the Institute of Solid Physics, Academy of Sciences of the SSSR (Chernogolovka), a Seminar was held which was devoted to the simulation of defects and processes of nonradiation origin. The transmission of a dislocation, the development of an assembly of dislocations, the interaction of point defects and dislocations, the connection between micro- and macroscopic processes in crystals, and also the crystallography of defects in polymers were discussed at the Symposium.

In the first group of reports, the work of V. I. Vydashenko and A. I. Landau (Kharkov Physicotechnical Institute) should be distinguished, concerning the movement of a dislocation through an arbitrary two-dimensional network of thermally surmountable point obstacles, with the presence in the glide plane of a small concentration of unsurmountable obstacles. Under the effect of the unsurmountable (or difficultly surmountable) stoppers a systemmatic reduction takes place of the average value of the angle $\alpha$, at which the dislocation attacks the easily surmountable obstacles encountered on its path. As a result, the average effective velocity of the thermoactivated motion of the dislocation in the glide plane decreases, which is equivalent to the origination of a local opposing stress. The model described serves as one of the possible microscopic mechanisms of deformation hardening. The same authors simulated on a computer the thermoactivated motion of the end of a dislocation, emerging at the surface of a crystal, and established the distribution of the migrations of the ends of the dislocation lines from one near-surface stopper to another, and also the distribution of the delay time at these stoppers.

G. V. Bushueva (M. V. Lomonosov Moscow State University) simulated the process of the passage of glide dislocations through plane grids of dislocations with a gradually increasing external stress, for different values of long-range interacting stress field. This allowed the stresses to be determined for the passage of a flexible dislocation through a network with a different value of the long-range interacting stress field. Moreover, by analyzing the elastic interaction of the circular boundary of the dislocation loop with the edge of the dislocation, migrating in planes which are parallel to the plane of occurrence of the loop, the possibility was shown of the origination of 3-9 equilibrium dislocation configurations.

V. S. Boiko (Kharkov Physicotechnical Institute) determined by mathematical simulation that the height of the Peierls energy barrier preventing movement of the spiral twinning dislocation along ⟨111⟩ in a microcrystal of tungsten is equal to 0.074 eV, and the Peierls stress can be defined as $\sigma_P \sim 10^{-2}\mu$ (where $\mu$ is the displacement modulus. S. B. Goryachev (Moscow Engineering Physics Institute) showed that the long-range interacting stress field of the original dislocation structure of the crystal does not affect the stress of the start of the internal Franck–Reid source. These approximate analytical calculations were confirmed by computer simulation.

The second group of reports at the Seminar was devoted to the simulation of the behavior of dislocation assemblies. S. B. Goryachev, by the Monte Carlo method, simulated the early stages of plastic deformation

hardening for the case when the plastic deformation process is determined by the evolution of the dislocation assemblies. In addition to this, he investigated the process of the formation of dipole dislocations by two sources which, by the action of a uniform external stress, radiate counter-clusters of edge dislocations of opposite sign, in parallel glide planes.

The simulation of the motion of dislocation assemblies during the growth of crystals in the initial stages of plastic deformation and recovery was carried out by V. M. Danilenko (Institute of Applied Mathematics, Academy of Sciences of the Ukrainian SSR) and it was shown by the example of molybdenum that in the absence of stoppers, the assembly of parallel dislocations is an extremely mobile system; in particular, the surplus dislocations of one sign are dispersed over 1 $\mu$sec to a distance of about 1 $\mu$m. Dipole dislocation systems are found to be more stable, but even in this case several active dislocations per second migrate to a distance greater than the average size of the dipole. In realistic conditions, dislocation systems are moving through the dislocation forest. Therefore, A. A. Predvoditelev (M. V. Lomonosov Moscow State University) has simulated the passage of a train of elastically interacting flexible dislocations, taking account of the fine structure of the long-range interacting stress field. For crystals of the NaCl type, the internal stress fields have a weak irregularity, due to which predominantly single detachments of the moving dislocation from the dislocation forest takes place, and the coefficient of resistance of the dislocation forest $\beta$, is increased by only 22% by comparison with the passage of a single dislocation. For hcp crystals the internal stresses, in consequence of the high degree of irregularity, cause bending by the glide dislocations, of a group of dislocations of the forest, which leads to the intensive formation of a loop and an increase of $\beta$ by 120%.

Point defects in crystals affect the different mechanisms of plastic deformation, and therefore a study of their behavior is one of the problems solved by computer simulation methods. V. S. Yushchenko (Institute of Physical Chemistry, Academy of Sciences of the USSR) investigated the diffusion of an interstitial impurity in a two-dimensional crystal, deformed by a perpendicularly densely packed series of atoms. It was shown that the single-axis tension, even in the absence of defects, can lead to a sharp increase of mobility of the dissolved component. The results are necessary for the analysis of the mechanism of adsorption, lowering of strength and the process of separation of a new phase during breakup of the solid solution. Model absorption calculations of point defects in an edge dislocation with the Burgers vector $a\langle 100\rangle$ in a three-dimensional crystal of $\alpha$-iron were carried out by É. Ya. Mikhlin (Institute of Engineering Physics). Vacancies, located near to the nucleus of a dislocation, remained in a train with the node, at which they were located previously, while the introduction of an internode atom in certain cases led to a marked rearrangement of structure. In particular, the additional atom was displaced to the central part of the train and occupied there the internode around the dislocation axis. The study of the absorption of point defects in a dislocation with a step allowed the parameter $\eta$ to be estimated, in an average way characterizing the preferential absorption of the internode atoms by dislocations. With a dislocation density of $10^{10}$ cm$^{-2}$ and with an average distance between steps of $\sim 50a$ (where $a$ is the average interatom distance), a value of $\eta = 1.037$ was obtained.

In several reports, the connection between micro-and macroscopic processes in crystals was discussed. In the simulation of the breakup of a chain of 41 atoms under conditions of constant deformation (A. I. Mikhailin, M. I. Kalinin Polytechnic Institute, Lvov), the origination of rupture of this chain was observed much later than the establishment of thermodynamic equilibrium, and the rupture preceded a high peak with a width of 4-5 atomic bonds on the kinetic energy distribution curve.

D. N. Karpinskii (Rostov State University) simulated on a computer the thermally activated processes of slippage and multiplication of dislocations in the plastic zone near the vertex of the crack for the case of its development in the cleavage plane (001) in $\alpha$-iron and slippage over the planes of the $\{110\}$ family. The hardening effect from an assembly of randomly arranged spherical coherent segregations in the body of the crystal was investigated by A. B. Popov (Moscow Engineering Physics Institute). Based on the results obtained, the deforming stress was calculated for crystals containing these segregations.

The macromolecular nature of the polymer crystals is due to their enhanced imperfection and the presence of specific crystallographic defects. A. P. Dreimanis (IMP, Academy of Sciences of the Latvian SSR) proposed a procedure for studying the structure and properties of an end defect, formed during chain rupture or by the presence of a molecular fold. It was established for orthorhombic polyethylene that the end defect represents a vacancy train or the nucleating center of spiral dislocations, and simultaneously it contains also a set of partial torsional dislocations. The lectures read in the school on the computer simulation of defects in metals, which took place simultaneously with the work of the Seminar, will be published.

# CHANGING YOUR ADDRESS?

**In order to receive your journal without interruption, please complete this change of address notice and forward to the Publisher, 60 days in advance, if possible.**

(Please Print)

Old Address:

name

address

city

state (or country) zip code

New Address

name

address

city

state (or country) zip code

date new address effective

name of journal

THE LANGUAGE OF SCIENCE
Plenum
PUBLISHING CORPORATION

**Plenum Publishing Corporation**
**227 West 17 Street, New York, New York 10011**

Declassified and Approved For Release 2013/02/15 : CIA-RDP10-02196R000800020002-3

# NEW RUSSIAN JOURNALS

## IN ENGLISH TRANSLATION

### BIOLOGY BULLETIN

*Izvestiya Akademii Nauk SSSR, Seriya Biologicheskaya*

The biological proceedings of the Academy of Sciences of the USSR, this prestigious new bimonthly presents the work of the leading academicians on every aspect of the life sciences—from micro- and molecular biology to zoology, physiology, and space medicine.

Volume 7, 1980 (6 issues) . . . . . $195.00

### SOVIET JOURNAL OF MARINE BIOLOGY

*Biologiya Morya*

Devoted solely to research on marine organisms and their activity, practical considerations for their preservation, and reproduction of the biological resources of the seas and oceans.

Volume 6, 1980 (6 issues) . . . . . $115.00

### WATER RESOURCES

*Vodnye Resursy*

Evaluates the water resources of specific geographical areas throughout the world and reviews regularities of water resources formation as well as scientific principles of their optimal use.

Volume 7, 1980 (6 issues) . . . . . $215.00

### HUMAN PHYSIOLOGY

*Fiziologiya Cheloveka*

A new, innovative journal concerned *exclusively* with theoretical and applied aspects of the expanding field of human physiology.

Volume 6, 1980 (6 issues) . . . . . $195.00

### SOVIET JOURNAL OF BIOORGANIC CHEMISTRY

*Bioorganicheskaya Khimiya*

Features articles on isolation and purification of naturally occurring, biologically active compounds; the establishment of their structure, methods of synthesis, and determination of the relation between structure and biological function.

Volume 6, 1980 (12 issues) . . . . . $245.00

### SOVIET JOURNAL OF COORDINATION CHEMISTRY

*Koordinatsionnaya Khimiya*

Describes the achievements of modern theoretical and applied coordination chemistry. Topics include the synthesis and properties of new coordination compounds; reactions involving intraspheral substitution and transformation of ligands; complexes with polyfunctional and macromolecular ligands; complexing in solutions; and kinetics and mechanisms of reactions involving the participation of coordination compounds.

Volume 6, 1980 (12 issues) . . . . . $255.00

### THE SOVIET JOURNAL OF GLASS PHYSICS AND CHEMISTRY

*Fizika i Khimiya Stekla*

Devoted to current theoretical and applied research on three interlinked problems in glass technology; the nature of the chemical bonds in a vitrifying melt and in glass; the structure-statistical principle; and the macroscopic properties of glass.

Volume 6, 1980 (6 issues) . . . . . $145.00

### LITHUANIAN MATHEMATICAL JOURNAL

*Litovskii Matematicheskii Sbornik*

An international medium for the rapid publication of the latest developments in mathematics, this quarterly keeps western scientists abreast of both practical and theoretical configurations. Among the many areas reported on in depth are the generalized Green's function, the Monte Carlo method, the "innovation theorem," and the Martingale problem.

Volume 20, 1980 (4 issues) . . . . . $175.00

### PROGRAMMING AND COMPUTER SOFTWARE

*Programmirovanie*

Reports on current progress in programming and the use of computers. Topics covered include logical problems of programming; applied theory of algorithms; control of computational processes; program organization; programming methods connected with the idiosyncracies of input languages, hardware, and problem classes; parallel programming; operating systems; programming systems; programmer aids; software systems; data-control systems; IO systems; and subroutine libraries.

Volume 6, 1980 (6 issues) . . . . . $115.00

### SOVIET MICROELECTRONICS

*Mikroelektronika*

Reports on the latest advances in solutions of fundamental problems of microelectronics. Discusses new physical principles, materials, and methods for creating components, especially in large systems.

Volume 9, 1980 (6 issues) . . . . . $160.00

**Send for Your Free Examination Copy**

**PLENUM PUBLISHING CORPORATION**, 227 West 17th Street, New York, N.Y. 10011
In United Kingdom: Black Arrow House, 2 Chandos Road, London NW10 6NR, England
Prices slightly higher outside the U.S. Prices subject to change without notice.